EFFECTS OF VOLTAGE UNBALANCE AND SYSTEM HARMONICS ON THE PERFORMANCE OFDOUBLY FED INDUCTION WIND GENERATORS

by

MORGAN MOZHGAN KIANI

Presented to the Faculty of the Graduate School of

The University of Texas at Arlington in Partial Fulfillment

of the Requirements

for the Degree of

DOCTOR OF PHILOSOPHY

THE UNIVERSITY OF TEXAS AT ARLINGTON

MAY 2009

ACKNOWLEDGEMENTS

I would like to express my gratitude to my supervisor Prof. Wei-Jen Lee for his continuous support, encouragement, and supervision. His guidance and valuable advises has been vital to my learning. I thank him for mentoring me for completion of the present dissertation.

I would like to thank Dr. Raymond R. Shoults, Dr. W. Dillon, Dr. R. Carter, and Dr. R. Kenarangui for serving in my supervising committee. Their views and suggestions have been valuable for completeness of this dissertation.

I wish to thank all the members from the Energy Systems Research Center for their support in completion of this dissertation.

I also want to thank members of the power electronics and controlled motion laboratory at University of Texas at Arlington for their cooperation.

April 17, 2009

DEDICATION

I would like to dedicate this to love of my life, my wonderful husband Babak and my sons, Shawn and Kevin.

ABSTRACT

EFFECTS OF VOLTAGE UNBALANCE AND SYSTEM HARMONICS ON THE PERFORMANCE OF DOUBLY FED INDUCTION WIND GENERATORS

MORGAN M. KIANI, PhD.

The University of Texas at Arlington, 2009

Supervising Professor: Wei-Jen Lee

Inherent difficulties in management of electric power in the presence of an increasing demand for more energy, non-conventional loads such as digital appliances, and non-sustainable imported fossil fuels has initiated a multi-folded effort by many countries to restructure the way electric energy is generated, dispatched, and consumed. Smart power grid is the manifestation of many technologies that would eventually transforms the existing power grid into a more flexible, fault resilient, and intelligent system. Integration of distributed renewable energy sources plays a central role in successful implementation of this transformation. Among the renewable options, wind

energy harvesting offers superior engineering and economical incentives with minimal environmental impacts. Doubly fed induction generators (DFIG) have turned into a serious contender for wind energy generators due to their flexibility in control of active and reactive power with minimal silicon loss. Significant presence of voltage unbalance and system harmonics in finite inertia transmission lines can potentially undermine the reliability of these wind generators. The present dissertation has investigated the impacts of system unbalances and harmonics on the performance of the DFIG. Our investigation indicates that these effects can result in an undesirable undulation in the rotor shaft which can potentially invoke mechanical resonance, thereby causing catastrophic damages to the installations and the power grid. In order to remedy the above issue, a control solution for real time monitoring of the system unbalance and optimal excitation of the three phase rotor currents in a DFIG is offered. The optimal rotor currents will create appropriate components of the magneto-motive force in the airgap that will actively compensate the undesirable magnetic field originated by the stator windings. Due to the iterative nature of the optimization procedure, field reconstruction method has been incorporated. Field reconstruction method provides high precision results at a considerably faster pace as compared to finite element method. Our results indicate that by just-in-time detection of the system unbalance and employment of the optimal rotor currents damaging torque pulsation can be effectively eliminated. The side effects of the proposed method in changing the core , copper, and silicon losses are minor and well justified when reliability of the wind generation units are considered.

TABLE OF CONTENTS

LIST OF ILLUSTRATIONS

LIST OF TABLES

CHAPTER 1

INTRODUCTION AND BACKGROUND

Continued economic growth and fulfillment of high standards in human life depends on reliable and affordable access to electricity. Over the past few decades, there has been a paradigm shift in the way electricity is generated, transmitted, and consumed. However, fossil fuels continue to form a dominant initial source of energy in the United States and other industrialized countries. The steady economic growth of China and India gradually exposed the unsustainable nature of the energy policy that is highly dependent on foreign fossil fuels. On the other hand, an aging power grid (see figure 1) that faces new challenges posed by higher demands and increasing digital and nonlinear loads has placed new reliability concerns as observed with frequent outages in the recent years. Sensitivity of digital equipments, such as data centers, and consumer electronics, into intermittent outages has redefined the concept of reliability. As a result, power generation, transmission, and consumption has been the focus of investigations as to see what remedies will address the above challenges thereby transforming the power grid into a more efficient, reliable, and communication-rich system. Smart power grid is a host of solutions that is aimed to realize these lofty goals by empowering customers, improving the capacity of the transmission lines and distribution systems, providing information and real time pricing between the utility and

clients, and higher levels of utilization for renewable energy sources to name a few. Diversifying the energy sources for generation of electricity and adaptation of a distributed generation with enhanced communication features is a central part of transformation into an intelligent grid. One may consider this as a true emergence of information technology (IT) into energy technology (ET). The present chapter describes the fundamentals of the existing power grid, potentials for integration of the renewable energy systems, and related technology challenges

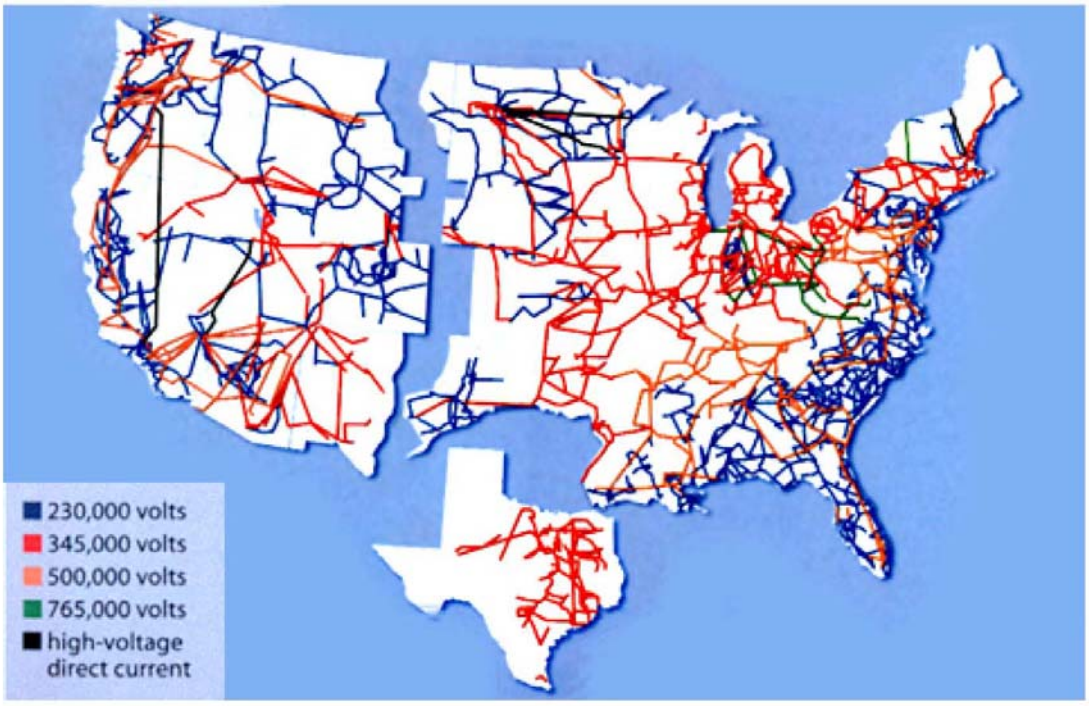

Figure 1.1 Electric power grid in the United States of America (Source: DOE)

1.1. Status of Generation and Transmission of Electricity in US Power Grid

Reliable and efficient generation and transmission of electricity presents a profound and undeniable impact on almost every aspect of the modern life. In spite of a continuous increase in use of electronic and nonlinear loads, the impact of these harmonic generating loads on the power grid has been neglected. Although over the past few decades substantial milestones in offering modern electricity operated appliances has been achieved development, maintenance, and improvement of performance in generation and transmission of electricity seems to be taken as granted. As the quest for consumption of reliable electricity with an affordable price turns into a necessary condition for continued economic growth, development of an efficient and reliable electric grid deserves a due attention. In view of the recent nationwide blackouts, high fuel prices, and security concerns, there has been a renewed attention to the survivability and efficiency of the generation and transmission of electricity. In this section, an overall assessment of the power generation and transmission in the United States will be offered.

1.1.1 Dependency of Generation on Fossil Fuels

An investigation of the existing power plants in our nation indicates that the majority of the electricity is generated from unsustainable and environmentally harmful fossil fuels. Figure 2 illustrates the breakdown of the resources used for generation of the electricity in the past and for the foreseeable future. Although the dependency on foreign oil is

primarily linked to the transportation sector, introduction of new hybrid electric and especially plug in hybrid vehicles in near term future will create a significant interdependence between our power grid and international affairs. What seems interesting is that the projected growth (in 2005) in use of renewable energy sources by the department of energy is still limited (close to 20% of the overall need by 2030) and needs to be augmented.

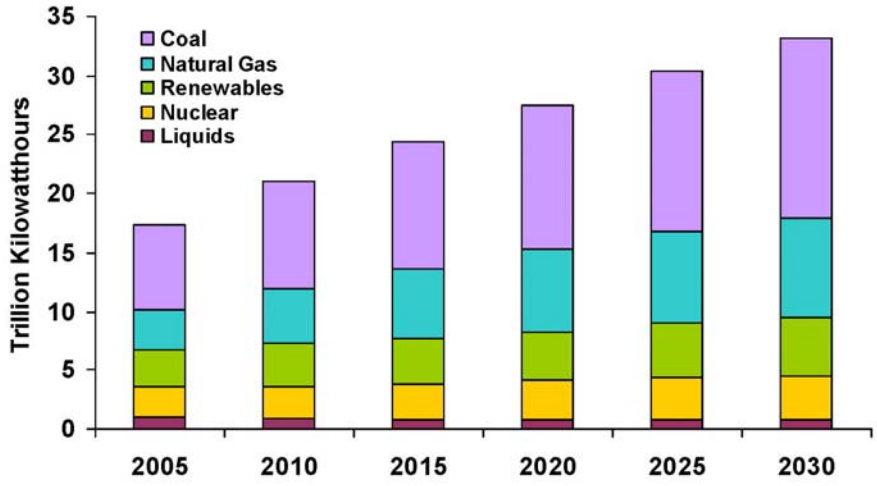

Figure 1.2 Sources of energy used in generation of electricity in USA(Source: DOE)

Environmental impact of a fossil fuel based energy policy has also raised many questions among research and governmental institutions. Figure 1.3 illustrates the existing records and projection in the rise of green house gases (GHG) and earth temperature. The alarming situation and the existing dependence between accumulation of GHG in biosphere and rise of temperature calls for restructuring of the electricity generation, optimal consumption of electricity and incorporation of clean coal

technology as well as development of new methods for capture and sequestration of excess GHG.

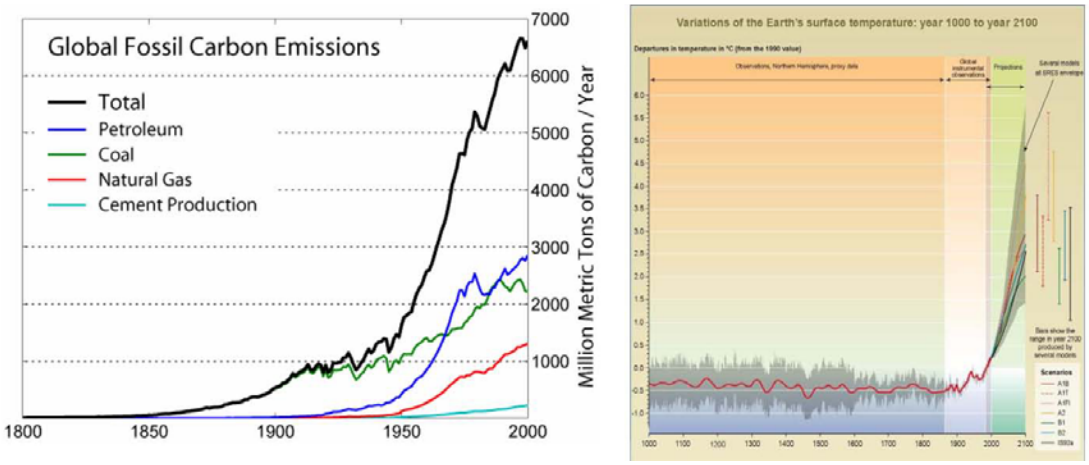

Figure 1.3 Generation of Carbon emission and rise of global temperature (Source:DOE)

1.1.2. Characteristics of Transmission Grid

Once recognized as a technological marvel by American Academy of Engineering, the US power grid is reaching its limits in the face of an asymmetric increase in demand for electricity. Lack of automation, effective energy management, exchange of information and limited available capacity in aging transmission lines has brought big segments of the US power grid to its knees on number of occasions over the past decade. The blackout of 2003 in the north east area has set an example how a cascading effects in the absence of surplus capacity and intelligent automated control can result in a major and extended outage, thereby resulting in significant financial damages. Distribution networks not only suffer from the above mentioned problems but also have to accommodate an increasing level of harmonics in the current. The change in perception of customers regarding reliability has originated another host of problems. It appears

that conventional methods in addressing the increase demand will become less effective in the future as the 21st century customers are less tolerant to intermittent outages while injecting significant amount of non-sinusoidal currents into the grid. Introduction of the plug-in hybrid electric vehicles and vehicle to grid (V2G) will amplify the dimensions of the existing problems. Smart power concept recommends empowering the customers by allowing distributed generation, smart purchase/sale of electricity, and effective communication between the utility (energy management) and local customers. Augmentation of existing renewable sources will certainly require construction of new transmission lines at the proper locations for generation are often distant from the metropolitan areas where the majority of consumers are located. This restructuring effort will require a system level evaluation of the protection, flow of power, stability, and voltage regulation issues. Although the overall expectations from the power grid of the future are almost known, the roadmap to accomplishing the objectives is less clear.

1.1.3. Changing Trends in Consumer Loads

Usage of electronic loads and appliances has become an inherent part of daily life in industrial countries. As information technology offers new products to the market the bi-products of these popular devices on the electric power grid has not been addressed properly. The common denominator between all new nonlinear loads can be summarized in (1) introduction of non-sinusoidal currents and (2) less tolerance to transient and intermittent outages. Figure 1.4 depicts a full wave rectifier circuit which forms the front-end circuit of most dc power supplies that are used in most electronic and digital appliances.

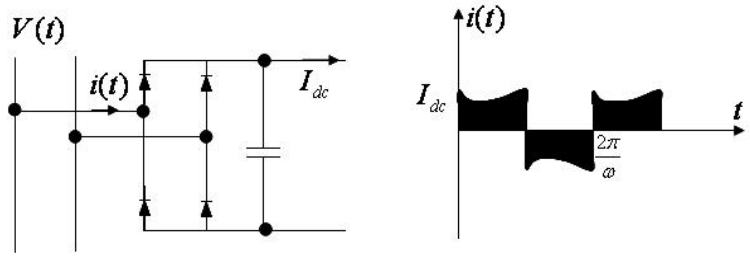

$$i(t) \approx \sum_{k=1}^{\infty} \frac{4I_{dc}}{k} Sin\left(\frac{k\pi}{2}\right).Cos(k\omega t)$$

Figure 1.4 Typical current waveform by a front end full-wave rectifier

As can be observed from figure 1.4, significant amount of odd harmonics are drawn from the grid by this type loads. One may note that single wave rectifiers as used in many low cost appliances can even worsen the situation by taking dc component of current as well as even harmonics which will have undesirable effects on the grid.

Reduced tolerance on temporary outage of power by digital loads is yet another challenge as most fault recovery methods and conventional reliability metrics used by utility companies have not been designed to address this growing demand. Uninterruptible supply of power with high quality requires new design elements such as integration of energy storage elements and more flexible and alternative path for delivery of power. This is a drastic change compared to the existing radial configuration and unidirectional delivery mechanism.

1.2. Renewable Sources of Energy

Potential resources for renewable energy include the following options:

- Wind energy
- Solar energy
- Geothermal energy
- Hydroelectric energy

One may include harvesting of hydrogen from bio-fuels into this list as hydrogen fueled fuel cells offer an alternative platform for generation of electricity. This method in fact has been proposed as a complimentary storage option for solar and wind energy systems.

As illustrated in figure 1.5, United States enjoys a rich exposure to renewable sources of energy, especially solar and wind energy sources [1], [2], [3]. However, wide harvest and integration of renewable energy sources would require solutions for (a) storage of energy as these resources are not readily available and can only be forecasted based on

meteorological information, (b) new transmission lines to transfer the energy, (c) economical incentives for currently expensive renewable energy sources, and (d) an intelligent energy management system that can perform load leveling across the United States and neighboring countries.

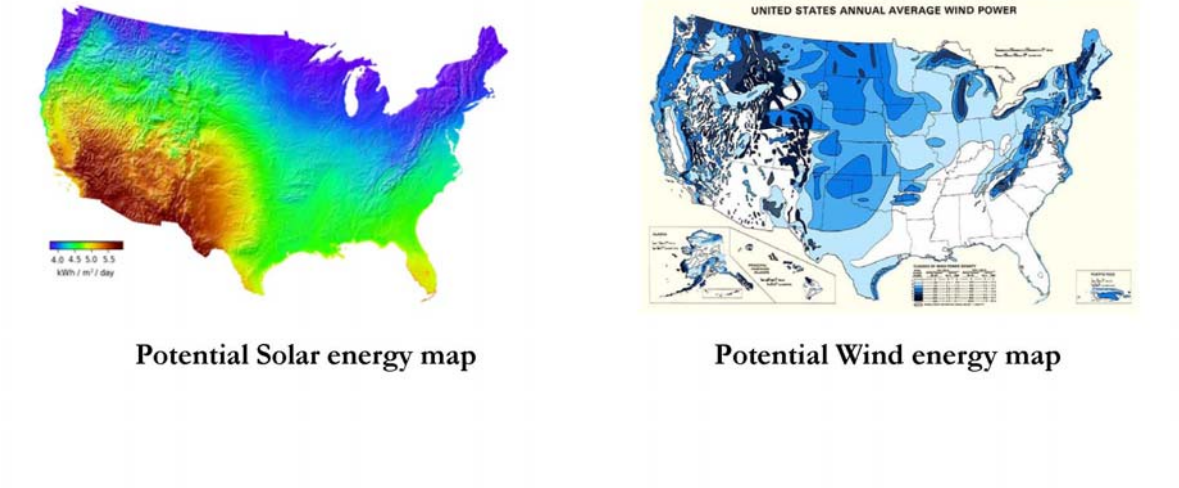

Figure 1.5 Potential resources of renewable wind and solar energies in United States

An inspection of the state-of-the-art in harvest and integration of the renewable sources of energy indicates that the existing resources and potentials are far from exhausted. Figure 1.6 shows the breakdown of the existing sources of energy and as can be observed renewable energy sources play a very minor role in overall distribution of the energy. One may also note that the current share of the renewable energy sources are dominated by hydroelectric power.

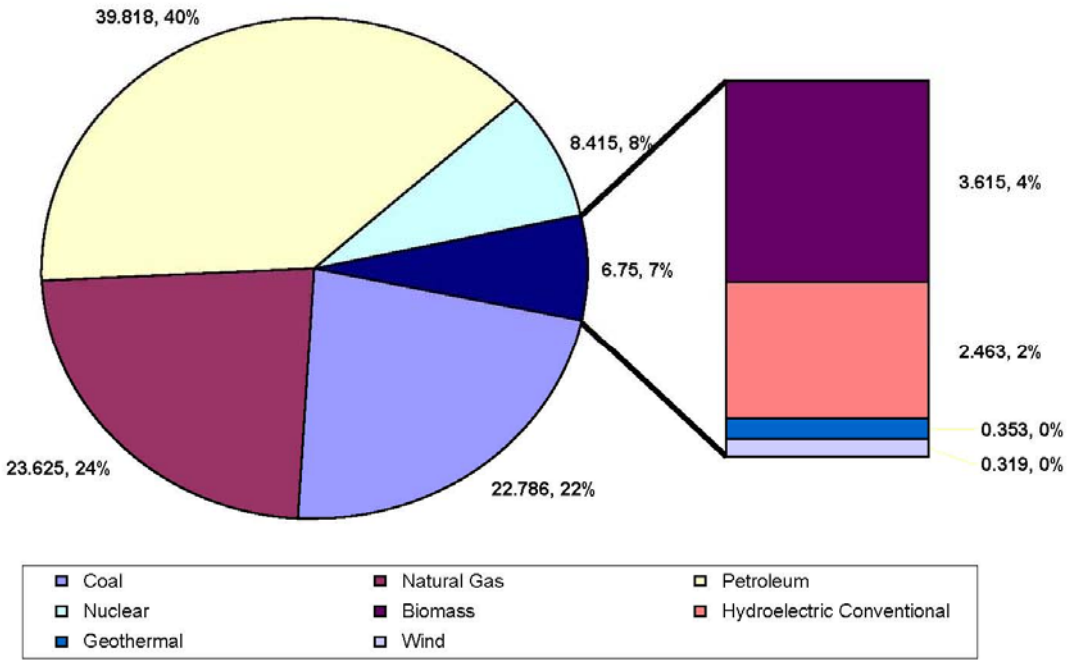

Figure 1.6 Breakdown of the energy sources in the United States

From the economical point of view, wind energy harvest represents a superior choice. The abundant nature of the existing wind resources, continued increase in size of the wind generation units, along with high efficiency solutions in electromechanical energy conversion has played a key role in this classification. From a technological point of view, doubly fed induction generators (DFIG) seem to offer efficient and flexible solutions for optimal harvest of wind energy. It must be noted that permanent magnet synchronous machines have also gained momentum for low power (less than 50kW) applications. However, at large powers (multi Megawatts) induction generators portray a superior choice.

The power contained in the wind passing through an area of A (homogenous distribution of the speed across the area is assumed) with a speed of v_1 is given by:

$$P_w = \frac{\rho}{2} A v_1^3 \tag{1.1}$$

Where ρ is the specific air mass which depends on air pressure and humidity. A typical value can be assumed to be $\rho \approx 1.2 kg/m^3$. Depending on the design of the wind turbine the effective (i.e. useful) rotor power can be approximated by:

$$P_{eff} = C_P \frac{\rho}{2} A v_1^3 \tag{1.2}$$

The maximum theoretical value for C_P will be around 0.6.However, maximum practical value for this coefficient is given by the range $C_{P,\max} = 0.4 \ldots 0.5$ due to profile loss, tip loss, and loss due to wake rotation. An important factor of the wind rotors is the tip-speed ratio given by:

$$\lambda = \frac{u}{v_1} = \frac{D}{2} . \frac{\Omega}{v_1} \tag{1.3}$$

In which $D, and\ \Omega$ represent the outer rotor diameter and the angular velocity of the rotor respectively. One can use (1.3) to obtain the useful torque harvested by the shaft of the rotor as given by:

$$T = \frac{C_P(\lambda)}{\lambda} . \frac{D}{2} . \frac{\rho}{2} A v_1^2 \tag{1.4}$$

1.3. Reliability of Power System and Penetration of the Renewable Energy Source

Distribution of the wind speed depends on seasonal and regional effects. Study of the wind regime is of high importance in optimal design of the wind generator. The wind velocity varies with the height of the turbine, and is influenced by the roughness of the surface. When the regime of the wind velocity is known for a specified height above the ground, the distribution of the power and energy yield can be evaluated by descriptive statistics.

The random nature of the wind energy would complicate the prediction of the available electric power and as such can undermine the reliability of the sources. Therefore, integration of a complimentary energy storage system is of paramount interest. Application of electrochemical batteries and hydrogen harvest plus fuel cell systems have been proposed in the literature. However, one needs to note that these technologies still suffer from poor efficiency and further improvement deems necessary.

1.4 Motivation and Objectives

One of the major factors in reliability of the wind generation units relates to their fault tolerant operation. These faults maybe of mechanical or electrical nature. Among electrical faults, short circuit, over voltage due to lightning and switching surges, and malfunction due to system unbalance and system harmonics are most probable. It is extremely important to protect the generation unit in the event of a fault. Furthermore, it is desirable to continue generation in the presence of tolerable faults with jeopardizing the wind generator. In this respect online condition monitoring and just-in-time maintenance of renewable wind generators plays a key role in reliability of the power system. The present dissertation aims to investigate the impact of voltage unbalance and system harmonics on the operation of doubly fed induction wind generators. Furthermore, a new method of real-time fault detection and treatment for unbalance and harmonics is developed. The fault treatment technique includes development of a control strategy that would remedy the potentially harmful torque undulations caused by system voltage unbalanced and harmonics. The real time fault detection and treatment form the main contributions of this dissertation both of which are based on the use of field reconstruction method.

CHAPTER 2

DOUBLY FED INDUCTION GENERATORS

The main factors for selection of a wind generator are ability of operation under variable speed condition, flexibility in control of the stator voltage magnitude and frequency, independent control of the active and reactive power, fault tolerant operation, and overall efficiency. Among the plausible candidate for this task the following configurations have gained momentum.

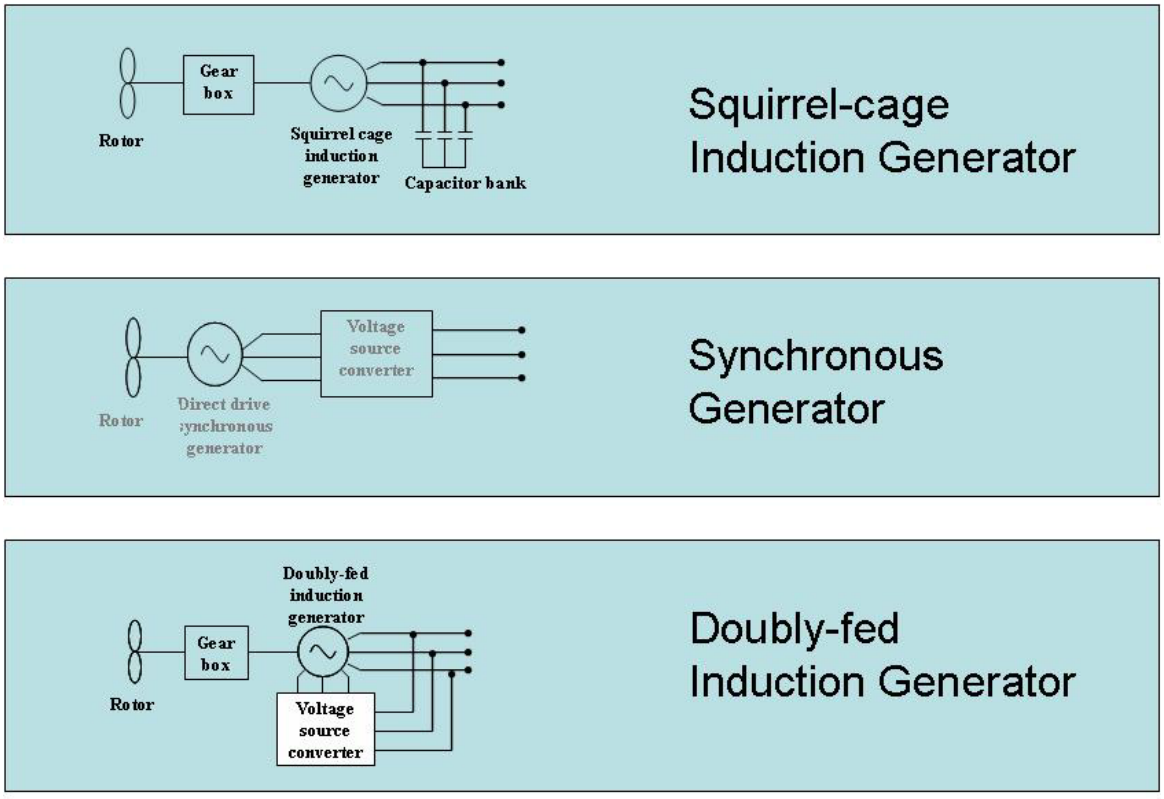

Figure 2.1 Primary candidates for wind energy harvest

The squirrel cage induction machine with a single stator supply is an adequate, low cost option. The stator frequency, rotor mechanical speed, and rotor current frequencies in an induction generator are related by the following equation:

$$\frac{P}{2} f_{mech} - f_s = f_r \tag{2.1}$$

Where $f_s, f_{mech}, f_r, and\ P$ represent stator frequency, mechanical frequency (revolutions per second), rotor current frequency and number of magnetic poles respectively. Since speed of the wind varies, using a gear box to bring the shaft speed to range sufficiently close to that of the stator deems necessary. However, this will add to the complexity of the design, and may not be a satisfactory solution at very low speeds resulting in inefficient operation of the drive (i.e. stator frequency is fixed at 60Hz). Moreover due to its singly fed construction (viz. rotor is formed by a short circuited set of bars with no access to external sources), the initial magnetizing current needs to be provided by a separate setoff capacitor banks or battery. In this design, independent control of the stator active and reactive power is not possible. Keeping in mind that this configuration is not capable of injecting reactive power to the grid hence it may lead to complications when voltage regulation is demanded.

The second option is formed by a synchronous machine. In small and medium range power (fractional horse power up to 100kW), permanent magnet synchronous machines are used in which the rotor is comprised of surface mounted permanent magnets. For higher levels of power wound rotor synchronous machines similar to those used in

turbo-generators are considered. Because the mechanical speed of rotation and electrical frequency of the stator are equal, i.e.:

$$f_s = \frac{P}{2} f_{mech} \tag{2.2}$$

To create a seamless synchronization, the use of a cascaded ac-dc followed by a dc-ac power electronic conversion is necessary. This unit has to process the total output power of the generator and as such will introduce significant amount of silicon loss which will have an adverse effect on efficiency.

The third option is presented by a doubly fed induction generator (DFIG). DFIG is formed by a wound rotor induction machine in which a set of three phase current can be injected into the rotor windings via slip rings[4]-[8]. The magnitude and frequency of the rotor currents can be controlled by a power electronics conditioner. Similar to synchronous generators, this power conditioner is consisted of an ac-dc followed by a dc-ac converter. The frequency and magnitude modulation is necessary to cope with the variable speed nature of the prime mover (i.e. wind). In order to obtain the 60Hz frequency in the stator circuit, the following relationship between the rotor current frequency and mechanical speed of the shaft should be maintained:

$$\frac{P}{2} f_{mech} - 60 = f_r \tag{2.3}$$

This relationship can be precisely followed by incorporating a pulse width modulation technique in control of the dc-ac stage of the rotor power conditioner. It must be mentioned that the rotor power is only a small portion of the output power and as such and unlike synchronous machines the overall impact of the silicon losses will be

limited. Given the fact that independent control of the active and reactive power is feasible in a DFIG, in consideration of the higher efficiency of the DFIG, it has received considerable attention among the research community over the past decade. It is expected that with larger penetration of the wind energy harvesting, DFIG turn into a superior candidate in large wind generation units.

2.1 Fundamentals of Operation

Like any electromechanical generator, DFIG converts mechanical energy into electric energy. The three phase windings of the stator and rotor along with their respective balanced sinusoidal current excitation will create two rotating electromagnets with fixed magnitudes. The electromagnet formed by stator will follow the one created by the rotor circuit hence trying to stop the rotor and in this phenomenon will apply a negative (decelerating) torque on the shaft. The absorbed mechanical power will boost the induced voltage in the stator coil resulting in generation of electric current flowing to the grid. In the following sections, a brief introduction of the electromagnetic field and electromechanical energy conversion in DFIG will be introduced.

2.1.1 Electromechanical Energy Conversion

Figure 2.2 illustrates a graphical interpretation of a DFI machine with rotor and stator windings represented by symbolic conductors. Each conductor represents a sinusoidally distributed winding for the respective phase.

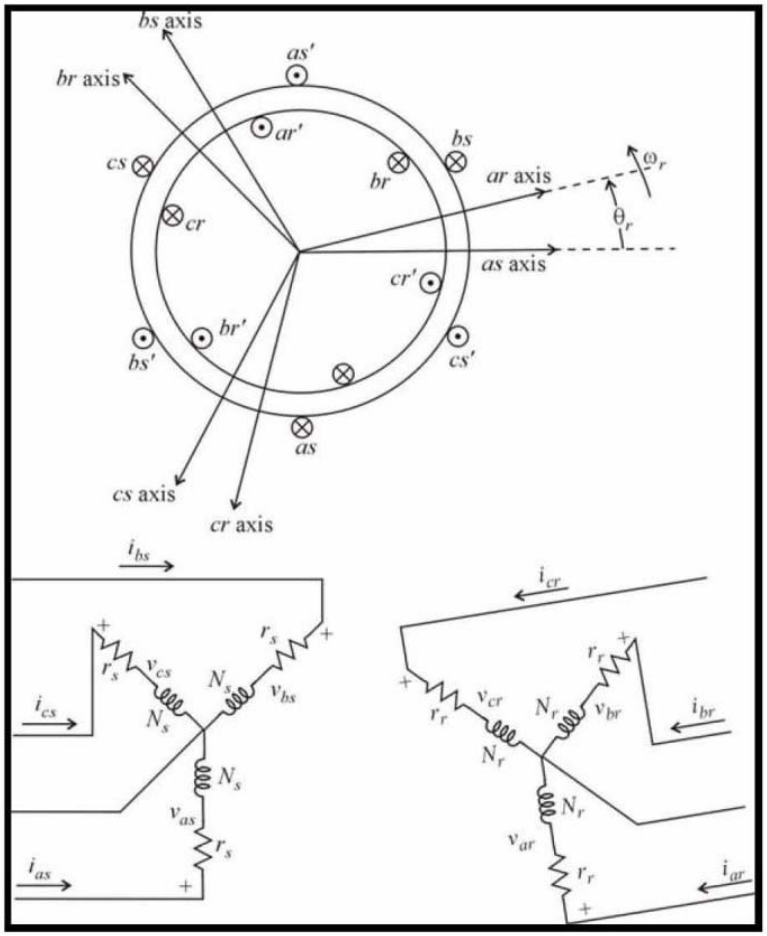

Figure 2.2 Symbolic representation of the stator and rotor windings

Assuming a sinusoidal distribution of the winding in the stator, one can formulate the total magneto-motive force of the stator by:

$$MMF_s = \frac{3}{2}.\frac{2N_s}{P} I_{s,\max} Cos(\omega_e t - \phi_s) \qquad (2.3)$$

Where $\phi_s, \omega_e, I_{s,\max} and\ N_s$ represent displacement on the stator, electrical velocity of the stator, maximum stator current magnitude, and effective number of conductors per phase in the stator windings respectively. Similarly, the rotor currents will originate a rotating magnetic field in the rotor as shown below:

$$MMF_r = \frac{3}{2}.\frac{2N_r}{P} I_{r,\max} Cos(\omega_r t - \phi_r) \tag{2.4}$$

In which $\phi_r, \omega_r, I_{r,\max} and\ N_r$ represent displacement on the rotor, rotor current frequency, maximum magnitude of the rotor current, and the effective number of the rotor windings per phase. Although the two fields rotate at different frequencies in their respective medium, they both travel at the same synchronous speed in the airgap. This would allow for uniform and ripple free electromagnetic torque. One may consider synchronous generator as a limit condition for DFIG when the rotor current frequency approaches zero. If the resulting magnetic flux densities of the stator and rotor are represented by $\mathbf{B}_S, \mathbf{B}_R$, the resulting electromagnetic force will follow the following expression:

$$\mathbf{F} = K.\mathbf{B}_S \times \mathbf{B}_R \tag{2.5}$$

Where K represents the impact of the geometry. It is apparent from the above equation that a pair of perpendicular flux densities of the rotor and the stator will enhance the force production. This is the underlying principle in maximum torque per Ampere control for doubly fed induction machines.

In the presence of imperfections in the stator and rotor windings, the winding function representing the stator and the rotor will contain harmonics (also known as

space harmonics). This will change the magneto-motive forces of the stator and the rotor to the following forms:

$$MMF_S = i_{as}\left(\sum_{k=1}^{\infty} N_{k,s} Cos(k\phi_s)\right) + i_{bs}\left(\sum_{k=1}^{\infty} N_{k,s} Cos(k(\phi_s - 120^0))\right) + i_{cs}\left(\sum_{k=1}^{\infty} N_{k,s} Cos(k(\phi_s + 120^0))\right) \quad (2.6)$$

$$MMF_r = i_{ar}\left(\sum_{k=1}^{\infty} N_{k,r} Cos(k\phi_r)\right) + i_{br}\left(\sum_{k=1}^{\infty} N_{k,r} Cos(k(\phi_r - 120^0))\right) + i_{cr}\left(\sum_{k=1}^{\infty} N_{k,r} Cos(k(\phi_r + 120^0))\right) \quad (2.7)$$

In which $i_{as}, i_{bs}, i_{cs}, i_{ar}, i_{br}, i_{cr}, N_{k,s}$, *and* $N_{k,r}$ stand for stator phase-a current, stator phase-b current, stator phase-c current, rotor phase-a current, rotor phase-b current, rotor phase-c current, magnitude of the k-th space harmonic in stator winding, and magnitude of the k-th rotor space harmonic respectively. Obviously, this formulation indicates that space harmonics can create components of the magneto-motive field that travel at speeds higher than the synchronous speed and therefore can cause significant pulsation in the electromagnetic torque.

If the rotor or stator currents contain harmonics, similar effects can be expected. Under a balanced sinusoidal condition the stator and rotor currents are given by:

$$\begin{aligned} i_{as} &= I_{s,\max} Cos(\omega_e t) \\ i_{bs} &= I_{s,\max} Cos(\omega_e t - 120^0) \\ i_{cs} &= I_{s,\max} Cos(\omega_e t + 120^0) \end{aligned} \quad (2.8)$$

$$
\begin{aligned}
i_{ar} &= I_{r,\max} Cos(\omega_r t) \\
i_{br} &= I_{r,\max} Cos(\omega_r t - 120^0) \\
i_{cr} &= I_{r,\max} Cos(\omega_r t + 120^0)
\end{aligned}
\tag{2.9}
$$

However, in the presence of stator and rotor harmonics (i.e. time harmonics) equations (2.6) and (2.7) will be further complicated as shown in (2.10) and (2.11):

$$
\begin{aligned}
MMF_S = &\left(\sum_{j=1}^{\infty} I_{sj,\max} Cos(j\omega_e t)\right) \bullet \left(\sum_{k=1}^{\infty} N_{k,s} Cos(k\phi_s)\right) + \\
&+\left(\sum_{j=1}^{\infty} I_{sj,\max} Cos(j(\omega_e t - 120^0))\right) \bullet \left(\sum_{k=1}^{\infty} N_{k,s} Cos(k(\phi_s - 120^0))\right) + \\
&+\left(\sum_{j=1}^{\infty} I_{sj,\max} Cos(j(\omega_e t + 120^0))\right) \bullet \left(\sum_{k=1}^{\infty} N_{k,s} Cos(k(\phi_s + 120^0))\right)
\end{aligned}
\tag{2.10}
$$

$$
\begin{aligned}
MMF_r = &\left(\sum_{j=1}^{\infty} I_{rj,\max} Cos(j\omega_r t)\right) \bullet \left(\sum_{k=1}^{\infty} N_{k,s} Cos(k\phi_s)\right) + \\
&+\left(\sum_{j=1}^{\infty} I_{rj,\max} Cos(j(\omega_r t - 120^0))\right) \bullet \left(\sum_{k=1}^{\infty} N_{k,s} Cos(k(\phi_s - 120^0))\right) + \\
&+\left(\sum_{j=1}^{\infty} I_{rj,\max} Cos(j(\omega_r t + 120^0))\right) \bullet \left(\sum_{k=1}^{\infty} N_{k,s} Cos(k(\phi_s + 120^0))\right)
\end{aligned}
\tag{2.11}
$$

As it can be observed existence of the space harmonics and time harmonics can initiate significant torque harmonics over a wide range of frequencies. Therefore it is imperative to make sure that the sinusoidal distribution of the stator and rotor windings are adhered to. The time harmonics introduced by the power electronics converter in the rotor circuit can be arbitrarily minimized so they do not pose any degrading effect on the performance of the DFIG. However, the grid induced harmonics can introduce low

order harmonic currents into the stator winding, thereby creating undesirable components of the field resulting in torque pulsation.

2.1.2. Control of Active and Reactive Power in DFIG

One of the major features of the doubly fed induction generator is related to its ability in independent control of the active and reactive power. In order to compute the active and reactive power in a DFIG, it is easier to perform a change in frame of references first. Reference frame transformation, in simple terms, will replace the stator or rotor windings with a pair of fictitious coils such that the resulting magneto-motive field in the airgap remains unchanged. The rotational speed of the new fictitious windings will be chosen such that they will carry direct currents (dc), thereby simplifying the terminal computations [9] - [12]. This is a conventional method for analysis of AC electric machines with lumped parameter models. In general, a change in frame of references can be described by the following relationship:

$$f_{qd0} = K_x^y(\theta_{x-y})\, f_{abc} \tag{2.12}$$

In which $f_{qd0}, f_{abc}, K_x^y, and\ \theta_{x-y}$ represent electrical quantity of interest (i.e. voltage, current, flux, charge, etc.) in the new set of frame of references, electrical quantity of interest in the original frame of reference (i.e. actual quantities), matrix of transformation, and the angle used for transformation respectively. The new set of frame of references that are usually referred to as quadrature (*q*) and direct (*d*) and zero sequence (0) are usually positioned in the rotor, on the stator, in the airgap, or on a separate synchronous frame of references. Although rotor frame of reference is a preferred selection in the case of synchronous machines (i.e. Park transformation) the

use of synchronous frame of references for placement of the fictitious coils are normally practiced in the case of the induction machines. This requires that both stator and rotor coils to be transferred to a frame of reference whose angular position is defined by:

$$\theta = \int_0^t \omega(\varsigma) d\varsigma + \theta(0) \tag{2.13}$$

The respective transformation matrices for transferring the stator and rotor quantities to this frame of reference are given by:

$$\mathbf{K}_s = \frac{2}{3}\begin{bmatrix} \cos(\theta) & \cos(\theta - 120^0) & \cos(\theta + 120^0) \\ \sin(\theta) & \sin(\theta - 120^0) & \sin(\theta + 120^0) \\ 0.5 & 0.5 & 0.5 \end{bmatrix} \tag{2.14}$$

$$\mathbf{K}_r = \frac{2}{3}\begin{bmatrix} \cos(\beta) & \cos(\beta - 120^0) & \cos(\beta + 120^0) \\ \sin(\beta) & \sin(\beta - 120^0) & \sin(\beta + 120^0) \\ 0.5 & 0.5 & 0.5 \end{bmatrix}, \beta = \theta - \theta_r \tag{2.15}$$

Keeping in mind that the angle θ_r is defined by:

$$\omega_r = \frac{d\theta_r}{dt} \tag{2.16}$$

Once the above transformations are performed the quantities shown in figure 2.2 can be transferred into our arbitrary chosen frame of references (with an angular speed of ω). In this new set of frame of references the phase voltage equations (for the new set of fictitious coils) can be described by:

$$\begin{aligned} \mathbf{v}_{qd0s} &= \mathbf{r_s}\mathbf{i}_{qd0s} + \omega\boldsymbol{\lambda}_{dq0s} + \frac{d\boldsymbol{\lambda}_{qd0s}}{dt} \\ \mathbf{v}'_{qd0r} &= \mathbf{r}'_r\,\mathbf{i}'_{qd0r} + (\omega - \omega_r)\boldsymbol{\lambda}'_{dq0r} + \frac{d\boldsymbol{\lambda}'_{qd0r}}{dt} \end{aligned} \tag{2.17}$$

One may note that the turn ratio between the rotor and stator windings have been taken into account in this transformation, i.e.:

$$\begin{aligned}
\mathbf{i}'_{abcr} &= \frac{N_r}{N_s}\mathbf{i}_{abcr} \\
\mathbf{v}'_{abcr} &= \frac{N_s}{N_r}\mathbf{v}_{abcr} \\
\boldsymbol{\lambda}'_{abcr} &= \frac{N_s}{N_r}\boldsymbol{\lambda}_{abcr}
\end{aligned} \tag{2.18}$$

Also it is important to note the following definition when using (2.17):

$$\begin{aligned}
(\boldsymbol{\lambda}_{dqs})^T &= \begin{bmatrix} \lambda_{ds} & -\lambda_{qs} & 0 \end{bmatrix} \\
(\boldsymbol{\lambda}'_{dqr})^T &= \begin{bmatrix} \lambda'_{dr} & -\lambda'_{qr} & 0 \end{bmatrix}
\end{aligned} \tag{2.19}$$

After performing mathematical simplifications the new set of phase voltage equations for transferred stator and rotor circuits will be given by:

$$\begin{aligned}
v_{qs} &= r_s i_{qs} + \omega\lambda_{ds} + \frac{d\lambda_{qs}}{dt} \\
v_{ds} &= r_s i_{ds} - \omega\lambda_{qs} + \frac{d\lambda_{ds}}{dt} \\
v_{0s} &= r_s i_{0s} + \frac{d\lambda_{0s}}{dt} \\
v'_{qr} &= r'_r i'_{qr} + (\omega - \omega_r)\lambda'_{dr} + \frac{d\lambda'_{qr}}{dt} \\
v'_{dr} &= r'_r i'_{dr} - (\omega - \omega_r)\lambda'_{qr} + \frac{d\lambda'_{dr}}{dt} \\
v'_{0r} &= r'_r i_{0r} + \frac{d\lambda'_{0r}}{dt}
\end{aligned} \tag{2.20}$$

Where $r_s, and\ r'_r$ represent the stator coil resistance and transferred rotor resistance values respectively. The transferred flux linkages are described by the following expressions:

$$
\begin{aligned}
\lambda_{qs} &= L_{ls} i_{qs} + L_M (i_{qs} + i'_{qr}) \\
\lambda_{ds} &= L_{ls} i_{ds} + L_M (i_{ds} + i'_{dr}) \\
\lambda_{0s} &= L_{ls} i_{0s} \\
\lambda'_{qr} &= L'_{lr} i'_{qr} + L_M (i_{qs} + i'_{qr}) \\
\lambda'_{dr} &= L'_{lr} i'_{ds} + L_M (i_{ds} + i'_{dr}) \\
\lambda_{0r} &= L'_{lr} i_{0r}
\end{aligned}
\tag{2.21}
$$

Where $L'_{lr}, L_{ls}, and\ L_M$ represent transferred rotor leakage inductance, stator leakage inductance and magnetizing inductance respectively. Under steady state and balanced sinusoidal conditions, the active and reactive powers at stator terminals can be expressed as:

$$
\begin{aligned}
P_e &= \frac{3}{2}(V_{qs} I_{qs} + V_{ds} I_{ds}) \\
Q_e &= \frac{3}{2}(V_{qs} I_{ds} - V_{ds} I_{qs})
\end{aligned}
\tag{2.22}
$$

The above equation can be further simplified if the arbitrary chosen frequency of the frame of reference (i.e. ω) is being fixed at synchronous frequency (ω_e) such that:

$$
\begin{aligned}
P_e &= \frac{3}{2} \frac{\omega_e L_M}{(L_{ls} + L_M)} \lambda_s I^e_{qr} \\
Q_e &= -\frac{3}{2} \frac{\omega_e}{(L_{ls} + L_M)} \lambda_s (\lambda_s - L_M I^e_{dr})
\end{aligned}
\tag{2.23}
$$

This equation shows that by proper control of the components of the rotor current an independent control of active and reactive power at stator terminals of a DFIG is possible. These equations, however, are subject to change in the presence of voltage unbalance and harmonics [13]-[42].

2.2 Power Electronic Control for DFIG

To implement the required functionalities of a doubly fed induction generator under variable speed mode of operation, the power electronic conditioner that supplies the rotor circuit need to provide modulation in the frequency as well as in magnitude of the injected currents. The circuit shown in figure 2.3 illustrates the basic elements and circuitry used to accomplish this task.

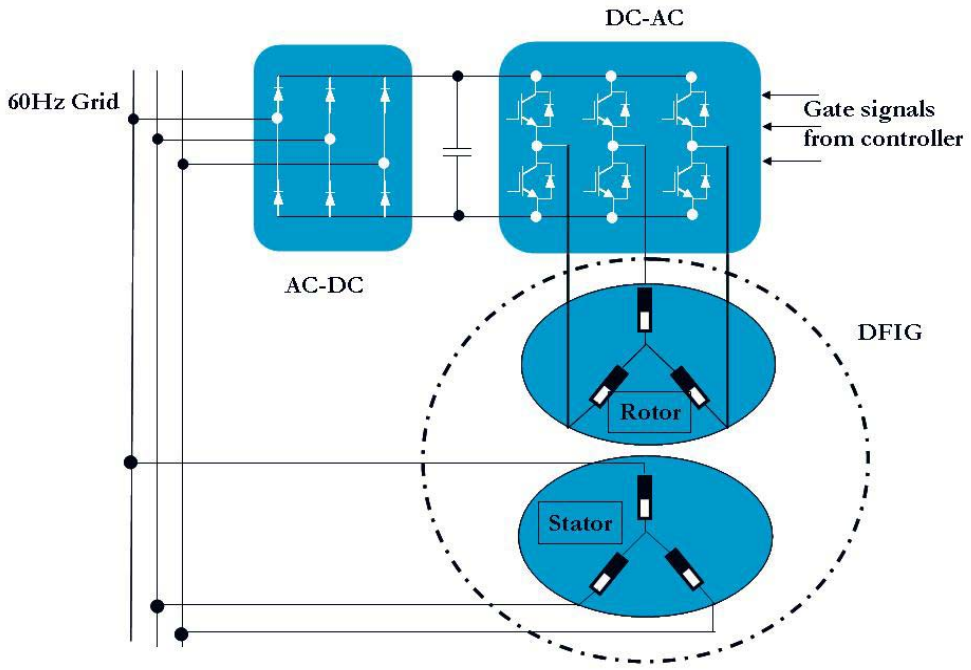

Figure 2.3 Power electronic converter used for control of the DFIG

The power electronic converter comprises of two sections, the front end rectifier that converts a 60Hz grid voltage into a rectified dc voltage and a three phase dc-ac inverter to generate the desired rotor currents. The front end rectifier can be a controlled rectifier so it can compensate the possible transient voltage swells. However, this will

add to the cost and complexity of the system. The dc link capacitor is primarily used to stabilize the voltage fluctuations. However, partial adjustment of the modulation index in the converter can compensate for possible voltage ripples that have not been taken care of by the capacitor bank. It must be noted that protection devices and measurement equipments such as dc link voltage sensor, dc link current sensor, and phase current sensors are not shown in figure 2.3. The usual devices used for low to medium level grid voltages are the IGBT (Insulated Gate Bipolar Transistors) devices. IGBT is a hybrid device that has the benefit of simplicity in electronic commutation (migrated from MOSFET) while capable of handling high levels of current and voltage in a single unit. Commercial samples for IGBT modules with capability of up to 6.5 kV and 0.6kA are readily available. These values correspond to power rating of 3.9MW of power in a single device which indicates that the required power electronics switches are already in the market for the range of power targeted in DFIG. Keeping in mind that electric machines tend to be current intensive devices (due to inherent challenges of insulation in limited stator slots) parallel operation of IGBT and Diodes can allow for even higher levels of power. The control of the devices can be done using digital signal controllers that usually used to control medium power electric drives. The control electronics, signal conditioning for the sensors and interface circuitry present a negligible part of the overall cost and space. In terms of control strategy for the three phase inverter there exist two possible options. These techniques are the Pulse Width Modulation (PWM) and hysteresis current control. In either case the three phase converter will act as a current source inverter (CSI). One may note that the switching frequency in PWM will

be a fixed value (i.e. carrier frequency) while the switching frequency in a hysteresis controller will follow a varying pattern. However, some articles suggest that hystersis control of the current exhibits higher levels of robustness. The main task of the CSI in this application is to compensate the induced voltage in the rotor circuit due to stator rotating field and enforce the desired current waveform.

2.3. Finite Element Model of DFIG

Finite element analysis (FEA) is a frequently used method for analysis of electromechanical converters. As a numerical analysis method, FEA allows for including any practical material, external excitation (voltage driven or current driven), inclusion of motion, and nonlinear effects such as magnetic saturation and eddy current effects. Due to the inherent symmetry of a conventional doubly fed induction machine and negligible end coil effects, a two dimensional analysis will be sufficient. It is also important to note that effects of magnetic saturation are not included in our model as existence of saturation is not allowed under normal modes of operation in power grid. In the absence of an experimental DFIG, a FE model of a targeted wound rotor induction machine (hereafter referred to as test machine) has been used in this analysis. Geometrical specification of the test machine can be found in Appendix-A. Figure 2.4 illustrates the distribution of the flux density in an arbitrary instant of time. As can be seen, the formation of four magnetic poles is apparent from this figure. The level of magnetic flux density confirms the absence of saturation. It is important to note that in order to obtain accurate results, the triangular mesh elements assigned to the airgap should have an aspect ratio close to one. A large aspect ratio between the sides of a

triangular element will result in accurate computation of the flux density and hence the electromagnetic torque. This model will be used in the remainder of the present dissertation for comparison purposes.

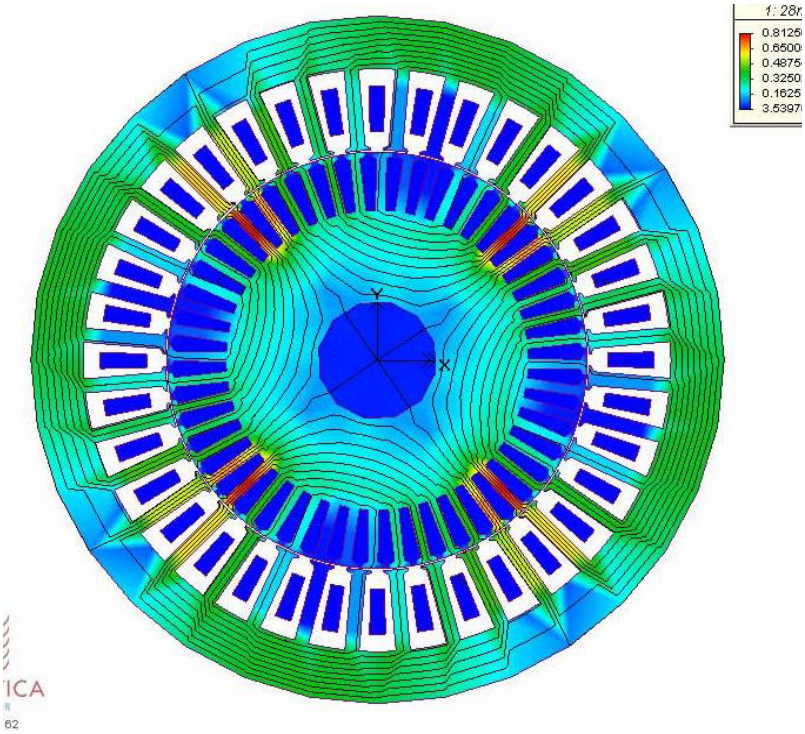

Figure 2.4 Distribution of the flux density in the test machine at an arbitrary point of Time

CHAPTER 3

EFFECTS OF UNBALANCE AND HARMONICS ON DFIG

Widespread usage of nonlinear and power electronic-based loads over the past two decades has profoundly influenced the concept of power quality. Once defined simply by the frequency, magnitude of voltage, and uninterrupted supply, the power quality is today identified by a range of new criterions that can potentially impact the operation of the sensitive loads such as electronic appliances. Table 1 shows some of these effects along with their definitions. Among all possibilities, sustained voltage harmonics and voltage unbalances can influence the operation, efficiency, and reliability of the power by a significant measure and as such deserve due attention. These effects can also alter and deteriorate the performance of distributed generator units like wind generators as these generators may to be installed in rural or residential areas with small inertia. At any rate penetration of system unbalance and harmonics is a growing concern which needs to be addressed. In this chapter, the origins of voltage unbalance and voltage harmonics will be addressed. Next, the impact of these effects on the performance of the doubly fed induction generators will be discussed.

Table 3.1 Power system electromagnetic phenomena (Cooper Industries)

Categories	Typical Spectral Content	Typical Duration	Typical Voltage Magnitude
Transients			
Impulsive			
Nanosecond	5-ns rise	<50 ns	
Microsecond	1-μs rise	50 ns–1 ms	
Millisecond	0.1-ms rise	>1 ms	
Oscillatory			
Low frequency	<5 kHz	0.3–50 ms	0–4 pu
Medium frequency	5–500 kHz	20 μs	0–8 pu
High frequency	0.5–5 MHz	5 μs	0–4 pu
Short-duration variations			
Instantaneous			
Interruption		0.50–30 cycles	<0.1 pu
Sag (dip)		0.50–30 cycles	0.1–0.9 pu
Swell		0.50–30 cycles	1.1–1.8 pu
Momentary			
Interruption		30 cycles–3 s	<0.1 pu
Sag (dip)		30 cycles–3 s	0.1–0.9 pu
Swell		30 cycles–3 s	1.1–1.8 pu
Temporary			
Interruption		3 s–1 min	<0.1 pu
Sag (dip)		3 s–1 min	0.1–0.9 pu
Swell		3 s–1 min	1.1–1.8 pu
Long-duration variations			
Interruption (sustained)		>1 min	0.0 pu
Undervoltages		>1 min	0.8–0.9 pu
Overvoltages		>1 min	1.1–1.2 pu
Waveform distortion			
dc offset		Steady state	0–0.1 %
Harmonics	0–100th harmonic	Steady state	0–20 %
Interharmonics	0–6 kHz	Steady state	0–2 %
Notching		Steady state	
Noise	Broadband	Steady state	0–1 %
Voltage fluctuations	<25 Hz	Intermittent	0.1–7 %
Voltage unbalance			0.5–2 %
Power frequency variations		< 10 s	

3.1 Origins of Voltage Unbalance and Harmonics in Electric Power Grid

System unbalance and harmonics are mainly generated in distribution systems when single phase consumers contribute greatly to the problem by employing a growing number of harmonic generating appliances (i.e. personal computers, electronic and digital appliances, etc.). However, one may note that transmission grid can also contribute to the problem during sustained overvoltages (saturation of power transformers) or asymmetric short circuit faults. Industrial consumers, over the past few decades have also contributed greatly to the problem by incorporating adjustable speed actuators that are controlled by power electronics converters, not to mention the nonlinear loads such as induction furnaces etc. The outlook for the future does not look any different as mass integration of plug-in hybrid vehicles (Vehicle to Grid interaction) and more digital and IT-enhanced home/industry appliances will be at hand. These trends suggest that new regulations for harmonic generating consumers will be necessary in the near future as they not only disturb the operation of the system, but also introduce additional losses hence undermining the efficiency among other implications. In this section we will address the sources and general implications of the harmonics and system unbalanced.

3.1.1 Voltage Unbalance and Symmetrical Components

A balanced three phase system of voltages is defined as a set of sinusoidal voltages with the same frequency and amplitude while their phase angle is shifted in clockwise direction by 120 degrees, i.e.:

$$\begin{aligned} V_a(t) &= \sqrt{2}V_{rms}Cos(\omega t) \\ V_b(t) &= \sqrt{2}V_{rms}Cos(\omega t - 120^0) \\ V_c(t) &= \sqrt{2}V_{rms}Cos(\omega t - 240^0) \end{aligned} \tag{3.1}$$

For steady state sinusoidal conditions, it is practical to only use the information related to magnitude and phase angle as presented in phasor notation:

$$\begin{aligned} \mathbf{V}_a &= V_{rms}\angle 0 \\ \mathbf{V}_b &= V_{rms}\angle -120^0 \\ \mathbf{V}_c &= V_{rms}\angle -240^0 \end{aligned} \tag{3.2}$$

One can prove that the sum of three balanced voltages would be zero, i.e.:

$$\mathbf{V}_a + \mathbf{V}_b + \mathbf{V}_c = V_{rms}(1\angle 0 + 1\angle -120^0 + 1\angle -240^0) = 0 \tag{3.3}$$

Any deviation from the above definition will constitute an unbalanced condition, although assuming sinusoidal waveforms at the same frequency usually any difference in magnitude or deviation from the designated phase angles is normally referred to as unbalanced. It must be mentioned that difference between the magnitude of the phase voltages is the most frequently occurring form of unbalanced under normal mode of operation and change in the phase normally occurs under faulty condition. Using the symmetrical component method one can convert an unbalanced set of voltages into a linear combination of (1) positive sequence voltages, (2) negative sequence voltages, and (3) zero sequence voltages. The positive and negative sequence

voltages represent two balanced systems in which the order of rotation between various phasors representing the phase voltages has been reversed. This means:

$$\begin{aligned} \mathbf{V}_a^{+} &= V^{+}\angle 0 \\ \mathbf{V}_b^{+} &= V^{+}\angle -120^0 \\ \mathbf{V}_c^{+} &= V^{+}\angle -240^0 \end{aligned} \tag{3.4}$$

$$\begin{aligned} \mathbf{V}_a^{-} &= V^{-}\angle 0 \\ \mathbf{V}_b^{-} &= V^{-}\angle 120^0 \\ \mathbf{V}_c^{-} &= V^{-}\angle 240^0 \end{aligned} \tag{3.5}$$

Where $V^{+}, and\ V^{-}$ represent the root mean square value of the positive and negative sequence voltages respectively. The zero sequence voltages are denoted by a set of voltages that have the same magnitude and the same phase angle. This means:

$$\begin{aligned} \mathbf{V}_a^{0} &= V^{+}\angle \phi \\ \mathbf{V}_b^{0} &= V^{+}\angle \phi \\ \mathbf{V}_c^{0} &= V^{+}\angle \phi \end{aligned} \tag{3.6}$$

In which ϕ represent an arbitrary chosen phase angle. The symmetrical component decomposition can be mathematically expressed as:

$$\mathbf{V}_{abc} = \mathbf{V}_{abc}^{+} + \mathbf{V}_{abc}^{-} + \mathbf{V}_{abc}^{0} \tag{3.7}$$

Figure 3.1 illustrates the above decompositions. It must be noted that similar transformation can be applied to other quantities such as current, flux, and charge.

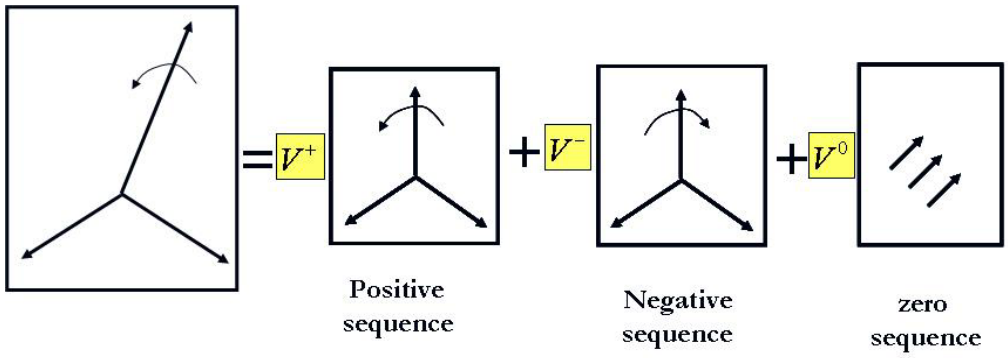

Figure 3.1 Decomposition of the unbalanced voltages into the symmetrical components

In order to find the magnitude of the positive, negative, and zero sequence voltages, the following transformation will be used:

$$\begin{bmatrix} \mathbf{V}^+ \\ \mathbf{V}^- \\ \mathbf{V}^0 \end{bmatrix} = \frac{1}{3}\begin{bmatrix} 1 & \alpha & \alpha^2 \\ 1 & \alpha^2 & \alpha \\ 1 & 1 & 1 \end{bmatrix}\begin{bmatrix} \mathbf{V}_a \\ \mathbf{V}_b \\ \mathbf{V}_c \end{bmatrix} \tag{3.8}$$

Where $\alpha = 1\angle 120^0$. Once the voltages or currents are decomposed into their symmetrical components, one can use the superposition theory to compute the individual response of the grid to each set of inputs. Since the positive and negative sequence form a balanced system, a single phase equivalent circuit can be used to solve the system. It must be noted that certain circuit configurations would not allow the flow of the zero sequence components. For instance, an ungrounded Wye connection does not allow the flow of zero sequence currents. It must be noted that , third, sixth, ninth harmonics constitute a zero sequence system and as such are not permitted to exist in line current where the ground connection is blocked.

3.1.2 Sources of Voltage Unbalance

Voltage unbalance can occur due to the following reasons:

- Unbalanced loading of the three phase systems in residential area (single phase users).This is more related to distribution networks.
- Asymmetrical faults such as single phase to ground fault.
- Unbalanced operation of the synchronous generators in power plants, due to eccentricity, etc.
- Large unbalanced industrial loads (such as multi-megawatts induction motors used in cement and mining industry) under single phase or two phase fault conditions.
- Asymmetric design practices in power transformers, transmission lines, etc.

Once the unbalance occurs, various parts of the system will face an unbalanced distribution of the load and hence non-uniform heating may occur which can potentially lead to the failure of the overloaded element. In recent years, there has been an increasing level of unbalanced due to increasing level of consumption in residential areas and aging of the main power generation, transmission, and distribution. As indicated in Table 3.1, the sustained unbalanced voltages should not exceed 2% of the nominal value. However, in the weak networks as seen in rural areas and heavily populated residential areas, the voltage unbalance can reach 10% for short durations of time (tens of seconds). This excessive level of unbalance, if occurring frequently, can be destructive to operation of many equipments. In the face of recent trends for integration of renewable wind energy generators, which are usually in distance from high inertia

power grid, the effects of system unbalance on the operation of these renewable sources should be investigated.

3.1.3 Sources of Harmonics

Harmonics are defined as sinusoidal voltage or currents having frequencies that are integer multiples of the power frequency which the system is designed to operate (fundamental). Most harmonic-producing devices are bilateral devices; that is, they behave the same in response to both positive and negative half-cycles of the sinusoidal signal. This produces only odd harmonics; that is, the odd multiples of the fundamental frequency (full wave rectifier). However, some equipments may produce both even and odd harmonics in their currents. These include half wave rectifier, transformer inrush current during magnetization, and arc furnaces during unstable arc periods. In general, the nonlinear nature of the load will result in significant current harmonics. These current harmonics are either filtered locally, or they will be provided by the power grid (i.e. generators). As long as the magnitude of these currents are limited, they will not disturb the other customers. As shown in figure 3.2 the harmonics will flow in the path with least impedance and that is the main feeder line and other laterals will not be influenced. However, one may note that while harmonics flow in a line they will induce a component of the voltage given by:

$$\Delta V = Z_k(k\omega) I_k(k\omega) \tag{3.9}$$

If the magnitude of the harmonic currents is sufficiently large, then the above voltage drop will be large enough to introduce a measurable harmonics in the line voltage.

Remembering that all other customers in neighboring laterals are connected in parallel to the grid, the voltage harmonics will find its way to their appliances.

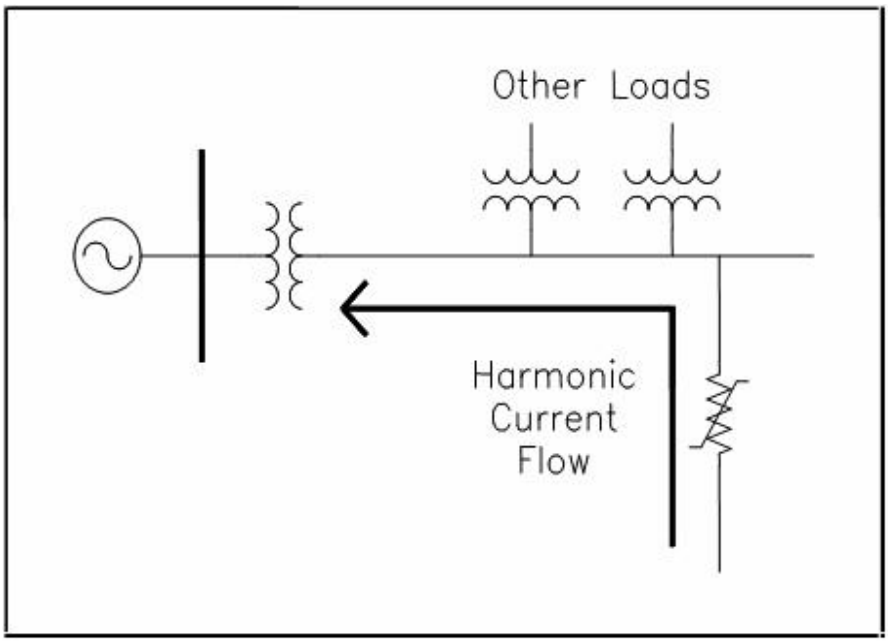

Figure 3.2 Flow of the harmonic current to the source

The main harmonic generating components in the grid are:

- Ferromagnetic Devices
- Arcing Devices
- Electronic Power Converters

Ferromagnetic devices such as power transformers and large induction motors can be the source of harmonics if subject to overvoltages. Over-voltage in the system can result in an increased level of magnetizing current in these equipments, thereby causing magnetic saturation. Magnetic saturation in turn will result in flat topped voltage waveforms that are viewed as a source of harmonics. Since these devices will create voltage harmonics, their impact on all consumers will be significant.

Arcing devices such as arc lamps and arcing furnaces present very nonlinear characteristics that will result in significant current harmonics. Recent criticisms of low efficiency in incandescent lamps and promotion of the arcing lamps will probably result in an increased level of harmonics in the future.

Electronic Power Converters encompass a wide variety of devices that basically, switch the line voltage at various times using semiconductors. Some commonly used power converters can be found in adjustable speed motor drives, rectifiers, uninterruptible power supplies to name a few. They can generate all sorts of harmonics many of which are represented in the "1/n" series form. Figure 3.3 shows the current waveform in a six step rectifier along with its frequency spectrum.

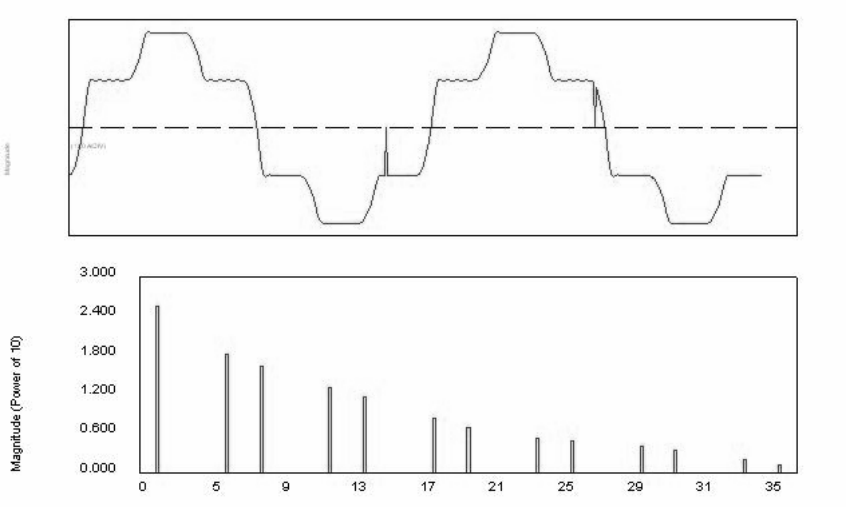

Figure 3.3 Simulated phase current waveform in a six-step, three phase converter(the spikes seen here are due to switching glitches which are caused by malfunction of the gating logic)

Some of the typical consequences of the voltage harmonics include:

- Overheating of motors
- Transformer heating

- Mis-operation of timing circuits
- Communication interference
- Failure of capacitors (resonance)
- Capacitor fuse blowing
- Increased line losses
- Meter errors (normally in users favor)

It must be noted that current harmonics only affect the element which they pass through whereas voltage harmonics will influence all customers and equipments. Tables 3.2 and 3.3 show the requirements imposed on distribution systems in regards to voltage and current harmonic contents.

Table 3.2 Requirement for voltage harmonic levels (IEEE-Std 519-1992)

Bus Voltage at PCC	Individual Voltage Distortion (%)	Total Voltage Distortion THD (%)
69 kV and Below	3.0	5.0
69.001 kV to 161 kV	1.5	2.5
161.001 kV and above	1.0	1.5

NOTE: High-voltage systems can have up to 2.0% THD where the cause is an HVDC terminal that will attenuate by the time it is tapped for a user.

Table 3.3 Requirement for current harmonic level (IEEE Std, 519-1992)

Maximum Harmonic Current Distortion in Percent of I_L

Individual Harmonic Order (Odd Harmonics)

I_{SC}/I_L	<11	11≤h<17	17≤h<23	23≤h<35	35≤h	TDD
<20*	4.0	2.0	1.5	0.6	0.3	5.0
20<50	7.0	3.5	2.5	1.0	0.5	8.0
50<100	10.0	4.5	4.0	1.5	0.7	12.0
100<1000	12.0	5.5	5.0	2.0	1.0	15.0
>1000	15.0	7.0	6.0	2.5	1.4	20.0

Even harmonics are limited to 25% of the odd harmonic limits above.

Current distortions that result in a dc offset, e.g. half-wave converters, are not allowed.

* All power generation equipment is limited to these values of current distortion, regardless of actual I_{SC}/I_L.

where

3.2. Impact of System Unbalance on the Performance of DFIG

Voltage unbalance can result in undesired components of magneto-motive force in the airgap of DFIG (similar cases can happen in PM or singly fed induction generators). In particular, existence of system unbalance in the magnitude of the stator currents can originate a clockwise and a counter clockwise field component in the airgap of the DFIG. Assuming a sinusoidal distribution of the stator winding, the resulting magneto motive force in the presence of the unbalanced stator currents is given by:

$$MMF_s = \frac{N_S}{2}\sqrt{2}\begin{bmatrix}\left(\frac{I_A+I_B+I_C}{2}\right)Cos(\omega_e t-\phi_s)+\\ \left(\frac{2I_A-I_B-I_C}{4}\right)Cos(\omega_e t+\phi_s)+\\ \frac{\sqrt{3}}{4}(I_B-I_C)Sin(\omega_e t+\phi_s)\end{bmatrix} \tag{3.10}$$

Where $\omega_e, I_A, I_B, I_C, \phi_S, N_S$ represent stator electrical frequency, magnitudes of phases A, B, and C currents, displacements on the stator, and number of total conductors per

phase respectively. As can be noted, intuitively, from (3.10), the clockwise component of the magneto-motive force will rotate opposite to the rotor field. Since both these two fields rotate at the synchronous speed in the airgap, their relative angular speed will reach $2\omega_e$ and as such one can expect an undulating component of the electromagnetic torque with a $2\omega_e$ frequency. This has been graphically shown in figure 3.4.

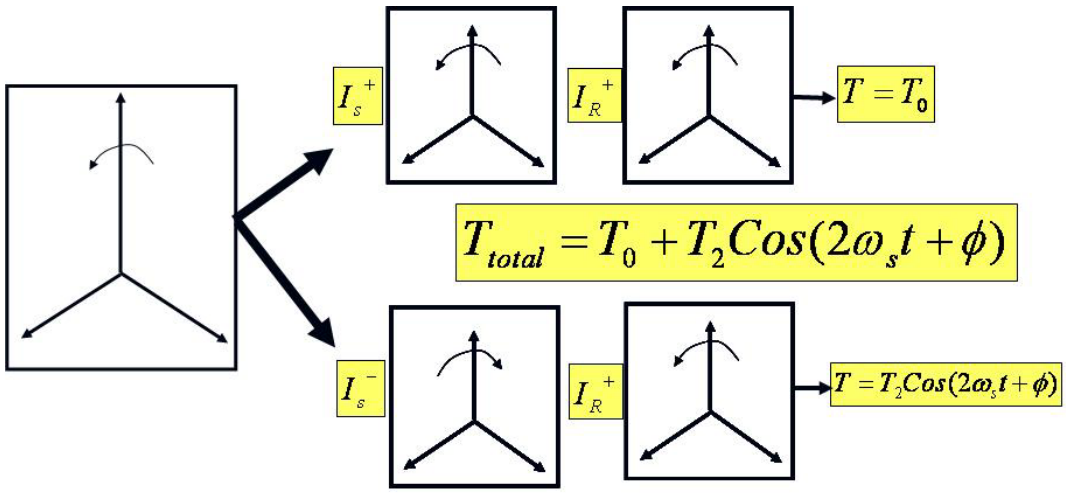

Figure 3.4 Decomposition of the electromagnetic torque in the presence of unbalance in stator current magnitudes

The low frequency (i.e. 120Hz) torque pulsation due to system unbalance can be a source of torsional vibration. One may note that the mechanical natural frequencies of the wind towers are inversely proportional to their size. As the size of these turbines increase, it is expected to reach lower resonance frequencies. This means that the odds for reaching a destructive mechanical resonance will increase as larger wind turbines with longer blades are introduced to the market. Therefore it is important to identify the

source of these torque pulsations and try to eliminate/mitigate them. Equation (3.11) gives an approximate formula for estimation of first natural frequency of a two blade rotor. As can be observed the natural frequency is inversely proportional to the mass and radius of the rotor blade.

$$\omega_n \approx \sqrt{\frac{EI}{MR^4}} \tag{3.11}$$

It must be noted that the unbalanced currents can occur in magnitude, phase angle or both. Also, if the configuration permits, zero sequence currents can flow in the stator windings. The zero sequence currents do not contribute to the magneto motive force and only increase the copper losses. In order to detect the unbalanced conditions, there are two opportunities. Figure 3.5 illustrates a diagram of the DFIG. The unbalanced currents can be identified by real time measurement of the stator currents. In the second method, and with an open circuited rotor terminals, one can measure the induced voltages in the rotor. Since an open circuited rotor acts as a transformer, the induced voltages in the rotor (secondary) will reflect the distribution of the primary voltages (stator, or the grid) and therefore one can use this information to detect possible unbalances.

One may note that unless in the presence of a catastrophic failure such as short circuit, a significant difference between the phase angles of the three phase stator voltages is not expected. Therefore in this dissertation, the effects of unbalanced are only modeled by changing magnitude. Furthermore, since the focus of the study is towards destructive effects of torque pulsation on the system, without a loss of generality, the impact of the

zero sequence currents can be omitted. It is acknowledged that zero sequence currents will increase the generator copper losses and hence will reduce the efficiency.

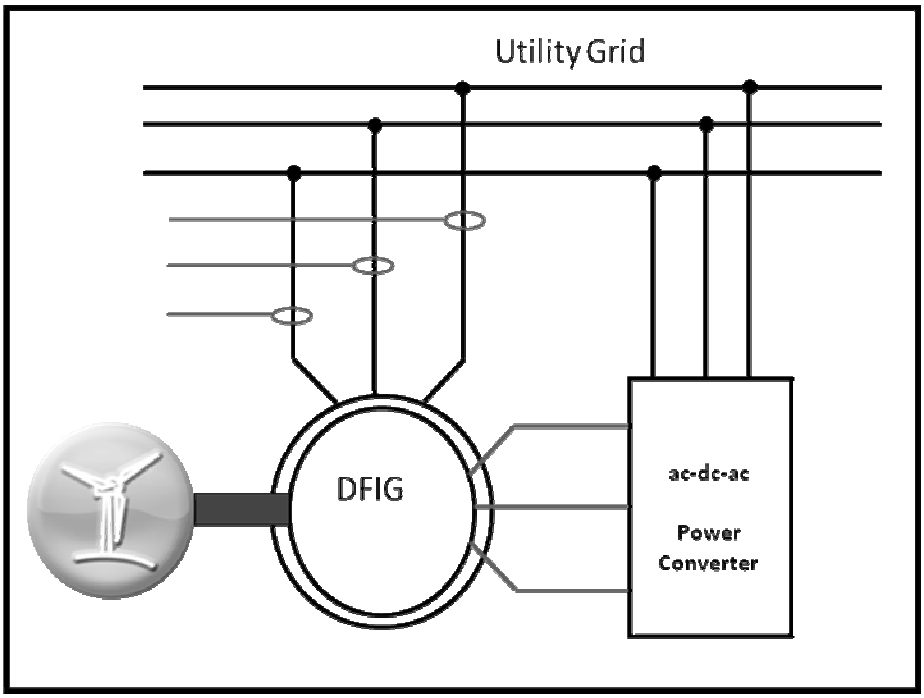

Figure 3.5 General block diagram of the DFIG

It must be noted that unbalanced distribution of the currents in the stator will not only create an unbalanced distribution of the copper losses but also will influence the core losses. Figure 3.6 illustrates the distribution of the flux density in the stator of our targeted DFIG under balanced and unbalanced stator excitation. One can notably identify an asymmetric distribution of the flux density in the stator. This is yet another aspect of the unbalanced operation of the DFIG which may complicate the cooling and thermal management of these generators.

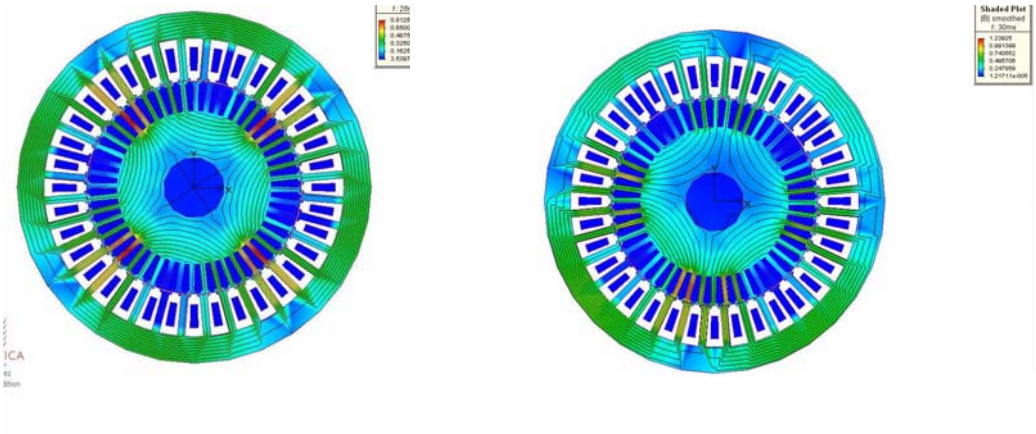

(a) (b)

Figure 3.6 Distribution of the flux density in (a) balanced and (b) unbalanced stator excitation

To illustrate the impact of the stator current unbalance, the following systems of excitation has been applied to the FE model of the targeted DFIG.

Case 1: Balanced condition:

$$\begin{aligned} i_{as} &= Cos(120\pi t)[p.u] & i_{ar} &= Sin(120\pi t)[p.u] \\ i_{bs} &= Cos(120\pi t - 120^0)[p.u] & i_{br} &= Sin(120\pi t - 120^0)[p.u] \\ i_{cs} &= Cos(120\pi t + 120^0)[p.u] & i_{cr} &= Sin(120\pi t + 120^0)[p.u] \end{aligned} \tag{3.12}$$

Case 2: Unbalanced condition (10% in magnitude):

$$\begin{aligned} i_{as} &= Cos(120\pi t)[p.u] & i_{ar} &= Sin(120\pi t)[p.u] \\ i_{bs} &= 0.9Cos(120\pi t - 120^0)[p.u] & i_{br} &= Sin(120\pi t - 120^0)[p.u] \\ i_{cs} &= Cos(120\pi t + 120^0)[p.u] & i_{cr} &= Sin(120\pi t + 120^0)[p.u] \end{aligned} \tag{3.13}$$

Figure 3.7 illustrates the results of the electromagnetic torque for each case. As can be seen, there exists a 120Hz component of the torque pulsation.

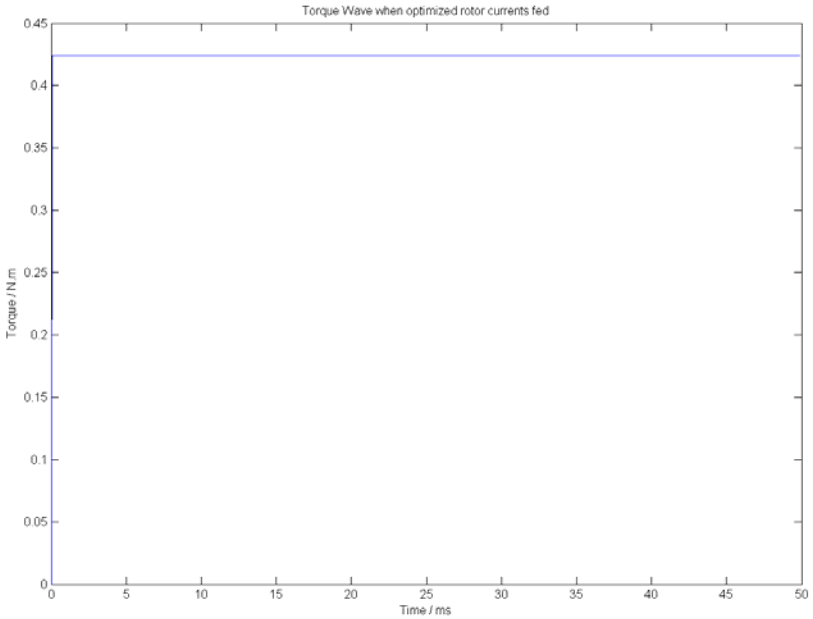

Figure 3.7 Electromagnetic torque under balanced excitation

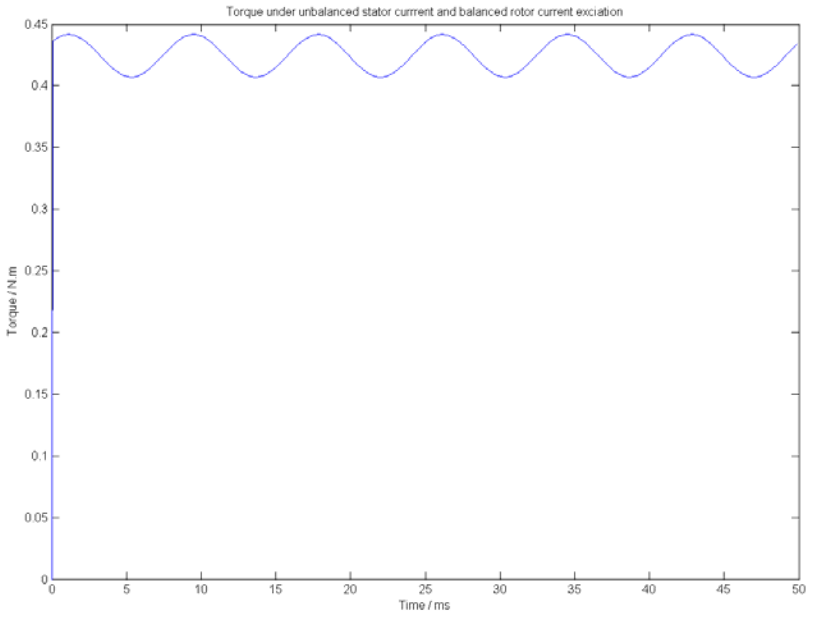

Figure 3.8 Electromagnetic torque under unbalanced excitation

3.3. Impact of System Harmonics on the Performance of DFIG

In the presence of a current harmonic the magneto-motive force resulting from the stator winding will be in the following form:

$$MMF_S = \frac{3N_S}{4}\sqrt{2}I_A Cos(k\omega_e t - \phi_s) \tag{3.14}$$

Where k represents the order of the harmonic. Existence of harmonics in the stator currents can create components of the magnetic fields that rotate at a speed other than the synchronous speed resulting in undesired torque harmonics. Therefore, by an intuitive approach and given a balanced magneto-motive force due to the rotor winding, one can expect the following:

- System harmonics will result in a torque harmonic at a frequency of $(k-1)\omega_e$.
- System harmonics along with the system harmonic will result in torque harmonics at the $0, 2\omega_e, (k-1)\omega_e$, and $(k+1)\omega_e$.

It may also note that harmonics will significantly alter the core losses as these losses are related to the frequency of excitation by:

$$P_{core} = K_h fB_m^2 + K_c (fB_m)^2 + K_e (fB_m)^{1.5} \tag{3.15}$$

Where $K_h, K_c, and\ K_e$ represent the hysteresis loss, eddy current loss, and excess loss coefficients.

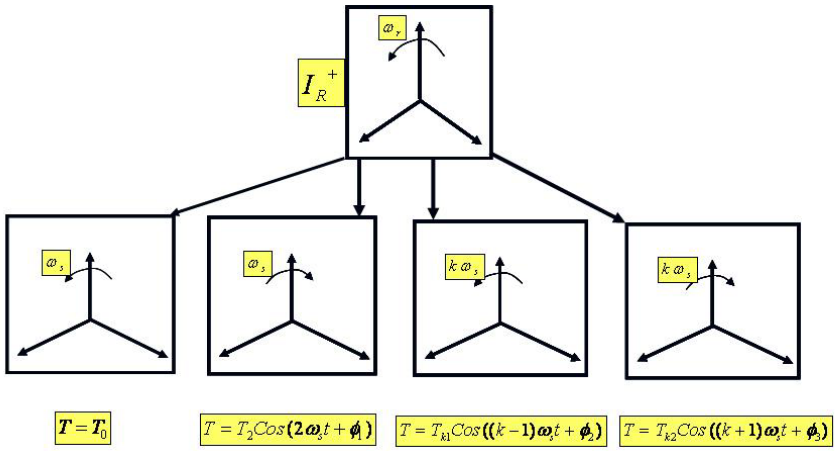

$$T_{total} = T_0 + T_2 Cos(2\omega_s t + \phi_1) + T_{k1} Cos((k-1)\omega_s t + \phi_2) + T_{k2} Cos((k+1)\omega_s t + \phi_3)$$

Figure 3.9 Creation of torque harmonics in DFIG due to grid harmonics

Figure 3.9 illustrates the generation of the torque harmonics due to the existence of the stator current harmonics. In order to validate the effects of the harmonic, a third harmonic component was injected to the stator current and the results of the torque was examined versus the healthy condition shown in figure 3.7.

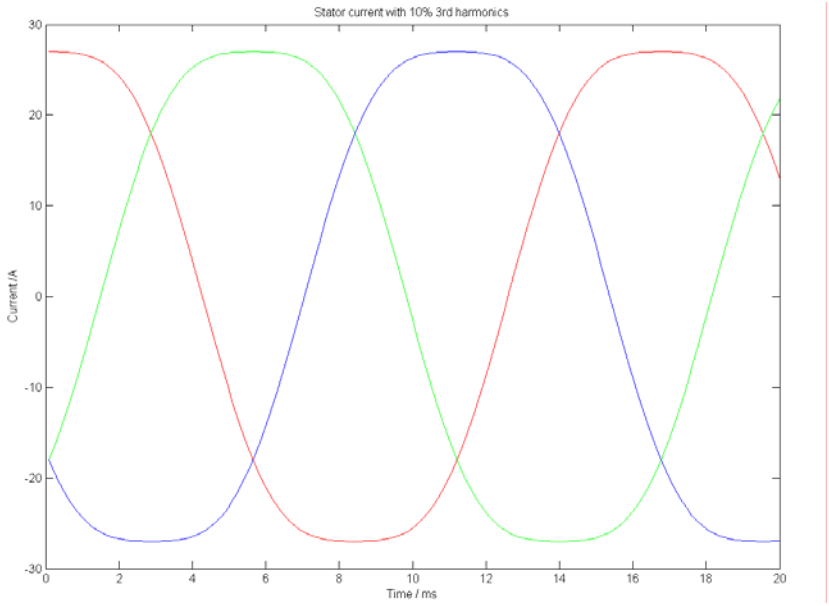

Figure 3.10 Stator currents along with the harmonics

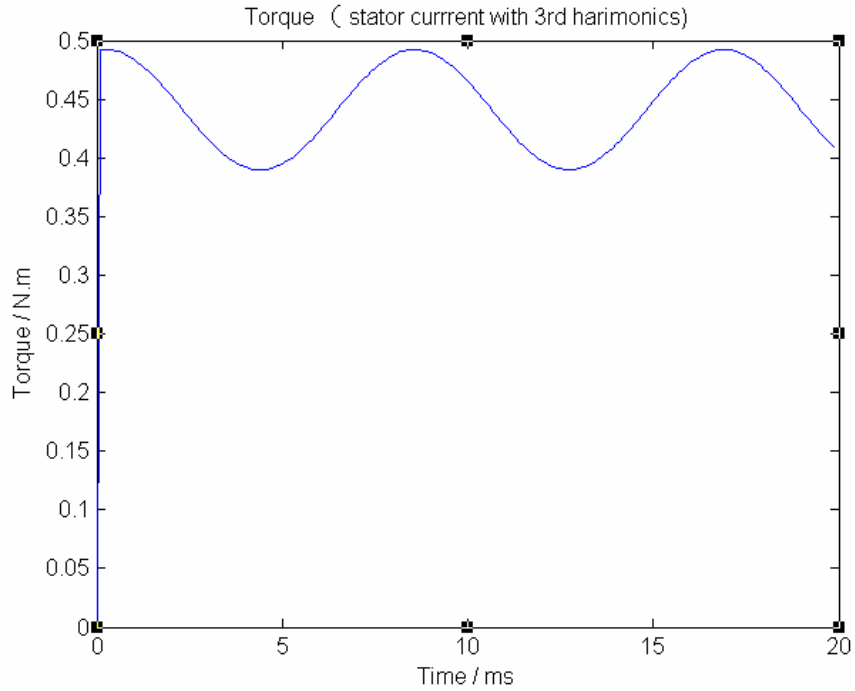

Figure 3.11 Torque pulsation due to the stator current harmonics

CHAPTER 4

FIELD RECONSTRUCTION METHOD

Finite difference (FD), finite element (FE) , and boundary elements (BA) methods have been used over the past three decades to numerically approximate the electromagnetic field within electromechanical energy converters. Within the same time frame, speed of numerical computations and efficiency of commercially available numerical packages used for implementation of these methods have witnessed significant improvements. However, given all the technological advances, Finite Element method (the flagship technique in majority of the packages) still suffers from long computational times. These deficiencies surface when iterative use of field quantities under various operational conditions are required. Performance optimization by means of varying the design quantities or supply optimization is a good example in this regard. Field reconstruction method in computation of the electromagnetic field quantities in the airgap of an unsaturated electric machine provides a significant reduction in computational time (more than two orders of magnitude) as compared to FEM. This is done by taking advantage from the periodical nature of the field solutions in the airgap of the machine. Since the majority of the magnetic energy, in an unsaturated machine, will be stored in the airgap, the accuracy of the results provided by FRM is comparable to those of FEM.

4.1 Fundamentals of FRM

Electromechanical energy converters convert energy from electrical to mechanical and vice versa, within a magnetic field. Magnetic fields are created by the virtue of a change in current density:

$$\nabla \times \vec{\mathbf{H}} = \vec{\mathbf{J}} \tag{4.1}$$

Where $\vec{\mathbf{J}}$ & $\vec{\mathbf{H}}$ represent the current density and magnetic field intensity respectively. In most apparent form, the current density may appear in the form of an electric current (free movement of electrons). The electromagnetic force will be then calculated using the following formula:

$$\vec{\mathbf{f}} = \vec{\mathbf{J}} \times \vec{\mathbf{B}} - \frac{\mathbf{1}}{\mathbf{2}}(\vec{\mathbf{H}}.\vec{\mathbf{H}})\nabla(\mu_1, \mu_2, ..., \mu_m) \tag{4.2}$$

In which $\vec{\mathbf{B}}, \mu_1, ..., \mu_m$ represent the flux density, and various permeabilities used in the composite used in the construction of the machines. Using Maxwell stress method one can compute the tangential and normal components of the electromagnetic force in the airgap using the tangential and normal components of the flux density in the airgap i.e.:

$$\begin{aligned} f_t &= \frac{1}{\mu_0} B_n B_t \\ f_n &= \frac{1}{2\mu_0}(B_n^2 - B_t^2) \end{aligned} \tag{4.3}$$

Where $\mu_0 = 4\pi \times 10^{-7} [1/H]$ represent the permeability of the air. Notably, a two dimensional problem has been assumed here. This means there exist an axial symmetry in design of the machine and three dimensional effects of the end coils are negligible.

Magnetic field in a two dimensional problem consist of a tangential and a normal component. As such in a cylindrical system of coordinates, the magnetic field can be expressed by:

$$\vec{\mathbf{H}} = H_n \vec{a}_n + H_t \vec{a}_t \tag{4.4}$$

In a linear (unsaturated) material such as air, the flux density and field intensity are related via:

$$\begin{aligned} &\vec{\mathbf{B}} = \mu \vec{\mathbf{H}} \\ &\mu = \mu_0 \mu_r \end{aligned} \tag{4.5}$$

Where μ_r denotes the relative permeability of the material. Similar to field intensity, flux density contains a normal and a tangential component, i.e.:

$$\vec{\mathbf{B}} = B_n \vec{a}_n + B_t \vec{a}_t \tag{4.6}$$

In a cylindrical electric machine, one can define a circular contour in the airgap and compute the total tangential force acting on the rotor using the following line integration:

$$F_t = \oint_C (f_t \vec{a}_t).\vec{dl} \tag{4.7}$$

To obtain the most accurate results, it is suggested to locate the circular path as far as possible from iron. That means the best choice for the contour will be a circular path that is located in the middle of the airgap. Figure 4.1 illustrates such a circular

path. By partitioning the circumference into n equal arcs, one can obtain a discretized version of the 4.7 using the local distribution of the flux density components on each segment.

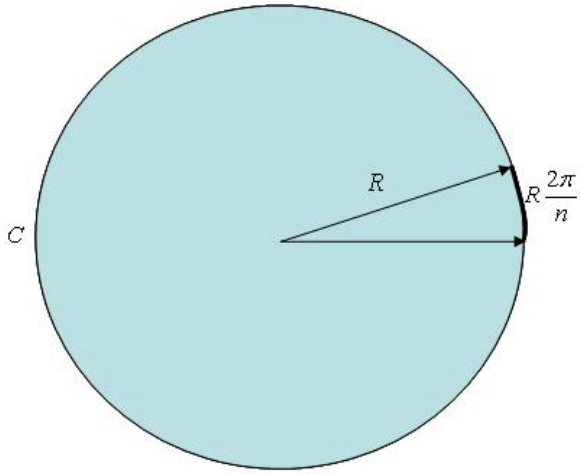

Figure 4.1 Circular path used for force calculation

$$F_t = \oint_C (f_t \vec{a}_t).\vec{dl} = \sum_{k=1}^{n} (\frac{2\pi R}{n\mu_0}) B_{n,k}.B_{t,k} = (\frac{2\pi R}{n\mu_0}) \sum_{k=1}^{n} B_{n,k}.B_{t,k} \quad (4.8)$$

Magnitude of the electromagnetic torque for the entire length of the machine (i.e. L) can be calculated using:

$$|\tau| = R|F_t| = (\frac{2\pi L R^2}{n\mu_0}) \left| \sum_{k=1}^{n} B_{n,k}.B_{t,k} \right| \quad (4.9)$$

Where R represents the radius of the circular contour (i.e. C).

4.1.1. Reconstruction of the Magnetic Field

In order to compute the local distribution of the tangential and normal components of the flux density (i.e. $B_{t,k}, B_{n,k}$) in (4.9), one can use Finite Element (FE) which is a iterative numerical method. However, examination of the magnetic field in

the airgap of the rotary electric machines indicates that there is a periodic pattern with respect to space and time. In other words, the magnetic field caused by a single conductor sufficient to reconstruct the total flux density without using redundant and time consuming FE calculations. The only necessary assumption in order to take advantage of this will be the linearity of the material. This means the magnetic saturation should not exist. However, the latter is the necessary condition for most high performance electric motors and generators. In the case of the doubly fed induction generators, this condition is very realistic as saturation in generators are not allowed by power utility companies as this may cause significant amount of harmonics. Therefore, the magnetic design and loading profile of the generators are adjusted such that magnetic saturation is avoided at all times.

In order to introduce the FRM, distribution of the magnetic field due to a single conductor carrying a dc current is shown in figure 4.2. This field has been calculated using a single magneto-static field calculation which is relatively a very quick calculation using FE method.

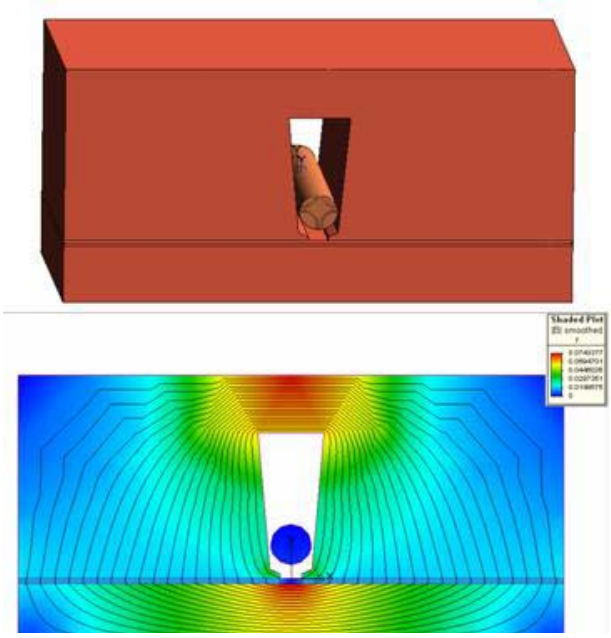

Figure 4.2 Magnetic field due to a single conductor carrying a dc current

Figure 4.3 illustrates the tangential and normal components of the flux density in the middle of the airgap. One can note that there exists an even symmetry in the tangential component of the flux density while the normal component of the flux density enjoys an odd symmetry with respect to the location of the conductor.

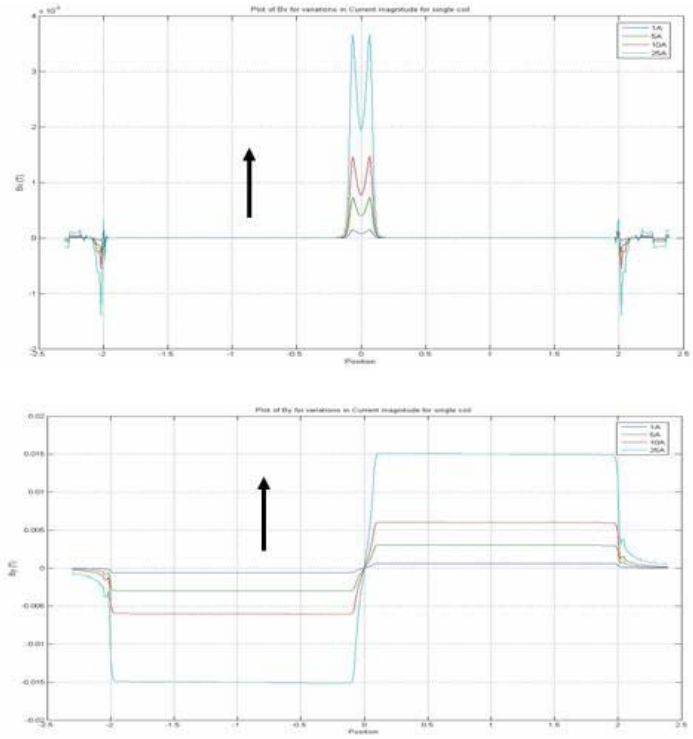

Figure 4.3 Tangential (top) and normal (bottom) components of the flux density at various current levels

One can note that the tangential and normal components of the flux density due to a 1 A current is defined as tangential and normal stator basis functions:

$$B_t\big|_{i=1A} = B_t(\phi_s) = h_t(\phi_s) \tag{4.10}$$

$$B_n\big|_{i=1A} = B_n(\phi_s) = h_n(\phi_s) \tag{4.11}$$

Where $0 \le \phi_s \le 2\pi$ represent various displacements on the circular contour. At this point if the instantaneous magnitudes of the current changes, in the absence of magnetic saturation, one can note that:

$$B_t(i, \phi_s) = ih_t(\phi_s) \tag{4.12}$$

$$B_n(i, \phi_s) = ih_n(\phi_s) \tag{4.13}$$

If the location of the conductor is shifted from $\phi_s = 0$ into an arbitrary chosen location such as $\phi_s = \phi_{s,j}$, then it can be seen that:

$$B_t(i, \phi_s) = ih_t(\phi_s - \phi_{s,j}) \tag{4.14}$$

$$B_n(i, \phi_s) = ih_n(\phi_s - \phi_{s,j}) \tag{4.15}$$

Using the superposition, the magnetic field caused by N conductors carrying currents of i_j and located at $\phi_{s,j}$, $j = 1 \cdots N$ is given by:

$$B_t(i_1, i_2, \cdots, i_j, \phi_s) = \sum_{j=1}^{N} i_j h_t(\phi_s - \phi_{s,j}) \tag{4.16}$$

$$B_n(i_1, i_2, \cdots, i_j, \phi_s) = \sum_{j=1}^{N} i_j h_n(\phi_s - \phi_{s,j}) \tag{4.17}$$

As a result the total flux density for any instant of time can be reconstructed as:

$$\vec{\mathbf{B}} = \left\{ \sum_{j=1}^{N} i_j h_t(\phi_s - \phi_{s,j}) \right\} \vec{a}_t + \left\{ \sum_{j=1}^{N} i_j h_n(\phi_s - \phi_{s,j}) \right\} \vec{a}_n \tag{4.18}$$

4.1.2. Basis Functions and their Role in FRM

A close inspection of (4.18) suggests that the tangential and normal components of the flux density follow the form of a truncated generalized Fourier series. Due to the even and odd symmetry of the tangential and normal basis functions, one can prove that:

$$\langle h_t(\phi_s), h_n(\phi_s)\rangle = \int_0^{2\pi} h_t(\phi_s) h_n(\phi_s) d\phi_s = 0 \tag{4.20}$$

The above equation suggests that with only the stator winding, it is impossible to create any tangential force [43], [44]. One may also note that due to even and odd periodic forms of the tangential and normal basis functions, they can be expanded using a trigonometric series and be stored after being calculated using a single magneto static solution of the field, i.e.:

$$\begin{aligned} h_t(\phi_s) &= \sum_{k=0}^{\infty} h_{t,k} Cos(k\phi_s) \\ h_n(\phi_s) &= \sum_{k=1}^{\infty} h_{n,k} Sin(k\phi_s) \end{aligned} \tag{4.21}$$

In development of an analytical model of the FRM, a finite number of terms will be used such that a judiciously chosen level of precision is achieved. It is also possible to store the basis functions in the form of look up table. In either case, once basis functions are calculated and properly stored, distribution of the magnetic field for any given value of the stator currents can be easily computed. It must be noted that the basis functions can also be computed for an entire phase winding as all the coils forming one phase will be carrying the same current at any given point of time. Figures 4.4 and 4.5 illustrate the tangential and normal basis functions for the phase- a of the stator in the targeted DFIG used in this study. There is an excellent match between Fourier approximation of the basis function and its actual values obtained from FE analysis.

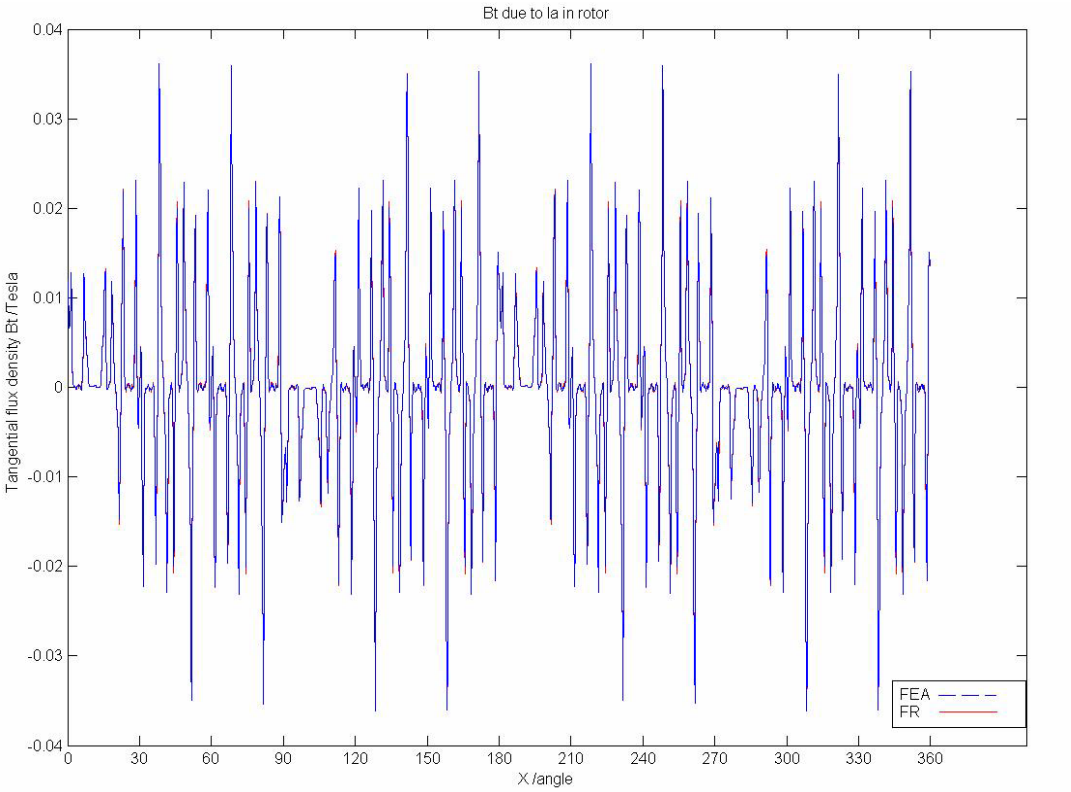

Figure 4.4 Tangential basis function of the phase-a in stator winding

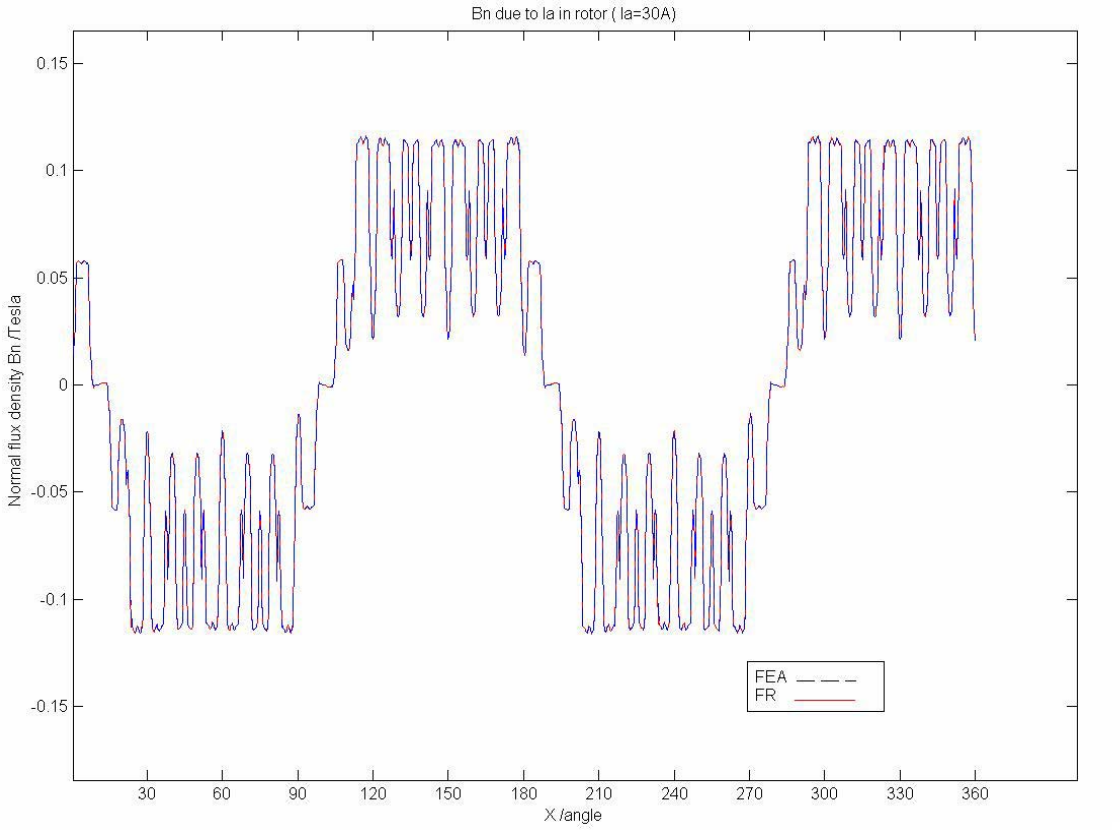

Figure 4.5 Normal basis function of the phase-a in stator winding

4.2. Application of FRM to DFIG

Doubly fed induction machines portray an ideal case for application of the FRM, as rotor and stator both contain a three phase winding. By computing the basis functions for each stator and rotor phase using two separate magneto-static field solution, one can compute their respective contributions to the tangential and normal components of the flux density in the airgap. Formulation of the field contributions from the stator and rotor windings are given below:

$$B_{t,s}(\phi_s) = h_{t,s}(\phi_s)i_{as} + h_{t,s}(\phi_s - \frac{2\pi}{3})i_{bs} + h_{t,s}(\phi_s + \frac{2\pi}{3})i_{cs} \tag{4.22}$$

$$B_{n,s}(\phi_s) = h_{n,s}(\phi_s) i_{as} + h_{n,s}(\phi_s - \frac{2\pi}{3}) i_{bs} + h_{n,s}(\phi_s + \frac{2\pi}{3}) i_{cs} \quad (4.23)$$

$$B_{t,r}(\phi_r) = h_{t,r}(\phi_r) i_{ar} + h_{t,r}(\phi_r - \frac{2\pi}{3}) i_{br} + h_{t,r}(\phi_r + \frac{2\pi}{3}) i_{cr} \quad (4.24)$$

$$B_{n,r}(\phi_r) = h_{n,r}(\phi_r) i_{ar} + h_{n,r}(\phi_r - \frac{2\pi}{3}) i_{br} + h_{n,r}(\phi_r + \frac{2\pi}{3}) i_{cr} \quad (4.25)$$

In which $h_{t,s}, h_{t,r}, h_{n,s}, h_{n,r}, \phi_s, \phi_r$ represent the tangential basis function for phase-a of the stator, tangential basis function for the phase-a of the rotor, normal basis function for the phase-a of the stator, normal basis function for the phase-a of the rotor, displacement with respect to the stator, and displacement with respect to the rotor respectively. The resulting field in the airgap will be a point-wise sum of the vectors representing the contribution of the stator and rotor fields. This is described in the following expression:

$$B_t(\phi) = B_{t,s}(\phi) + B_{t,r}(\phi) \quad (4.26)$$

$$B_n(\phi) = B_{n,s}(\phi) + B_{n,r}(\phi) \quad (4.27)$$

In which ϕ represent a displacement in the airgap. Figures 4.6 and 4.7 illustrate the resulting normal and tangential components of the flux density due to a balanced excitation of the stator and rotor windings in our targeted DFIG at one arbitrary chosen point of time. It must be noted that once the FRM model is established, the time stepping in updating the position of the rotor as well as currents in stator and rotor circuit can be done in a negligible amount of time and hence the entire computation time is related to the necessary time for computation of (4.22)-(4.27). As can be seen,

results obtained from the FRM are in good agreement with those obtained using the FE analysis.

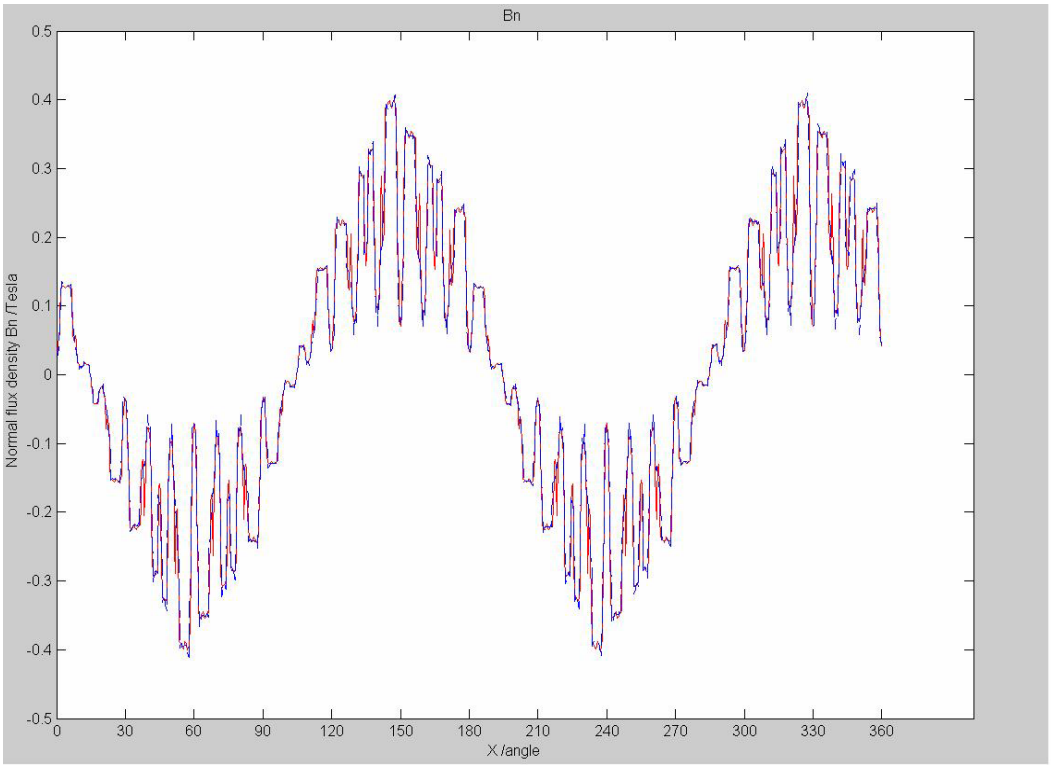

Figure 4.6 Normal component of the flux density in the airgap of the targeted DFIG

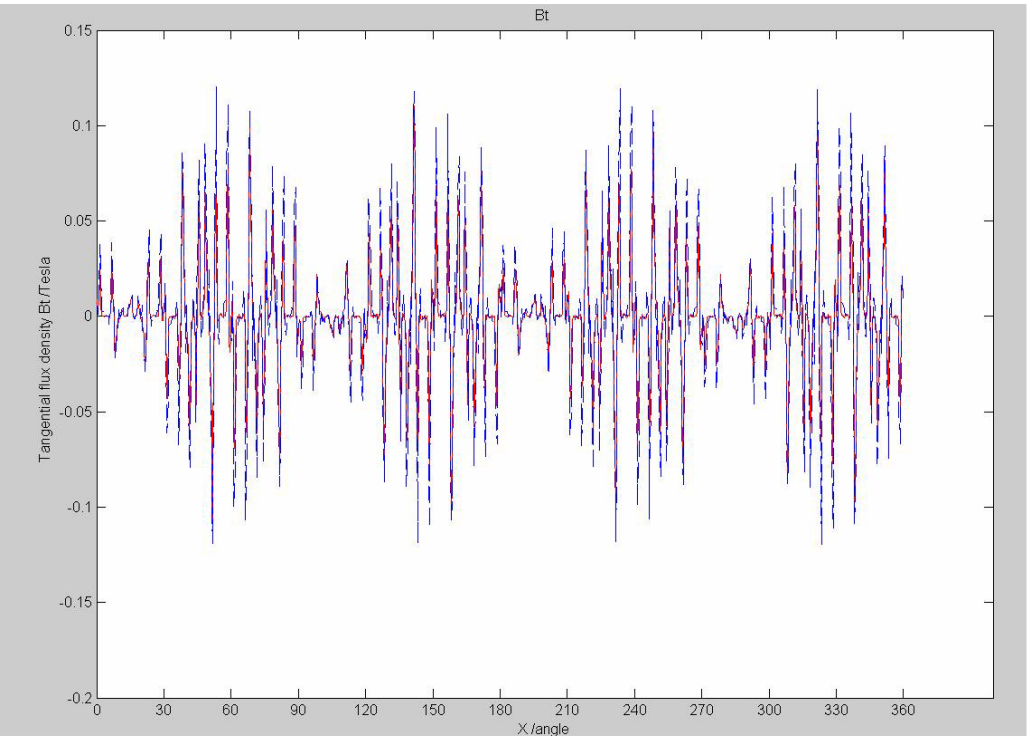

Figure 4.7 Tangential component of the flux density in the airgap of the targeted DFIG

4.3 An Introduction to Optimization Methods Incorporating FRM

An optimization routine in general can be described by:

$$\begin{aligned} &\underset{x}{Min}\, f(x) \\ &C(x) \le 0 \end{aligned} \tag{4.28}$$

In which the $f(x), C(x)$ represent the optimizing function and the boundary conditions respectively. The vector x comprises of the controlled variables. In the present investigation, optimal values of the rotor currents over one full electrical cycle forms the controlled variables. This means:

$$x = \{\{i_{ar}\}, \{i_{br}\}, \{i_{cr}\}\} \tag{4.29}$$

In which $\{i_{ar}\},\{i_{br}\},and\ \{i_{cr}\}$ represents the set of N samples that are uniformly collected over one electrical cycles:

$$\begin{aligned}\{i_{ar}\} &= \{i_{ar}[1], i_{ar}[2], \cdots i_{ar}[N]\}\\ \{i_{br}\} &= \{i_{br}[1], i_{br}[2], \cdots i_{br}[N]\}\\ \{i_{cr}\} &= \{i_{cr}[1], i_{cr}[2], \cdots i_{cr}[N]\}\end{aligned} \tag{4.30}$$

The boundary conditions are used to make sure that the results of the optimization do not violate the thermal limitation of the rotor phase currents. It is also important to note the type of connection used in the rotor winding. If there is an ungrounded wye connection, it is important to make sure that the instantaneous sum of the three phase currents equates zero i.e..

$$\begin{aligned}&|i_{ar}|,|i_{br}|,|i_{cr}| \le i_{thermal}\\ &i_{ar} + i_{br} + i_{cr} = 0\end{aligned} \tag{4.31}$$

The optimizing function is the torque pulsation over one full electrical cycle. Figure 4.8 illustrates the general block diagram of the optimization program. The optimization toolbox of the Mathlab has been used for this purpose. We have developed a M-file that includes the FRM model of the targeted DFIG in which given the values of the stator and rotor currents the torque pulsation over one electrical cycle can be calculated. This program provides the entire torque profile and as such contains more information. In the optimization routine for any given set of the stator currents, the optimized values of the rotor currents at various speeds have been calculated. Since the nonlinear effects of saturation are not included here, at any known speed and stator power angle, the rotor currents can be calculated for a specific normalized unbalance/harmonics and then for other stator current magnitudes at the same speed and

power angle, the rotor currents will be adequately modulated (amplified or decreased with the same rate). The comprehensive results of this investigation will be stored in a look up table and will be used for real time implementation. It must be noted that although updating the rotor currents can occur for any incremental change in the unbalance or harmonic contents of the stator currents, to avoid complexity, the entire range of the possible unbalance and harmonics can be partitioned into a finite number of regions and as such the rotor currents will be updated once a switching between regions occur. The steepest descent method has been used as the optimization method in Mathlab. Appendix-B contains a copy of the M-file representing the FRM model of the DFIG.

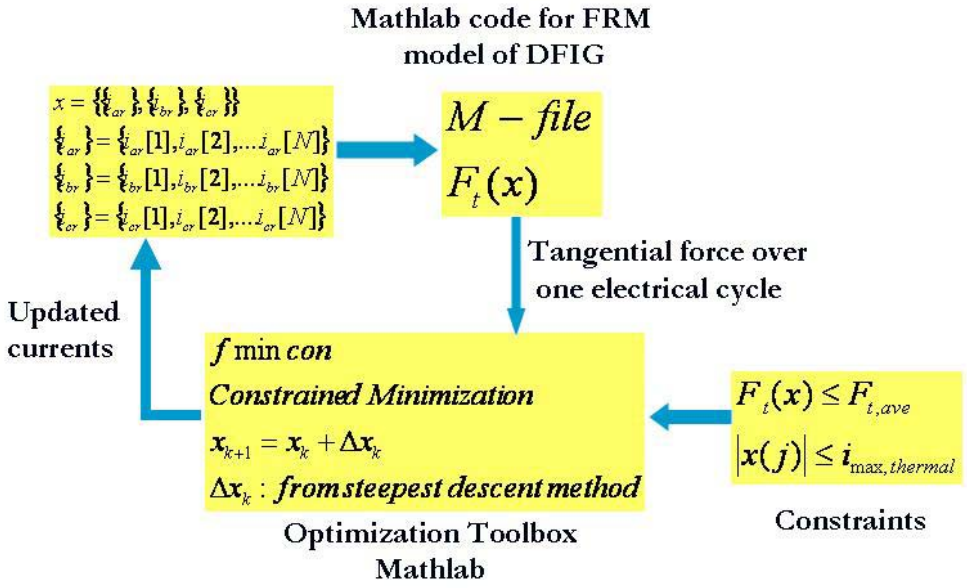

Figure 4.8 Basic configuration of the optimization routine

CHAPTER 5

FAULT TOLERANT CONTROL OF DFIG FOR DISTRIBUTED GENERATION

Wide spread installation of ac wind generators for distributed generation of electricity is one of the most important steps towards creation of a smart grid. Whether for concentrated generation by utility companies or individual installation by industrial and residential consumers, fault tolerant and reliable operation of these will be an integral part of their control strategy. As mentioned in earlier chapters, system induced mechanical vibrations originated by voltage unbalance and harmonics can jeopardize the safe operation of these units. Among available options for wind generators, DFIG provides room for effective mitigation of these undesirable vibrations which can potentially lead to mechanical resonance and eventual destruction of these generators.

Figure 5.1 Wind generation unit at fault

Considering the cost associated with the lost generation capacity and replacement of the unit, development of a fault monitoring and fault treatment for DFIG wind generators is of high importance. In this chapter, a new method of control is introduced. FE analysis has been used to demonstrate the effectiveness of the proposed method.

5.1 Elimination of Torque Pulsation via FRM-based Control of Rotor Currents in DFIG

Figure 5.2 illustrates a general arrangement of distributed wind generation in the power grid in which various generation units with various size and characteristics are tied together. If the transmission lines connecting these units to a high inertia line are subject to system induced voltage unbalance and harmonics, the generation units will experience mechanical vibrations that can potentially lead to their failures. Although local compensation for active and reactive power may be at hand timely mitigation of torque undulations is an important precaution. This can be accomplished by in-time detection of system induced unbalance and harmonics and proper adjustment of the rotor currents in DFIG. Other types of wind generators such as permanent magnet and squirrel cage induction drives do not provide this degree of freedom and as such can not be treated the same way. In this section, statement of problem and our suggested method will be presented. Finite Element method, due to its precision, has been used to validate the claims.

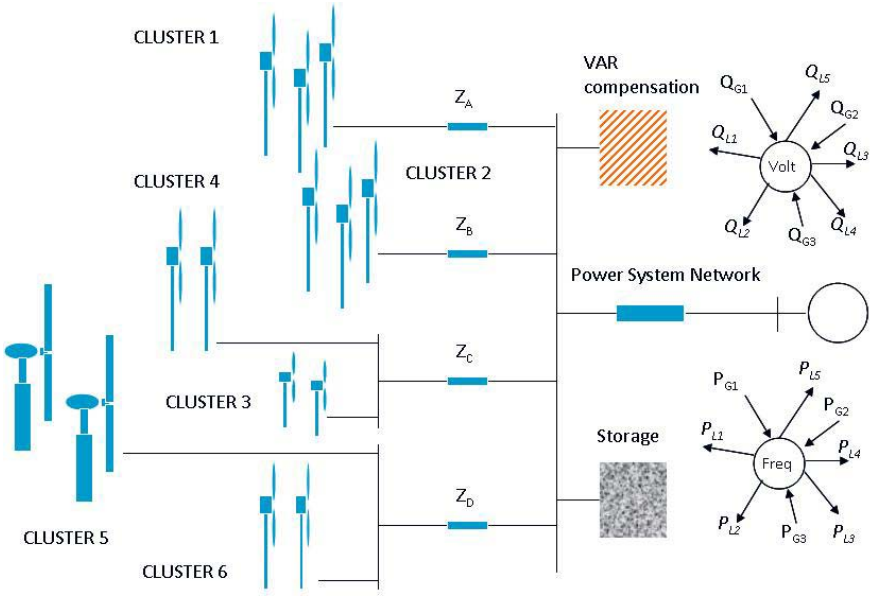

Figure 5.2 Example of an interconnected distributed wind generation

5.1.1 Statement of the Problem

Under normal mode of operation, active and reactive powers, as demanded by the system, can be accommodated in a doubly fed induction generator via regulation of direct and quadrature axis components of the rotor current (see Figure 5.3). Since the stator is connected to the grid, its voltage and frequency is set and it is not expected to observe significant changes in the magnetic inductances of the machine. The realization of the three phase currents in a hysteresis type current source inverter is a known technology and can be done very effectively. Measurement of the electrical angle for the stator as well as mechanical angle of the rotor can be done by using sensors or sensorless technique. For the purpose of the present dissertation, these technologies are well mature and do not require further discussion.

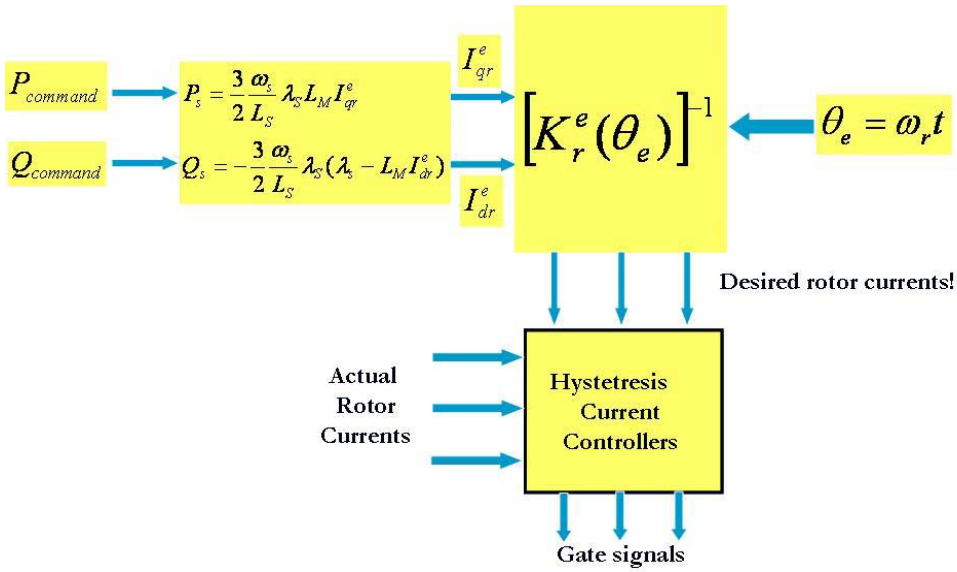

Figure 5.3 Basic control structure of DFIG under normal mode of operation

The focus of this section is to obtain optimal set of rotor currents such that in the presence of unbalance or harmonics in the stator currents, adequate rotor currents are injected such that torque pulsations can be eliminated or mitigated to a tolerable extent. This approach will require two main components:

- Detection of the voltage unbalance and harmonics
- Change of rotor currents according to the system condition to mitigate torque pulsation.

This approach has been graphically demonstrated in figure 5.4. As can be noted that the detection system will continuously monitor the real time values of the actual stator currents for abnormal conditions, i.e. voltage unbalance and harmonics. If these conditions do not exist (with an appreciable extent), the conventional system of figure 5.3 will dictate the required rotor currents so the desired active and reactive powers are

obtained. In the case of a voltage unbalance (more than 1% change in the magnitude) or voltage harmonics (more than 1% harmonic magnitude), the new set of rotor currents will be provided by a separate controller. This controller will contain a look up table of optimal currents for various probable voltage unbalance and system harmonics at every speed. If the extent of the unbalance or harmonics exceed a predetermined threshold value, i.e. 10%, the unit will be shut down for safety reasons. It is assumed that the DFIG is operating under unsaturated conditions, so the look up table will be precise for up to 100% of the rated stator load.

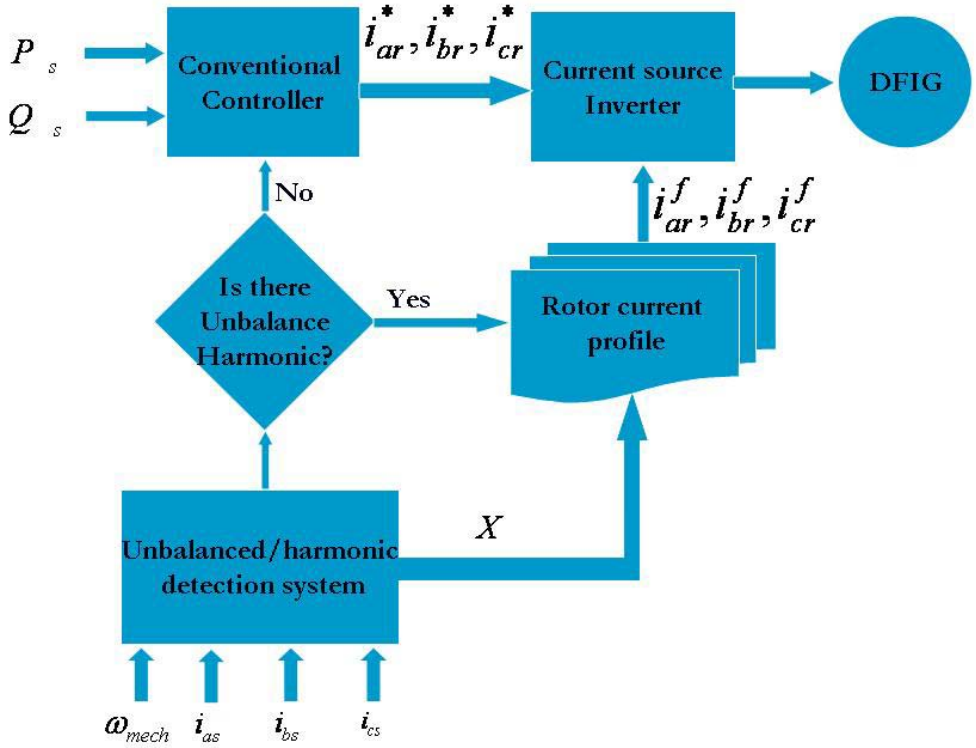

Figure 5.4 General layout of the controller system

The detection system can also be designed by monitoring the open circuited rotor voltages. However, this would only allow for testing the grid condition at no-load condition and will not be feasible for load conditions. As such the focus of the detection method is based on monitoring of the real time stator currents. Figure 5.5 illustrates the basic structure of the detection system. As can be seen a Park transformation will be applied to the measured values of the stator currents over one full electrical cycle (i.e. 16.6 msec). The transformation matrix is given by:

$$K_s(\theta_e) = \begin{bmatrix} Cos(\theta_e) & Cos(\theta_e - 120^0) & Cos(\theta_e + 120^0) \\ Sin(\theta_e) & Sin(\theta_e - 120^0) & Sin(\theta_e + 120^0) \\ 1 & 1 & 1 \end{bmatrix} \qquad (5.1)$$

$$\theta_e = 120\pi t$$

If there is a balanced system of currents with no harmonics, the result of this transformation will be two dc values corresponding to direct and quadrature axis and no zero sequence current. Any sustained deviation from this will indicate the presence of abnormal conditions in the stator supply. For instance, in the case of a balanced system of currents the following output vector will be expected:

$$\begin{bmatrix} i_{qs}^e \\ i_{ds}^e \\ i_0 \end{bmatrix} = \begin{bmatrix} \frac{3}{2} I_{\max} \\ 0 \\ 0 \end{bmatrix}, i.e. \quad \begin{bmatrix} i_{as} \\ i_{bs} \\ i_{cs} \end{bmatrix} = \begin{bmatrix} I_{\max} Cos(\theta_e) \\ I_{\max} Cos(\theta_e - 120^0) \\ I_{\max} Cos(\theta_e + 120^0) \end{bmatrix} \qquad (5.2)$$

Where $I_{\max}$ represents the maximum magnitude of the phase currents. If the stator currents contain harmonics in addition to the fundamental component, then one can see that:

$$\begin{bmatrix} i_{qs}^{e} \\ i_{ds}^{e} \\ i_{0} \end{bmatrix} = \begin{bmatrix} \frac{3}{2} I_{\max} + \frac{3}{2} \hat{I} Cos((k-1)\theta_e) \\ \frac{3}{2} \hat{I} Sin((k-1)\theta_e) \\ 0 \end{bmatrix}, i.e. \quad \begin{bmatrix} i_{as} \\ i_{bs} \\ i_{cs} \end{bmatrix} = \begin{bmatrix} I_{\max} Cos(\theta_e) + \hat{I} Cos(k\theta_e) \\ I_{\max} Cos(\theta_e - 120^0) + \hat{I} Cos(k(\theta_e - 120^0)) \\ I_{\max} Cos(\theta_e + 120^0) + \hat{I} Cos(k(\theta_e + 120^0)) \end{bmatrix} \quad (5.3)$$

As can be seen, the impact of the harmonic will be detected as an additional frequency component located at $(k-1)60[Hz]$.Similarly, decomposition of the unbalanced system into a positive and negative sequence suggest that there will be a dc component along with a component at 120Hz. In fact, one can think of Park transformation as a clockwise rotation of the current phasors with an amount of θ_e.

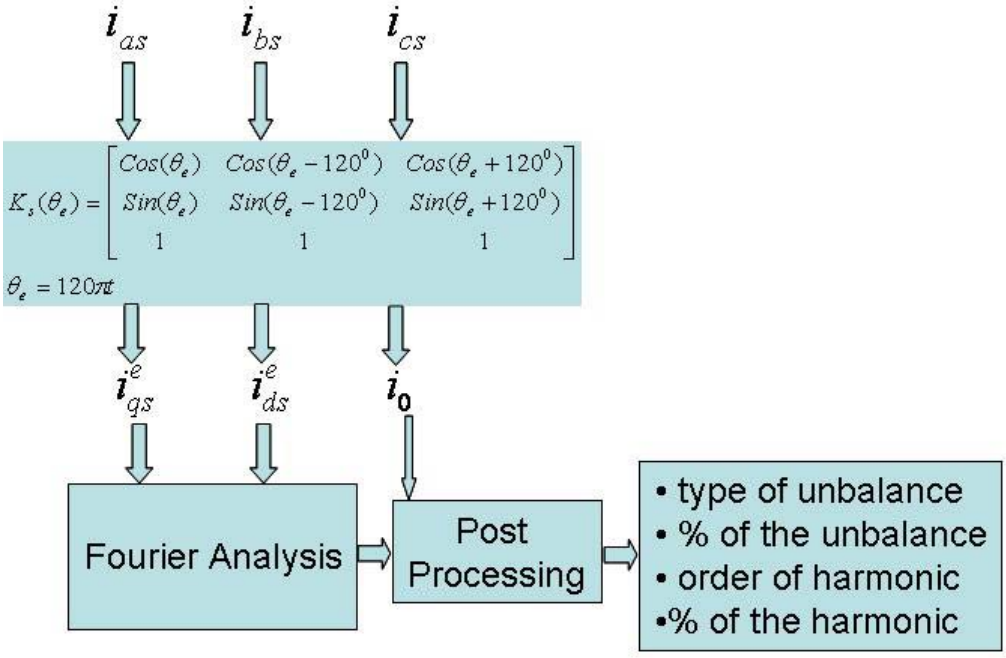

Figure 5.5. Detection of the unbalance and harmonics

The second step of the process includes the correction of the rotor current in such a way that the system induced torque pulsations are rejected. In order to accomplish this task, first a FRM model of the DFIG is formed and verified by FE analysis or direct measurement when possible. The reported accuracy of the FE is within +/-5% of the measured values in an unsaturated electric machine. Figure 5.6 illustrates the optimization process through which the optimal profile of the rotor currents are found.

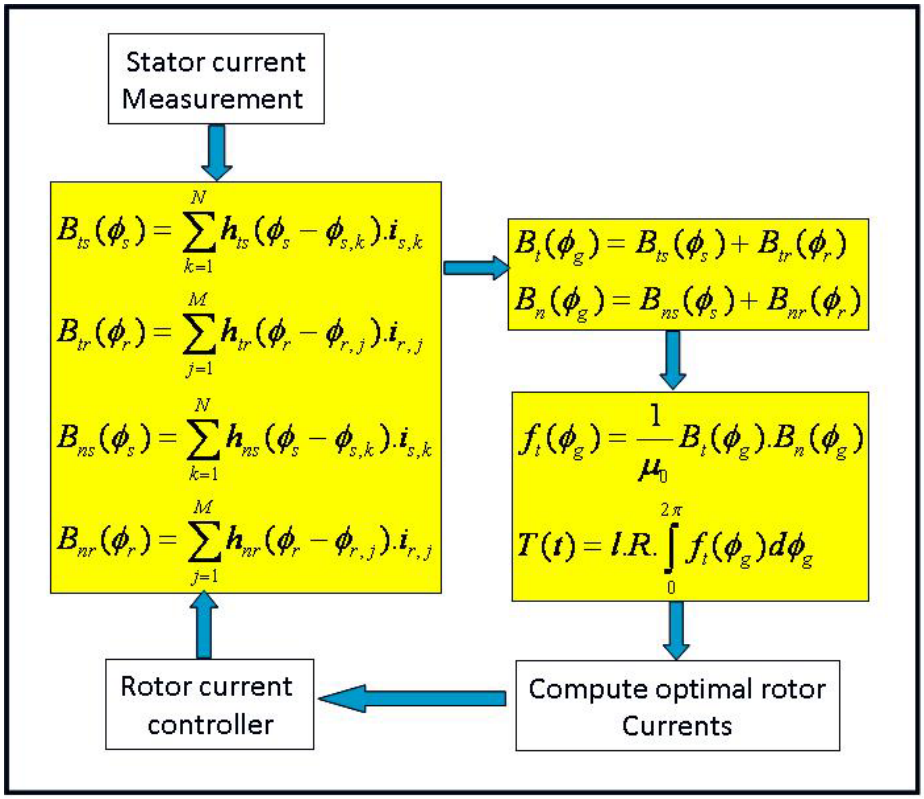

Figure 5.6 Optimization of the rotor currents to minimize/cancel torque pulsation within one electrical cycle

In this process, it is assumed that the stator current profiles are available and the set of unknowns only includes the rotor currents. The optimization toolbox of Mathlab along with a FRM model of the DFIG under investigation has been used for this study.

5.1.2. Discussion of the Results

In the first experiment, effects of the system unbalance have been presented by 10% drop in the magnitude of the stator phase-B current as shown below:

$$\begin{aligned} i_{as}[p.u.] &= Cos(120\pi t) \\ i_{bs}[p.u.] &= 0.9Cos(120\pi t - \frac{2\pi}{3}) \\ i_{cs}[p.u.] &= Cos(120\pi t + \frac{2\pi}{3}) \end{aligned} \tag{5.4}$$

As can be seen in figure 5.7, given a set of balanced rotor currents, the electromagnetic torque at standstill exhibits an oscillation with a frequency of 120 Hz. This is twice as high as the system frequency. The source of this undulation is the clockwise component of the stator field.

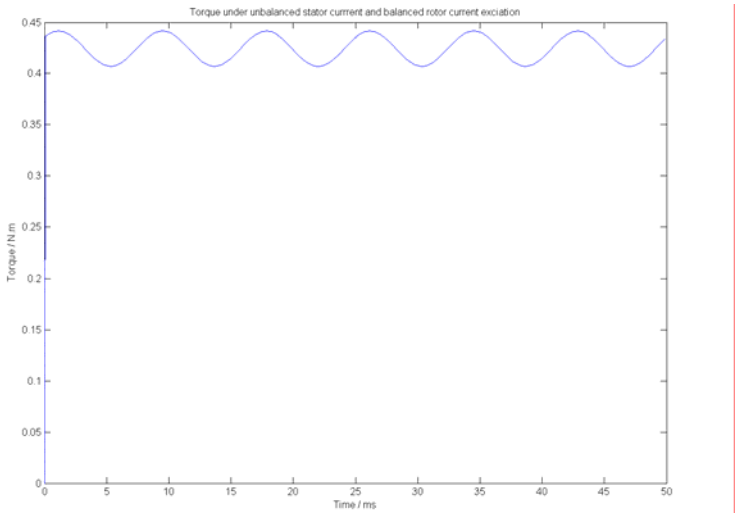

Figure 5.7 Torque pulsation at a frequency of 120 HZ due to 10% system unbalance condition

By applying the proposed optimization procedure, the optimal set of rotor currents have been computed. The objective in this optimization is to mitigate the torque pulsation without exceeding the thermal limitation on the rotor currents. For comparison purposes, the balanced sinusoidal currents are plotted so the deviation from the conventional excitation is highlighted (see figure 5.8). Figure 5.9 illustrates the optimized torque profile. As can be observed the torque pulsation has been significantly mitigated while the average torque has been maintained.

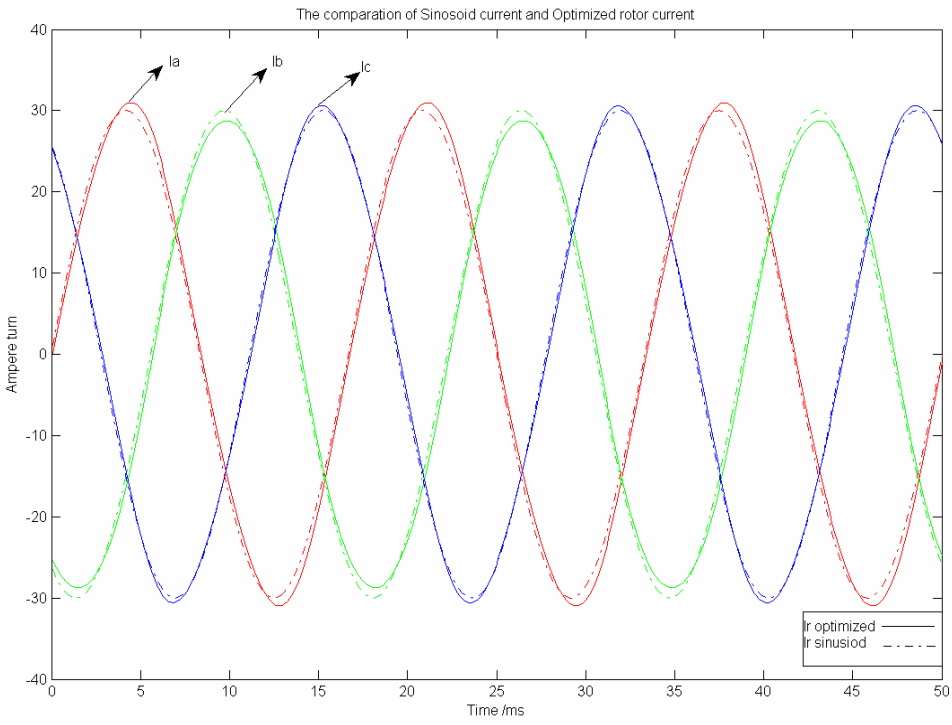

Figure 5.8 Optimal rotor currents for torque ripple cancellation

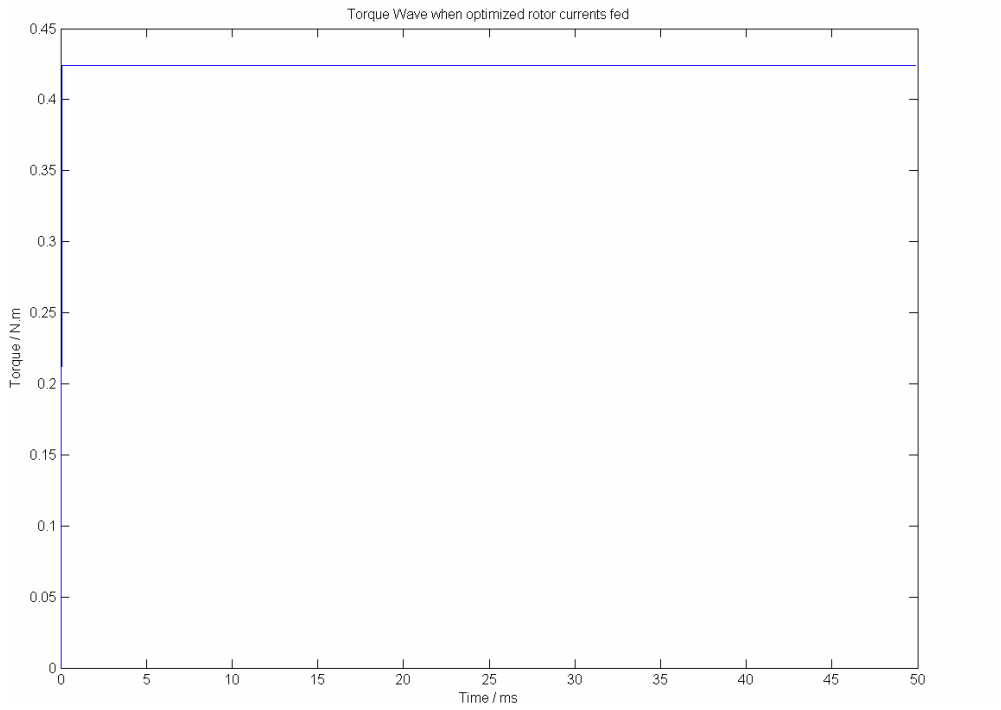

Figure 5.9 Optimized torque profile

In the second experiment, effects of system harmonics are examined. Figure 5.10 depicts the stator currents containing 10% 3rd harmonic. Stator connection has been modified to allow the flow of the current harmonics. Although the magnitude of the harmonic is very high, the machine will not exhibit any nonlinear effects of the saturation.

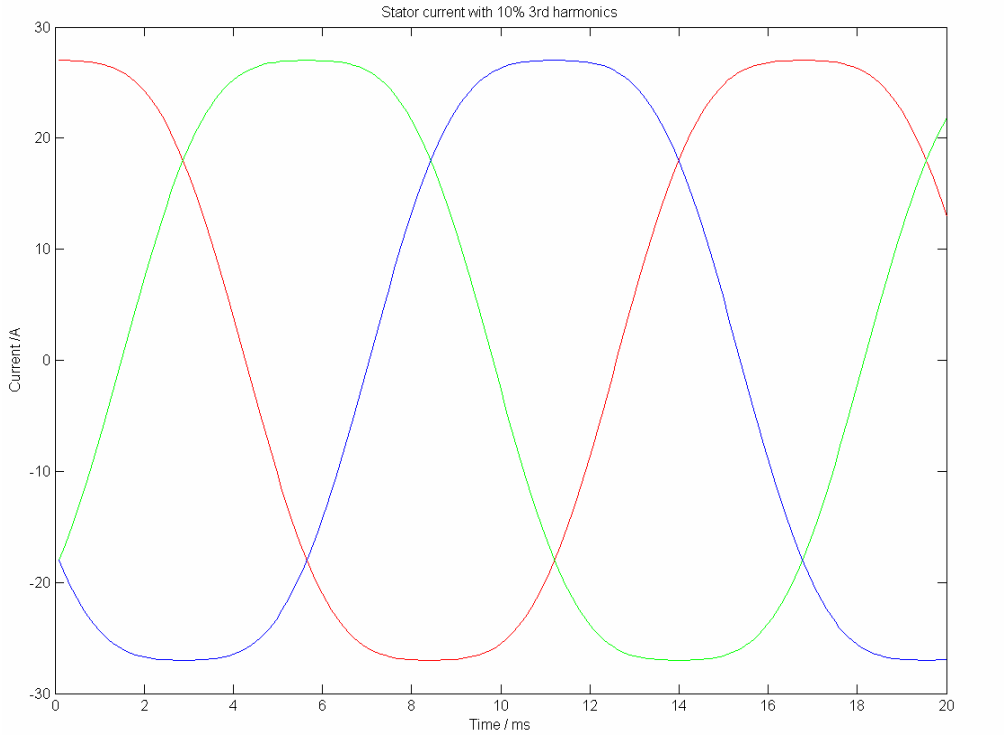

Figure 5.10 Stator current in the presence of the third harmonic

As can be noted from figure 5.11, the third harmonics will induce a 120 Hz component of the torque. This torque pulsation is targeted in our optimization process and accordingly a set of optimized rotor currents have been found and illustrated in figure 5.12. The new set of rotor currents will effectively cancel the system induced torque pulsation as shown in figure 5.13. One may note that all of the above two experiments have been performed at standstill and as such fundamental frequencies of the rotor and stator are equal. This should not be viewed as a loss of generality for steady state operational conditions as the optimal rotor currents are obtained as a function of rotor electrical angle $\theta_r = \omega_r t + \theta_r(0)$ and as the speed changes appropriate adjustment can be made to generate the optimal rotor current profiles. One, however, should not extend

this to computation of the core losses in the rotor as these losses are influenced greatly by the frequency of the magneto-motive field.

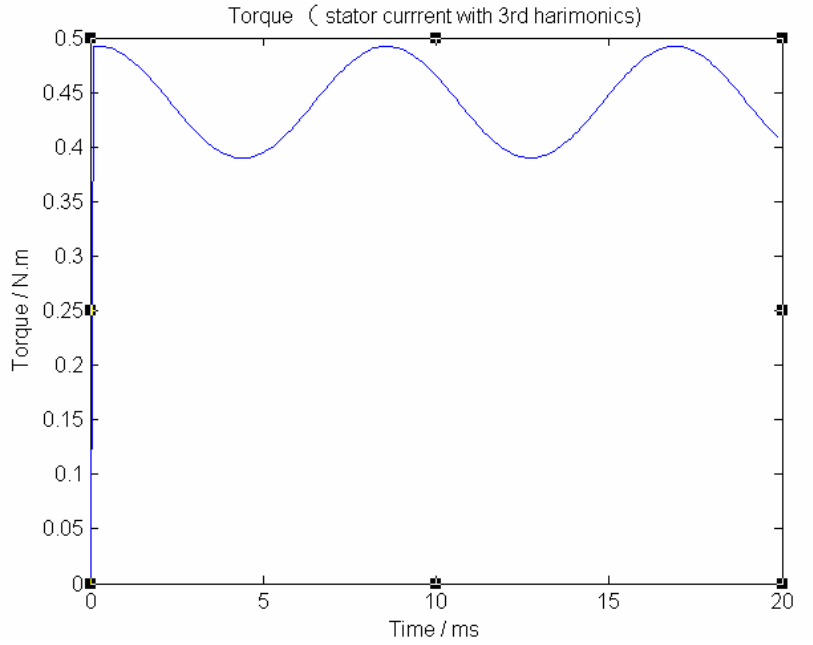

Figure 5.11 Torque pulsation due to system harmonics

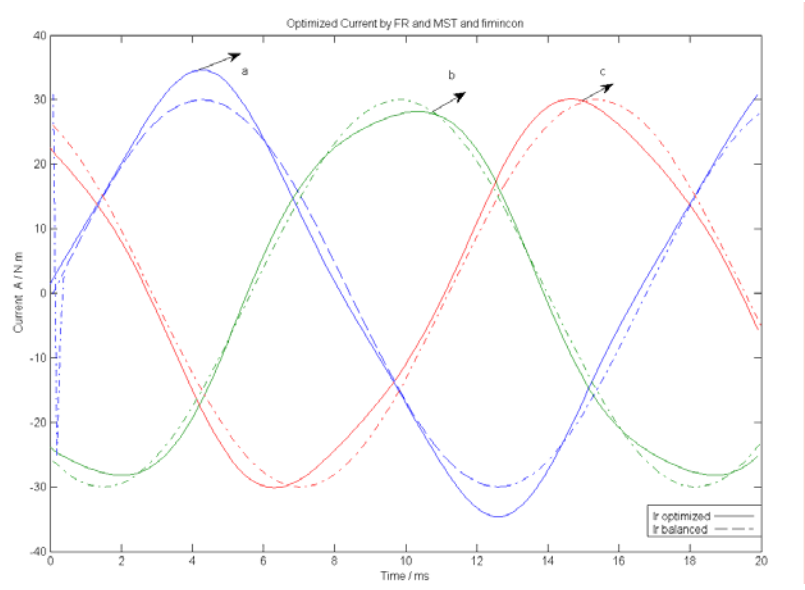

Figure 5.12 Optimized rotor currents to cancel system induced torque pulsation

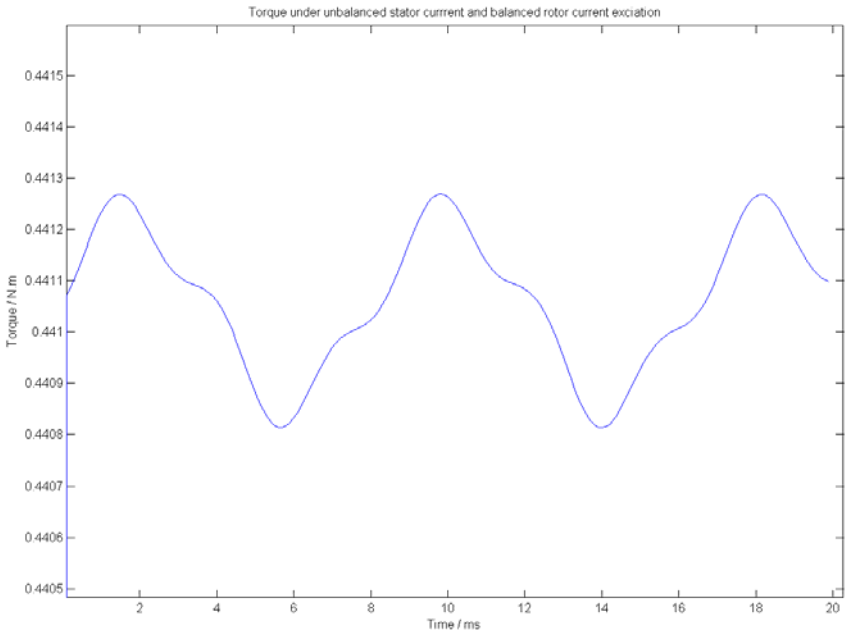

Figure 5.13 Optimized torque profile

5.2 Operation as a Variable Speed Drive

Due to the variable speed of the wind, it is important to formulate the proposed optimization technique such that the changing speed of wind can be accommodated. Considering the fact that fluctuations in the speed of wind occur at a much larger time scale as compared to the electrical period of a 60Hz network, the DFIG will operate in its steady state mode of operation for a dominant majority of time. The flow chart shown in figure 5.4 portrays the control strategy. Vector "X" as shown in figure 5.4 contains very important information regarding the type and extent of existing unbalance and harmonics. In addition, it contains information regarding the mechanical speed of rotation. This information is either recorded explicitly using an external position sensor

or has been alternatively provided using an implicit approach such as position sensorless technique. In either case, a look up table is formulated in the form of:

$$\begin{aligned} i_{ar}(\theta_r) &= i_{ar}(\theta_{mech} - \theta_e) \\ i_{br}(\theta_r) &= i_{br}(\theta_{mech} - \theta_e) \\ i_{cr}(\theta_r) &= i_{cr}(\theta_{mech} - \theta_e) \end{aligned} \tag{5.5}$$

Accessing online information regarding the value of the rotor position and by monitoring the real time value of the stator electrical angle, one can effectively decide on the instant of the engagement for the optimal set of rotor currents at any desired rotor frequency. This will guarantee an optimal steady state performance for the wind generation system. There maybe some transients mismatch while the instant of the commutation to optimal rotor currents is being decided. However, this is a short time as compared to mechanical time constants of the wind turbine system and tolerable. In general, it is expected to find the optimal point of synchronization within one electrical cycle of the stator (16.6 msec).

It is important to remember that using the current profiles obtained from standstill are very accurate in terms of torque ripple minimization at any desired speed. However, changes in the rotor core losses will differ depending on the actual value of the rotor current frequency. Therefore, it is important to perform the experiments at the exact rotor current frequency to collect rotor core losses. Finally it must be reminded that due to the linearity of the DFIG, for any level of the unbalance and harmonics, value of the base stator current and base rotor currents are known and a per unit system with linear interpolation will be used to project the optimal rotor current which may occur within the boundaries of the current.

5.3. Impact on Efficiency and Power Converter

One of the most important performance features in a wind generator is the efficiency of the unit. The efficiency is defined as:

$$\eta = \frac{\tau.\omega_{mech} - P_{core} - P_{copper} - P_{si}}{\tau.\omega_{mech}} \tag{5.6}$$

Where $\tau, P_{core}, P_{copper}, P_{si}$ represent electromagnetic torque, core losses, copper losses, and silicon losses in the rotor power converter.

The copper losses in the DFIG can be approximated by:

$$P_{copper} = R_s(I^2_{rms,as} + I^2_{rms,bs} + I^2_{rms,cs}) + R_r(I^2_{rms,ar} + I^2_{rms,br} + I^2_{rms,cr}) \tag{5.7}$$

Where $R_s, and\ R_r$ represent the effective resistance of the stator and rotor phase windings respectively. The silicon losses in the rotor power converter can be approximated by:

$$P_{si} = 6V_{D,FF}.I_{rms,D} + 6V_{CE,IGBT}.I_{rms,IGBT} + P_{Switching} \tag{5.8}$$

Where $V_{D,FF}, I_{rms,D}, V_{CE,IGBT}, I_{rms,IGBT}, and\ P_{switching}$ represent the forward drop of the diodes used in the front end rectifier, the root mean square current in diodes, collector to emitter voltage drop in IGBT, rms current in IGBT and switching losses. Since the power in the rotor circuit constitutes a small portion of the full power and switching frequency of the PWM is normally kept at low levels (2 - 4kHz for medium size drives), the overall impact of the silicon losses, due to change in rotor current profile, on the efficiency of the generation unit will be small.

Finally, the core losses in the stator and the rotor can be decomposed into the eddy current (changing flux in laminations) losses and hysteresis losses (energy used for orientation of ferromagnetic material within laminations). While the stator frequency is fixed at 60Hz, because of the changes in the wind speed and in accordance with (2.1) the rotor frequency will be variable. However, the rotor frequency will be normally less than the stator frequency. Strong dependency of the core losses upon the frequency of the respective magnetic field in a given part of the generator is demonstrated in:

$$P_v = K_h f B_m^{\ 2} + K_c (f B_m)^2 + K_e (f B_m)^{1.5} \tag{5.9}$$

In which, K_h, K_c, K_e refer to the hysteresis loss, eddy current loss, and excess loss coefficients respectively, which only related with material properties and B_m is the magnitude of flux density. Figure 5.14 demonstrates the core losses in the targeted DFIG before and after optimization of the rotor currents for the elimination of the torque ripple due to unbalanced stator currents.

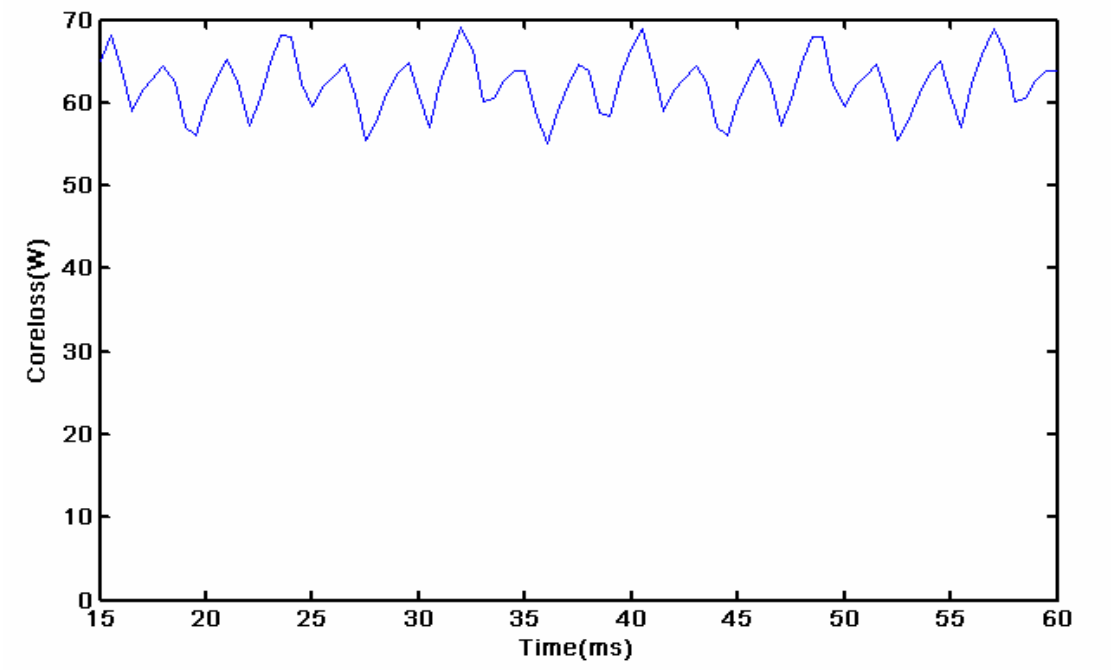

Figure 5.14 Core losses before optimization of the rotor current

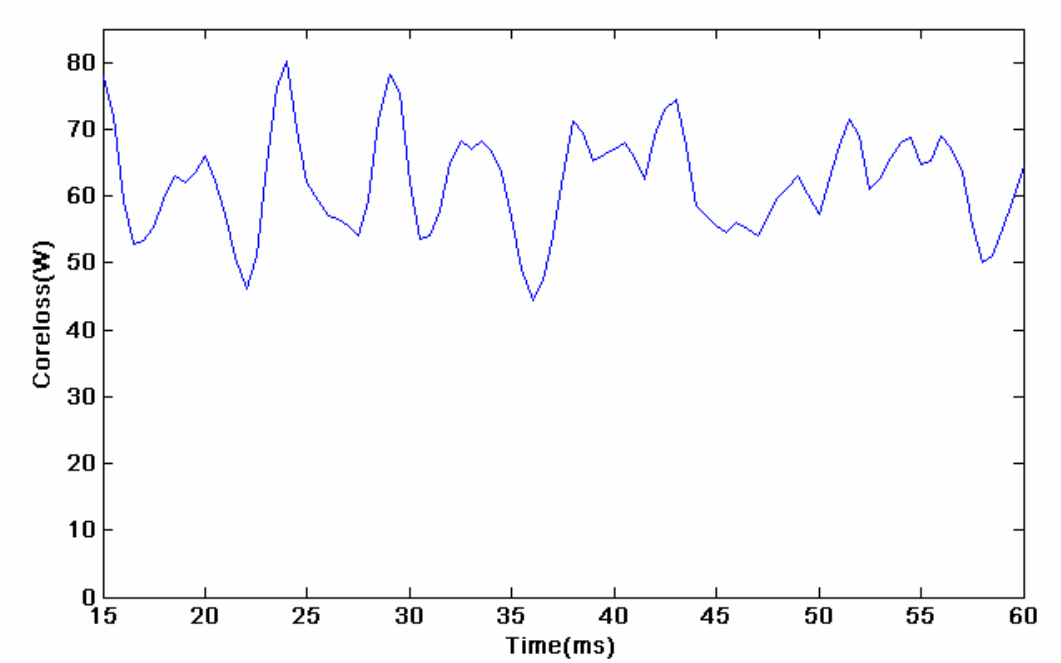

Figure 5.15 Core losses after optimization of the rotor currents

A close inspection of the average value of the core losses before and after current profiling in this case indicates that there are no significant changes in the core losses. In

fact the total core losses are virtually the same. The core loss distributions shown in figures 5.14and 5.15 have been obtained using finite element method as implemented in the software package Magnet from Infolytica ©.

It is notable that within the optimization technique, the efforts have placed to maintain the average torque (i.e. average tangential force) while the pulsation has been cancelled. This has been done by placing a boundary condition on the average value of the torque. Therefore, at any given speed the arrangement of losses is not going to change dramatically and the DFIF remains as productive as it was in the presence of harmonics. Although existent, the drop of the efficiency due to the proposed current profiling is less than 1% in targeted range of unbalance and harmonics.

CHAPTER 6

CONCLUSIONS AND FUTURE RESEARCH

Among various options that are considered for renewable energy harvest, distributed wind energy systems seem to be of prime interest. This is primarily due to the abundant, economical, and efficient generation of this renewable energy system. Because of their high efficiency, flexible structure for variable speed operation, and independent control of the active and reactive power, doubly fed induction generators have been a superior candidate for large power units. It has been noticed that system unbalance and system harmonics exhibit a rising trend in distribution and finite inertia power systems. This can undermine the safe operation of AC generation units, by reducing their efficiency (increase in core and copper losses, i.e. skin effects) as well as introducing undesirable torque undulations. Low frequency undulation of the electromagnetic torque can ignite mechanical resonance and severe damage to the unit if it is not properly detected and mitigated. This dissertation offers a real time solution for detection of system unbalance and harmonics and their treatment by using a field reconstruction method (FRM). Simulation results show that the proposed method can effectively eliminate the system induced mechanical vibrations with no noticeable drop in average torque. This forms a performance improvement management system that can provide safe operation of the generation unit for up to 10% system unbalance and system harmonics.

Finite element has been used to validate the effectiveness of the proposed approach. Findings of this investigation will pave the way for real-time fault detection and fault tolerant operation of DFIG for wind energy harvest that are connected to a finite inertia (weak) grid. Elimination of torque pulsation without a noticeable sacrifice in average torque not only will avoid possible mechanical resonance but also will improve the durability of the wind turbine and its rotating components.

For the future research, one can augment the proposed method not only for motoring mode of operation, but also including faults that are either caused by mechanical components (i.e. gear box, turbine, bearings) or due to eccentricity of the rotor, bent rotor, and or asymmetric design of the stator and rotor stacks.

The use of artificial neural networks in place of look up tables may be pursued as well. It is also possible to augment the proposed method to a wind farm and evaluate the impact of the rotor currents on the overall current harmonic level of the wind farm. It is expected that the result of this research will be applicable to dissemination of the wind energy harvest units to commercial and residential units as well as large wind farms. This is a very important step towards empowering the consumers which is an integral part of smart power grid vision.

APPENDIX A

SPECIFICATIONS OF DFIG

Parameter	Value
Rated power	5Hp
Rated voltage	208 V
Synchronous speed	1800 r.p.m.
Number of stator slots	36
Number of rotor slots	48
Stator/rotor coil material	copper
Stator/rotor core material	M-19
Core length	3.5 inches
Airgap length	0.05 inches
Stator outer diameter	9 inches

APPENDIX B

FRM MODEL FOR DFIG

```
%%%%%%%%%%%%%%%%%%%%%%%%%%%%%%%%%%%%%%%%%%%%%%%%%%%%%%%%%%%%%%%%%%%%%%%
%%%%
%  This code loads previously stored  basis functions of phase A of
stator  and rotor from files
%  calculates the Bnk, Btk due to current in Phase B,Phase C
% calculates the the total Bn,Bt,Fn,Ft in the airgap of Induction
machine
% calculates force density and torque  of DFIG
%%%%%%%%%%%%%%%%%%%%%%%%%%%%%%%%%%%%%%%%%%%%%%%%%%%%%%%%%%%%%%%%%%%%%%%
%%%
clear workspace
clc
%------The definition of Parameters----------------------------------
----
Dn=1440;                          %Number of Points in the intergral
contour
micro0=4*pi*1e-7;
Rg=2.7375*25.4*1e-3;       % The radias of the mid of airgap
2.7375inch, transfer to Meter
stacklength=3.5*25.4*1e-3; % the effective stack length
PPn=2;                              % Pole Pair Number
phy_s=0;                          % the angle difference between stator
and rotor axis, it is default in this calculation

%--by change Theta_R, we can verify if the calculated field is
corrected or not
Theta_R=1440*45/360; % the Mechanical angle of rotor relative to
stator axis

%------Parameters of Stator
Ns=30;                             %Number of turns in one slot of
stator
Ks=36;                               %Number of slots in stator
Ks_angle=Dn/Ks;             % stator slot pitch angle
R_angle=Dn/3/PPn;           % the angle difference between phase wind

%------Parameters of Rotor
Nr=30;                           % Number of conductor turns in one
slot of rotor
Kr=48;                           % Number of slots in rotor
Kr_angle=Dn/Kr;             % rotor slot pitch angle
S_angle=Dn/3/PPn;       % the angle difference between phase wind


%-----stator exciation
% leave stator and rotor current 90 degree difference , rotate the
rotor by 45 mechanical degree
angle_s=pi/2;
angle_r=0;
Isa=5*Ns*cos(angle_s);%+ 0.5*5*Ns*cos(5*angle_s+pi/2);%+
0.05*Isa*Ns*cos(5*(angle_s+pi/2));
```

```
Isb=5*Ns*cos(angle_s-2*pi/3);%+0.5*5*Ns*cos(5*(angle_s-
2*pi/3)+pi/2);%+ 0.05*Isb*Ns*cos(5*(angle_s-2*pi/3+pi/2));
Isc=5*Ns*cos(angle_s-4*pi/3);%+0.5*5*Ns*cos(5*(angle_s-
4*pi/3)+pi/2);%+ 0.05*Isc*Ns*sin(5*(angle_s-4*pi/3+pi/2));
Is(1)=Isa
Is(2)=Isb
Is(3)=Isc



%---rotor excitation
Ira=5*Nr*cos(angle_r);%+ 0.375*5*Nr*cos(5*angle_r-pi/2);
Irb=5*Nr*cos(angle_r-2*pi/3);%+ 0.375*5*Nr*cos(5*(angle_r-2*pi/3)-
pi/2);
Irc=5*Nr*cos(angle_r-4*pi/3);%+ 0.375*5*Nr*cos(5*(angle_r-4*pi/3)-
pi/2);
Ir0(1)=Ira
Ir0(2)=Irb
Ir0(3)=Irc

%--rotor current optimization
%Ir_op=minimize(Bsn,Bst,Brn,Brt,Is,Ir0,0);
%Ira=Ir_op (1)
%Irb=Ir_op (2)
%Irc=Ir_op (3)

%%%%%%%%%%%%%%%%%%%%%%%%%%%%%%%%%%%%%%%%%%%%%%%%%%%%%%%%%%%%%%%%%%%%%%
%
%Basis function code is in FR_basis.m
%%%%%%%%%%%%%%%%%%%%%%%%%%%%%%%%%%%%%%%%%%%%%%%%%%%%%%%%%%%%%%%%%%%%%%
%%

%%%%%%%%%%%%%%%%%%%%%%%%%%%%%%%%%%%%%%%%%%%%%%%%%%%%%%%%%%%%%%%%%%%%%%
%%%%
% Read data from stored basis function
%%%%%%%%%%%%%%%%%%%%%%%%%%%%%%%%%%%%%%%%%%%%%%%%%%%%%%%%%%%%%%%%%%%%%%
%%%%
Bs_Vector=dlmread('C:\Matlab\DFIG_FR\Basis\Bs_Ia44A.txt');
Br_Vector=dlmread('C:\Matlab\DFIG_FR\Basis\Br_Ia44A.txt');
Bs_Vector=dlmread('C:\Matlab\DFIG_FR\Basis\Bs_Ia44A.txt');
Br_Vector=dlmread('C:\Matlab\DFIG_FR\Basis\Br_Ia44A.txt');
for B_index=1:1:Dn;
    Bsn(B_index)=Bs_Vector(B_index,2);
    Bst(B_index)=Bs_Vector(B_index,3);
    Brn(B_index)=Br_Vector(B_index,2);
    Brt(B_index)=Br_Vector(B_index,3);
end

%%%%%%%%%%%%%%%%%%%%%%%%%%%%%%%%%%%%%%%%%%%%%%%%%%%%%%%%%%%%%%%%%%%%%%
%%%%%
%If you want to watch basis function, you can plot it here
```

```
%%%%%%%%%%%%%%%%%%%%%%%%%%%%%%%%%%%%%%%%%%%%%%%%%%%%%%%%%%%%%%%%%%%%%%%%
%%%%%
%B_index=1:1:Dn
% figure(1)
% plot(B_index, Bsn(B_index))
% title('Bsn basis function')

%%%%%%%%%%%%%%%%%%%%%%%%%%%%%%%%%%%%%%%%%%%%%%%%%%%%%%%%%%%%%%%%%%%%%%%%
%%%%%
% Field Reconstruction use basis function
%%%%%%%%%%%%%%%%%%%%%%%%%%%%%%%%%%%%%%%%%%%%%%%%%%%%%%%%%%%%%%%%%%%%%%%%
%%%%%
%Bsn(B_index) is the basis function for Bsn
%Bst(B_index) is the basis function for Bst
%Brn(B_index) is the basis function for Brn
%Brt(B_index) is the basis function for Brt
%-------------shift the phase/angle to get function for each phase----
-----
for B_index=1:1:Dn;

    Bsa_index=B_index;
    Bsb_index=Bsa_index+S_angle;    %physical angle difference between
Phasewinding A and Phasewinding B
    Bsc_index=Bsb_index+S_angle;    %physical angle difference between
Phasewinding B and Phasewinding C

    Bra_index=B_index;
    Brb_index=Bra_index+R_angle;
    Brc_index=Brb_index+R_angle;

    if(Bsb_index>1440)
        Bsb_index=Bsb_index-1440;
    end
    if(Bsb_index<1)
        Bsb_index=Bsb_index+1440;
    end
    if(Bsc_index>1440)
        Bsc_index=Bsc_index-1440;
    end
    if(Bsc_index<1)
        Bsc_index=Bsc_index+1440;
    end

    if(Brb_index>1440)
        Brb_index=Brb_index-1440;
    end
    if(Brb_index<1)
        Brb_index=Brb_index+1440;
    end
    if(Brc_index>1440)
        Brc_index=Brc_index-1440;
    end
```

```
    if(Brc_index<1)
        Brc_index=Brc_index+1440;
    end
Bsan(Bsa_index)=  Isa*Bsn(B_index);
Bsbn(Bsb_index)=  Isb*Bsn(B_index);
Bscn(Bsc_index)=  Isc*Bsn(B_index);

Bsat(Bsa_index)=  Isa*Bst(B_index);
Bsbt(Bsb_index)=  Isb*Bst(B_index);
Bsct(Bsc_index)=  Isc*Bst(B_index);

Bran(Bra_index)=  Ira*Brn(B_index);
Brbn(Brb_index)=  Irb*Brn(B_index);
Brcn(Brc_index)=  Irc*Brn(B_index);

Brat(Bra_index)=  Ira*Brt(B_index);
Brbt(Brb_index)=  Irb*Brt(B_index);
Brct(Brc_index)=  Irc*Brt(B_index);



end
%-----------------------------------------------------------
%standstill
%-----------------------------------------------------------
 %
BN(B_index)=Bsan(B_index)+Bsbn(B_index)+Bscn(B_index)+Bran(B_index)+Br
bn(B_index)+Brcn(B_index);
 %
BT(B_index)=Bsat(B_index)+Bsbt(B_index)+Bsct(B_index)+Brat(B_index)+Br
bt(B_index)+Brct(B_index);

 %-----------------------------------------------------------
 %  rotating condition
 % calculate Bsn, Bst,Brn,Brt repespectively and shift Brn,Brt by
rotor mechanical angle
 %-----------------------------------------------------------
for B_index=1:1:Dn;

    BSN(B_index)=Bsan(B_index)+Bsbn(B_index)+Bscn(B_index);
    BRN(B_index)=Bran(B_index)+Brbn(B_index)+Brcn(B_index);
    BST(B_index)=Bsat(B_index)+Bsbt(B_index)+Bsct(B_index);
    BRT(B_index)=Brat(B_index)+Brbt(B_index)+Brct(B_index);
end
%-----------------------------------------------------------
%rotating,  rotate the rotor field by rotor mechanical angle
%-----------------------------------------------------------
for B_index=1:1:Dn;
    index= B_index - Theta_R;

    if(index== fix(index));
```

```
        %-------temp_BRN, temp_BRT is for watching the final BRN,BRT
        temp_BRN(B_index)=BRN(data_index(index,1440));
        temp_BRT(B_index)=BRT(data_index(index,1440));

        BN(B_index)=BSN(B_index)+BRN(data_index(index,1440));
        BT(B_index)=BST(B_index)+BRT(data_index(index,1440));
    elseif (index > fix(index));
        temp_BRN(B_index)=BRN( data_index(fix(index),1440) )+(index-
fix(index))*( BRN( data_index( (fix(index)+1),1440 ) )  - BRN(
data_index(fix(index),1440 ) )  );
        temp_BRT(B_index)=BST(B_index)+BRT(
data_index(fix(index),1440) )+(index-fix(index))*(  BRT( data_index( (
fix(index)+1),1440 ) ) -  BRT( data_index( fix(index),1440 ) ) );

        BN(B_index)=BSN(B_index)+BRN( data_index(fix(index),1440)
)+(index-fix(index))*( BRN( data_index( (fix(index)+1),1440 ) )  -
BRN( data_index(fix(index),1440 ) )  );
        BT(B_index)=BST(B_index)+BRT( data_index(fix(index),1440)
)+(index-fix(index))*(  BRT( data_index( ( fix(index)+1),1440 ) ) -
BRT( data_index( fix(index),1440 ) ) );
    elseif (index < fix(index));

        temp_BRN(B_index)=BRN( data_index(fix(index),1440)
)+(fix(index)-index)*( BRN( data_index( fix(index),1440 ) )  - BRN(
data_index((fix(index)-1),1440 ) )  );
        temp_BRT(B_index)=BST(B_index)+BRT(
data_index(fix(index),1440) )+(fix(index)-index)*(  BRT( data_index(
fix(index),1440 ) ) -  BRT( data_index( (fix(index)-1),1440 ) ) );

        BN(B_index)=BSN(B_index)+BRN( data_index(fix(index),1440)
)+(fix(index)-index)*( BRN( data_index( fix(index),1440 ) )  - BRN(
data_index((fix(index)-1),1440 ) )  );
        BT(B_index)=BST(B_index)+BRT( data_index(fix(index),1440)
)+(fix(index)-index)*(  BRT( data_index(  fix(index),1440 ) ) -  BRT(
data_index( (fix(index)-1),1440 ) ) );
    end

end

%----plot Bn created by stator
Bnt_index=0:1:(Dn-1);
figure(201);
plot(Bnt_index/4,BSN(Bnt_index+1),'r');
set(gca,'XTick',0:30:360)
ylabel('Normal Flux Density (Tesla)','fontsize',11);
xlabel('Angular position in the airgap','fontsize',11);
title('Normal Flux Density Bsn created by stator ','fontsize',11)
set(findobj(gca,'type','line'),'linewidth',1.0)
set(gca,'fontsize',11); % axis tick size11
set(gca,'linewidth',1.5);% axis linewidth 1.5
set(gcf,'color',[1,1,1]); % figure backgroudn color
hold on
```

```
%---------plot Bn created by rotor
figure(202)
plot(Bnt_index/4,temp_BRN(Bnt_index+1),'b');
set(gca,'XTick',0:30:360)
ylabel('Normal Flux Density (Tesla)','fontsize',11);
xlabel('Angular position in the airgap','fontsize',11);
title('Normal Flux Density Brn created by rotor ','fontsize',11)
set(findobj(gca,'type','line'),'linewidth',1.0)
set(gca,'fontsize',11); % axis tick size11
set(gca,'linewidth',1.5);% axis linewidth 1.5
set(gcf,'color',[1,1,1]); % figure backgroudn color
hold on

%----plot Bt
figure(203);
plot(Bnt_index/4,BST(Bnt_index+1),'r');
set(gca,'XTick',0:30:360)
ylabel('Tangential Flux density (Tesla)','fontsize',11);
xlabel('Angular position in the airgap','fontsize',11);
title('Tangential Flux density created by stator','fontsize',11)
set(findobj(gca,'type','line'),'linewidth',1.0)
set(gca,'fontsize',11); % axis tick size11
set(gca,'linewidth',1.5);% axis linewidth 1.5
set(gcf,'color',[1,1,1]); % figure backgroudn color
%hold on
figure(204);
plot(Bnt_index/4,temp_BRT(Bnt_index+1),'b');
set(gca,'XTick',0:30:360)
ylabel('Tangential Flux density (Tesla)','fontsize',11);
xlabel('Angular position in the airgap','fontsize',11);
title('Tangential Flux density created by rotor','fontsize',11)
set(findobj(gca,'type','line'),'linewidth',1.0)
set(gca,'fontsize',11); % axis tick size11
set(gca,'linewidth',1.5);% axis linewidth 1.5
set(gcf,'color',[1,1,1]); % figure backgroudn color
%hold on

%%%%%%%%%%%%%%%%%%%%%%%%%%%%%%%%%%%%%%%%%%%%%%%%%%%%%%%%%%%%%%%%%%%%%%%%%%%
%
% Plot fn and ft
%%%%%%%%%%%%%%%%%%%%%%%%%%%%%%%%%%%%%%%%%%%%%%%%%%%%%%%%%%%%%%%%%%%%%%%%%%%
%%
%----plot Bn

for B_index=1:1:Dn;
ft(B_index)=BN(B_index)*BT(B_index)/micro0;
fn(B_index)=(BN(B_index)^2 - BT(B_index)^2)/micro0/2;
end
B_index=1:1:Dn;
figure(205);
plot(B_index/4,ft(B_index),'b');
set(gca,'XTick',0:30:360)
ylabel('Tangential Force density (N/m2)','fontsize',11);
```

```
xlabel('Angular position in the airgap(degree)','fontsize',11);
title('Tangential Force density','fontsize',11)
set(findobj(gca,'type','line'),'linewidth',1.0)
set(gca,'fontsize',11); % axis tick size11
set(gca,'linewidth',1.5);% axis linewidth 1.5
set(gcf,'color',[1,1,1]); % figure backgroudn color
hold on
figure(206);
plot(B_index/4,fn(B_index),'b');
set(gca,'XTick',0:30:360)
ylabel('Normal Force density (N/m2)','fontsize',11);
xlabel('Angular position in the airgap(degree)','fontsize',11);
title('Normal Force density','fontsize',11)
set(findobj(gca,'type','line'),'linewidth',1.0)
set(gca,'fontsize',11); % axis tick size11
set(gca,'linewidth',1.5);% axis linewidth 1.5
set(gcf,'color',[1,1,1]); % figure backgroudn color
hold on

%%%%%%%%%%%%%%%%%%%%%%%%%%%%%%%%%%%%%%%%%%%%%%%%%%%%%%%%%%%%%%%%%%%%%%%%%%%%%%%
% Calculate the Fn,Ft,T
% BN,BT is generated by FR method
%%%%%%%%%%%%%%%%%%%%%%%%%%%%%%%%%%%%%%%%%%%%%%%%%%%%%%%%%%%%%%%%%%%%%%%%%%%%%%%
%
Dtheta=(2*pi/Dn);
Ft=0;
Fn=0;
Integral_ft=0;
Integral_fn=0;
torque=0;
for B_index=1:1:Dn;
ft(B_index)=BN(B_index)*BT(B_index)/micro0;
fn(B_index)=(BN(B_index)^2 - BT(B_index)^2)/micro0/2;
Ft=Ft+ft(B_index)*Rg*Dtheta;
Integral_ft=Integral_ft+ft(B_index);
Fn=Fn+fn(B_index)*Rg*Dtheta;
Integral_fn=Integral_fn+fn(B_index);
end
Integral_ft
Ft
Integral_fn
Fn
torque = Ft*Rg*stacklength

%%%%%%%%%%%%%%%%%%%%%%%%%%%%%%%%%%%%%%%%%%%%%%%%%%%%%%%%%%%%%%%%%%%%%%%%%%%%%%%
%
%FFT of the Bt
%%%%%%%%%%%%%%%%%%%%%%%%%%%%%%%%%%%%%%%%%%%%%%%%%%%%%%%%%%%%%%%%%%%%%%%%%%%%%%%
F_s=1440*30;
% use fft to compute y and its power
m=length(BT); % windows length
n= pow2(nextpow2(m)); % transform length to 2^N
%lp=600;
```

```
%wn1=2*lp/F_s;
%[z1,p1,k1]=cheby1(2,0.5,wn1);
%[b1,a1]=CHEBY1(2,0.5,wn1);
%b1=b1/(8*1.0711);
%a1=a1/(8*1.0711);
%data=filter(b1,a1,BN)
Fcomponet=fft(BT,n)/m;
figure(207)
%-----plot magnitude-----------------------
fp=F_s/2 * linspace(0,1,n/2);
plot(fp,2*abs(Fcomponet(1:n/2)));
```

APPENDIX C

ADDITIONAL SIMULATION RESULTS

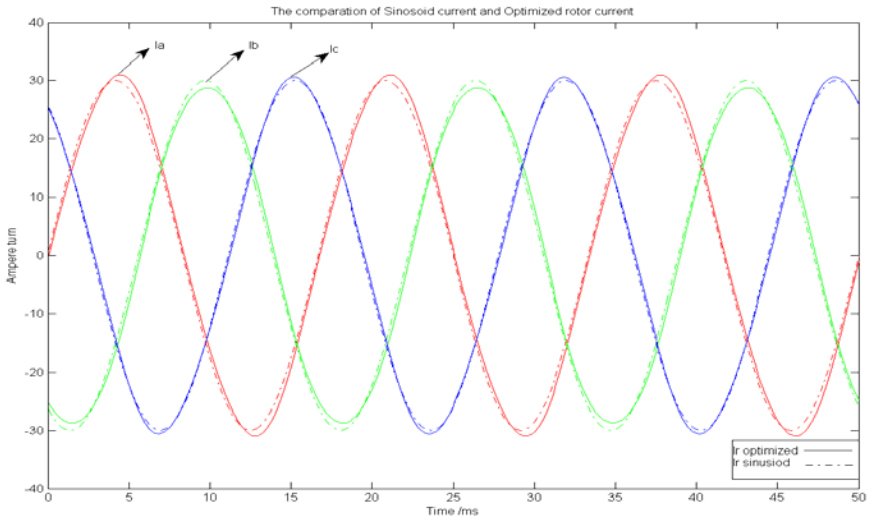

Figure C. 1 Optimal and balanced rotor current

Torque under optimized rotor excitation

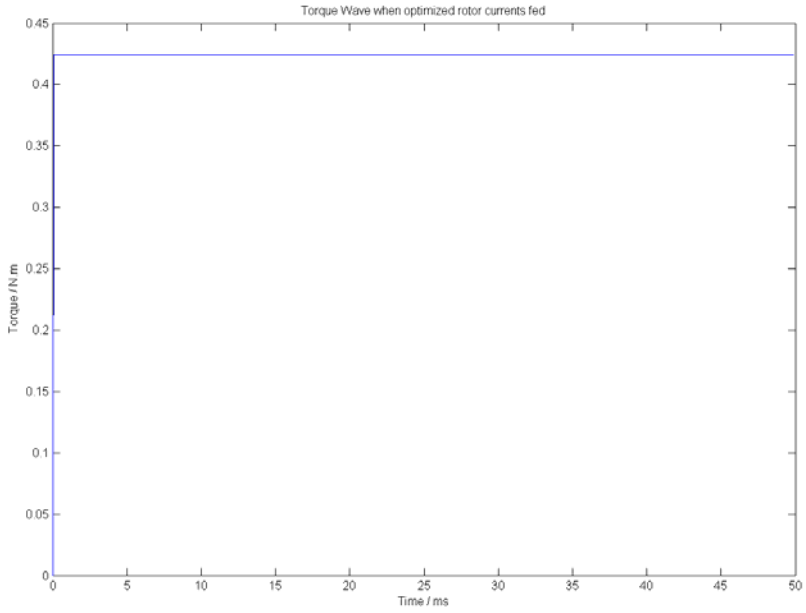

Figure C.2 Torque under optimized rotor excitation and unbalanced stator excitation

Optimal and balanced rotor current at 5A

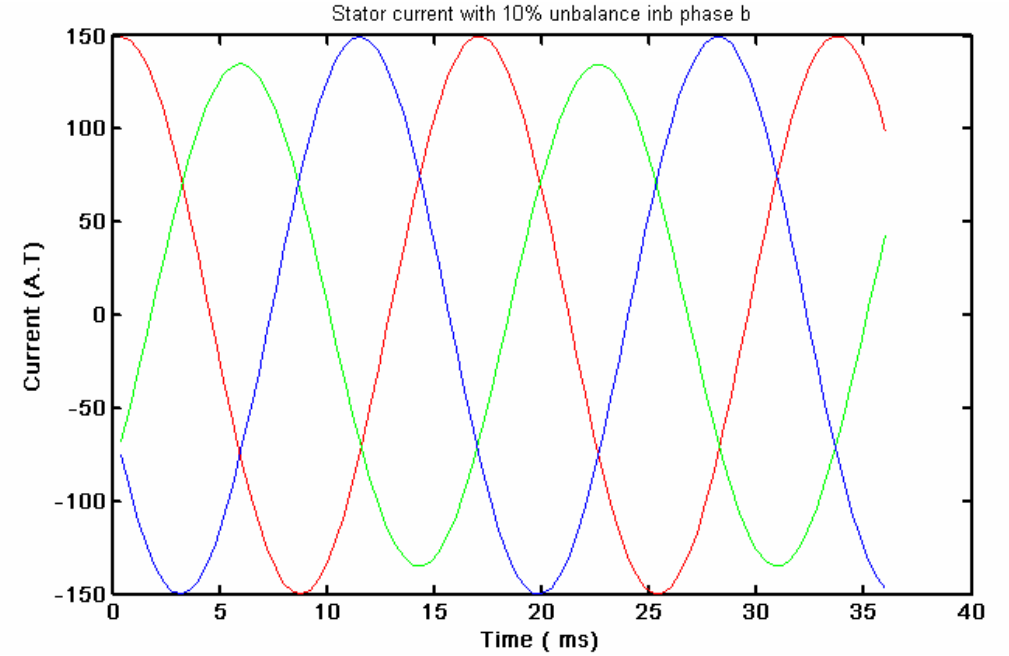

Figure C.3 Unbalanced stator current

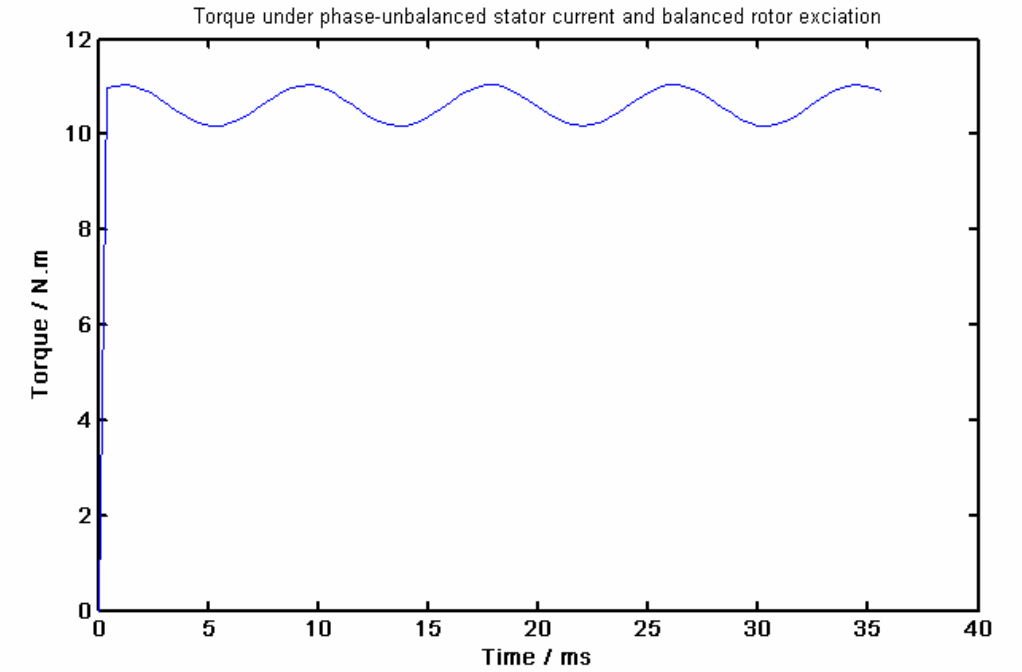

Figure C.4 Torque under balanced rotor excitation and unbalanced stator excitation

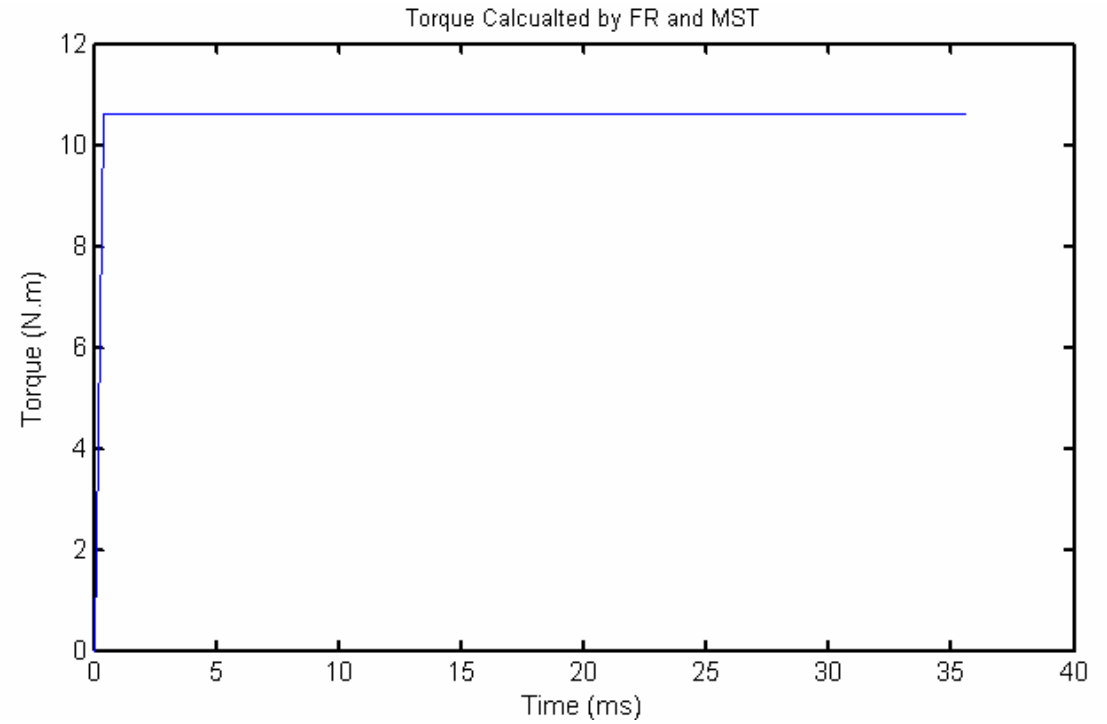

Figure C. 5 Torque under optimized rotor excitation and unbalanced stator excitation

Core loss before optimization

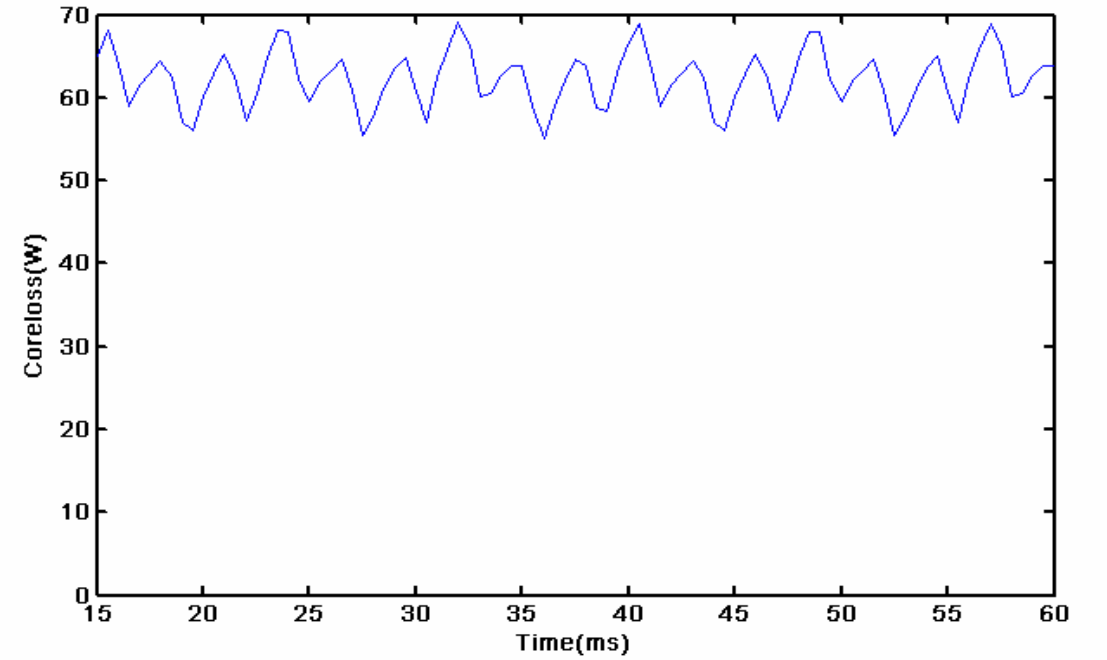

Figure C.6 Core loss under balanced rotor excitation and unbalanced stator excitation

Core loss after torque optimization

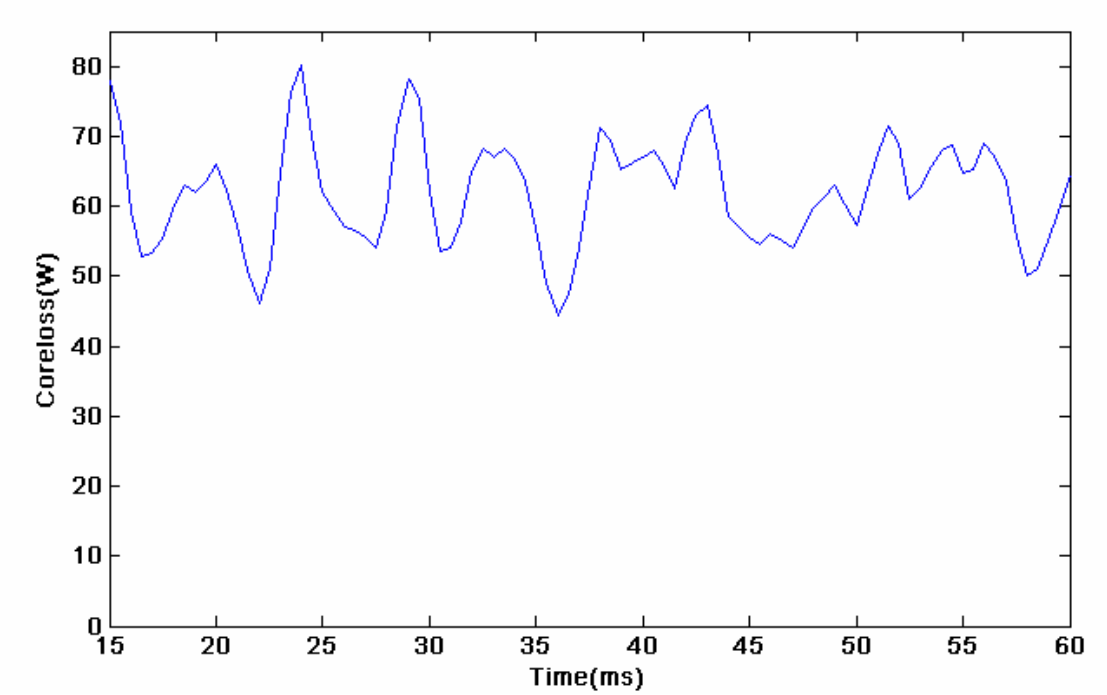

Figure C.7 Core loss under optimal rotor excitation and unbalanced stator excitation

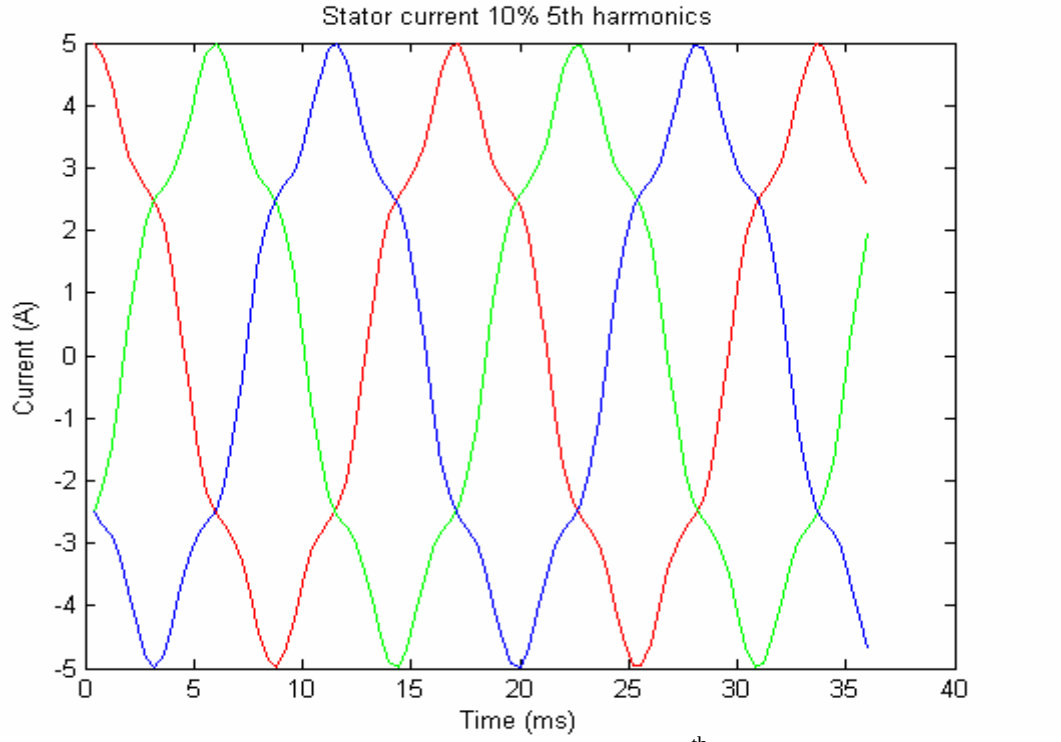

Figure C.8 stator current with 10% 5th harmonic

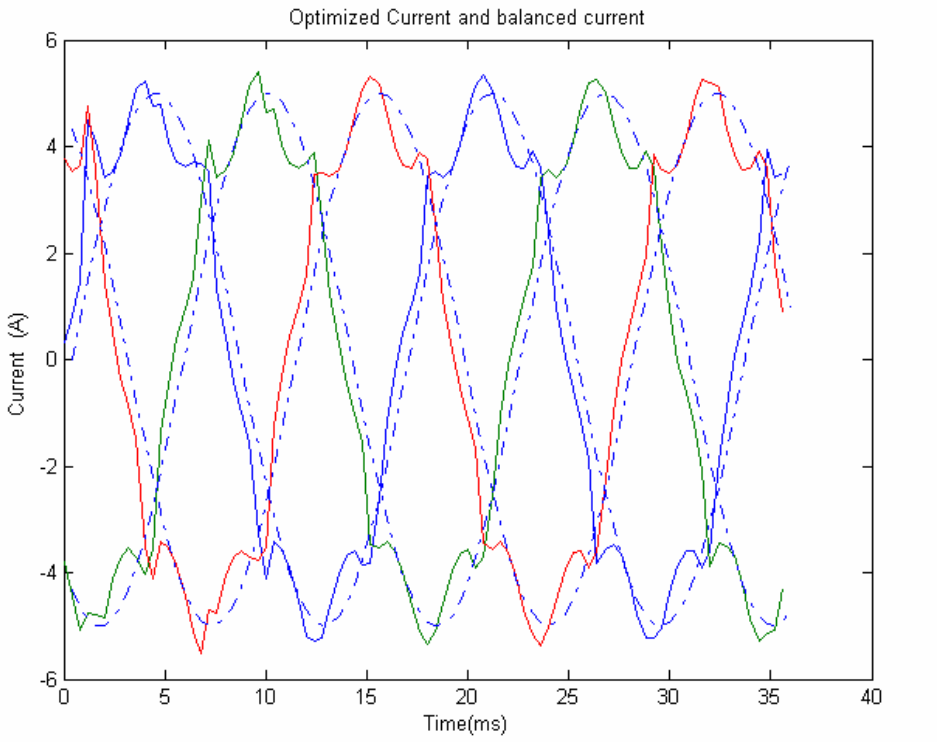

Figure C.9 Optimal rotor current

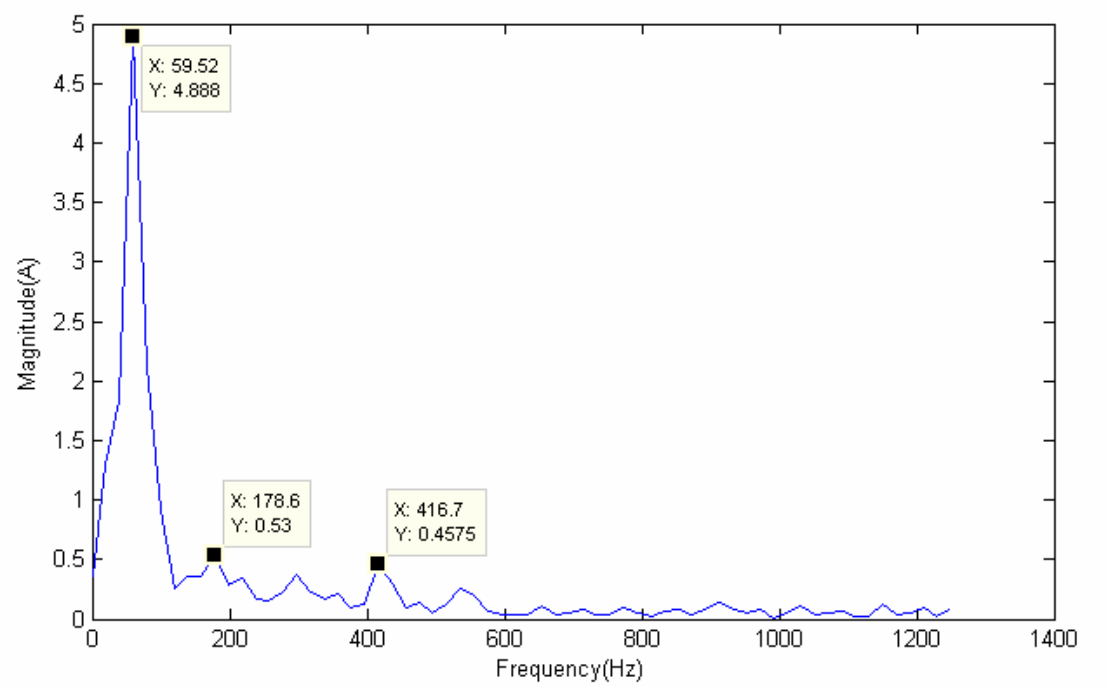

Figure C.10 FFT Analysis of optimal rotor current

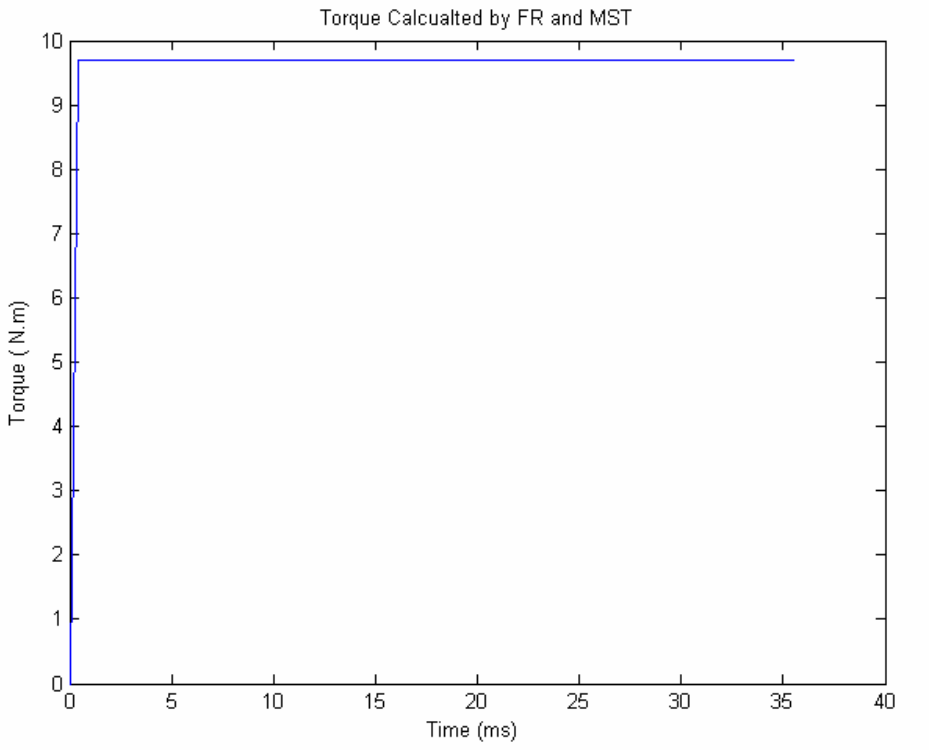

Figure C.11 Torque under optimal rotor current excitation

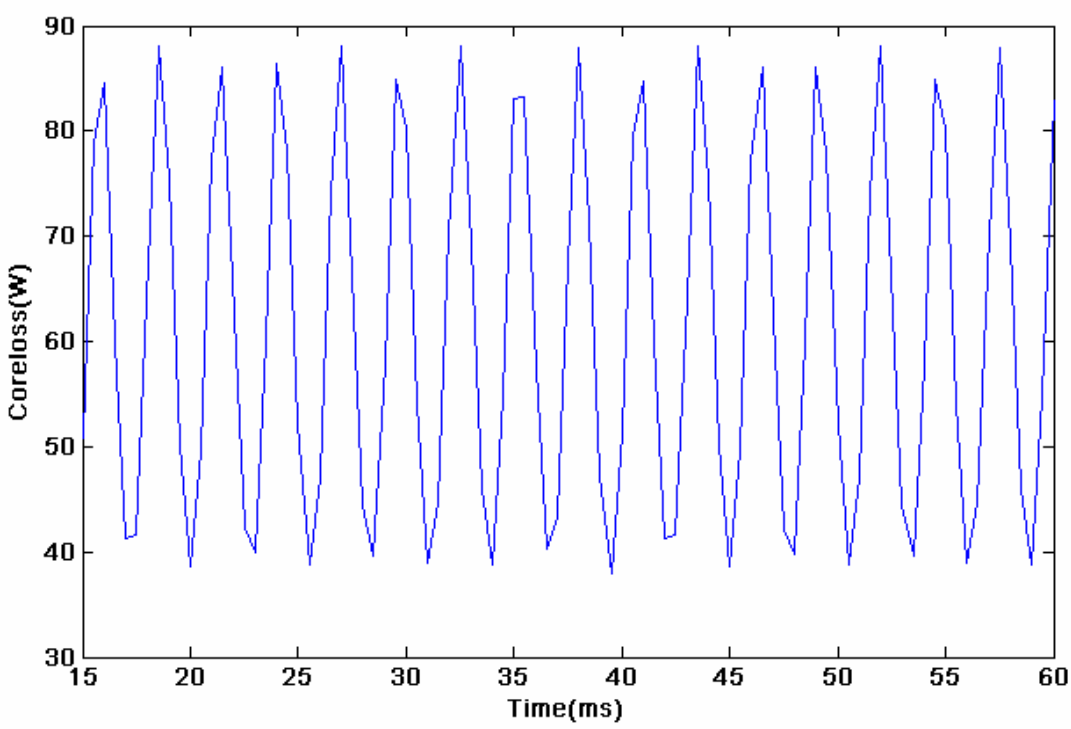

Figure C.12 Core loss before optimization

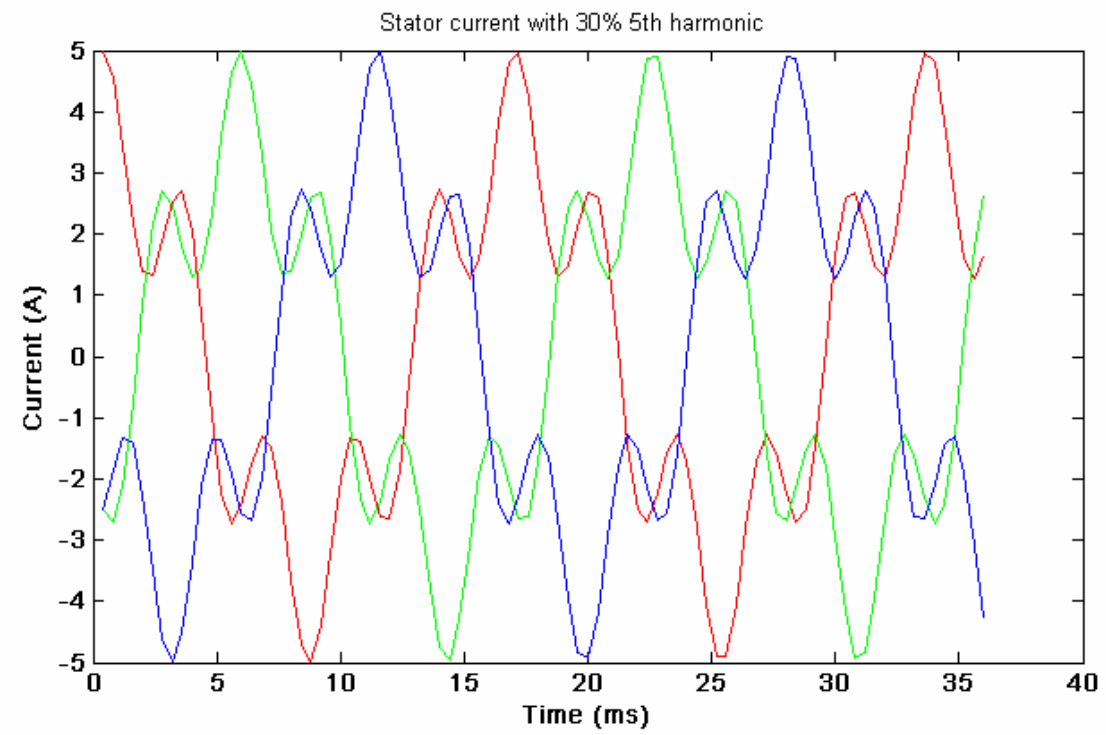

Figure C.13 Stator current

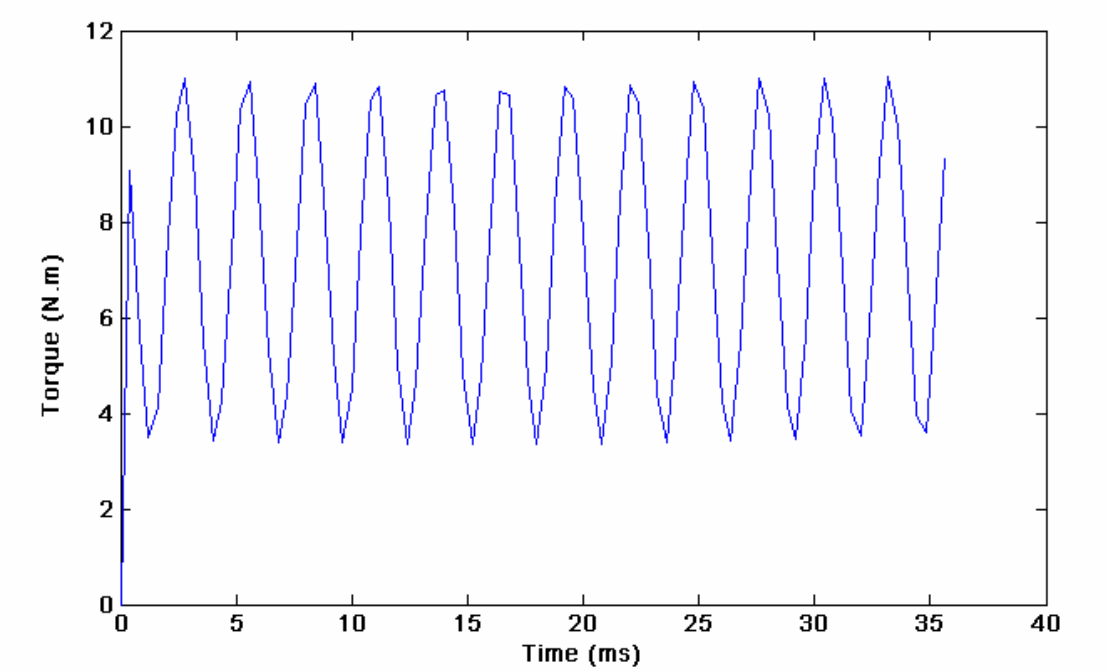

Figure C.14 Torque under balanced rotor excitation
Average Torque = 7.2 N.M

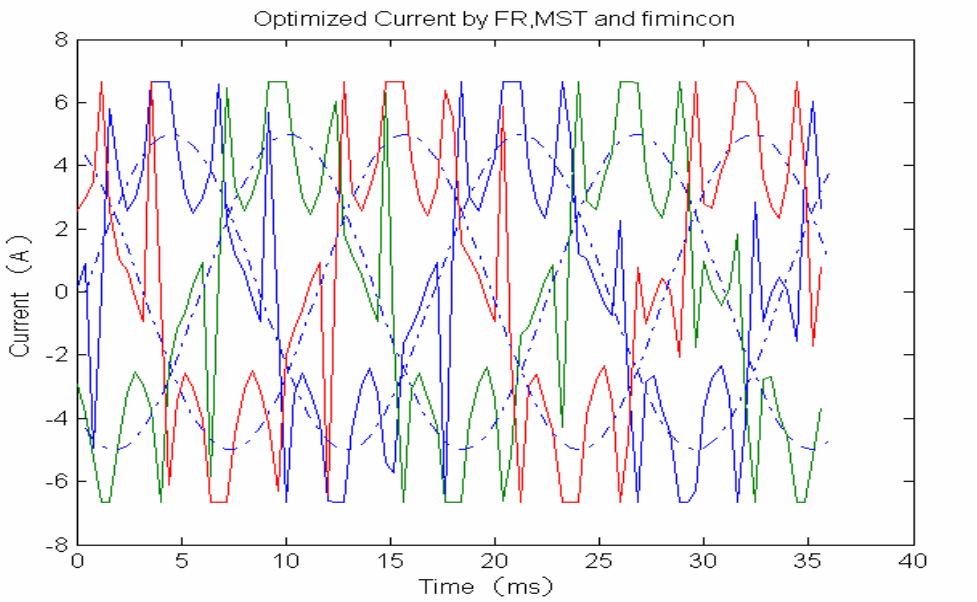

Figure C.15 Optimal rotor currents

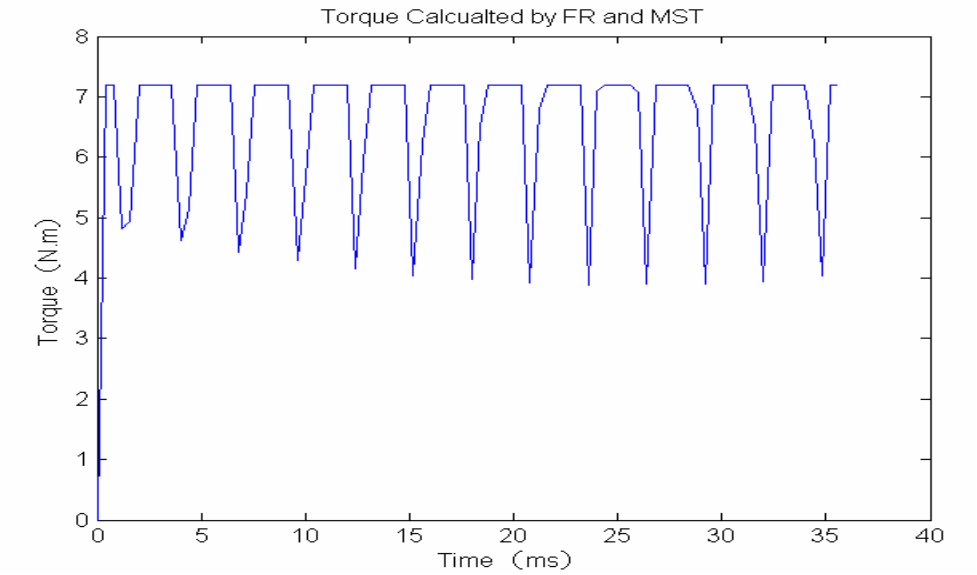

Figure C.16 Torque under optimal rotor current excitation

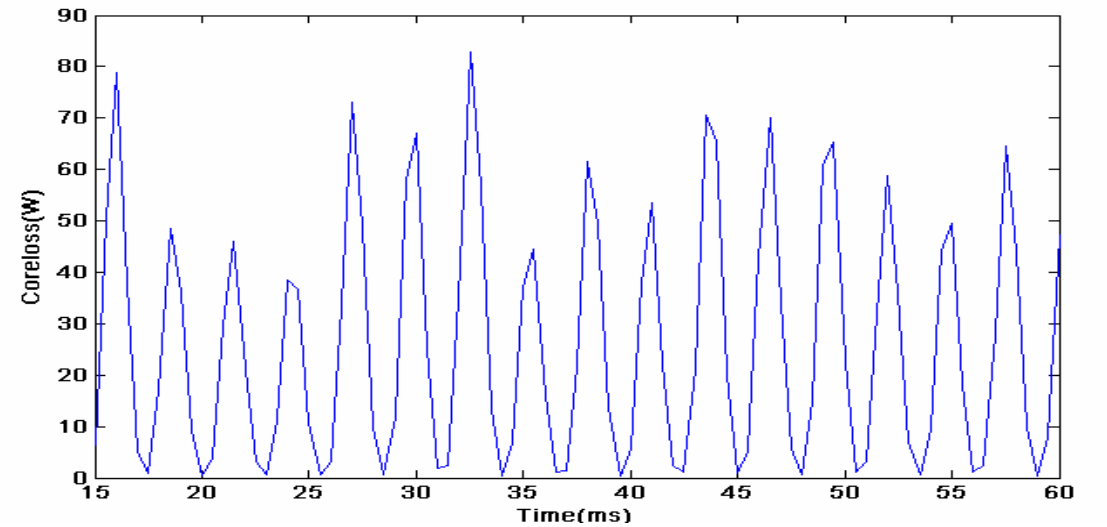

Figure C.17 Core loss after torque optimization

REFERENCES

[1] Chen, L.L.; Fan, S.S.; Lee, W.W.-J.; Liao, J.J. R.; Yokoyama, R.R.," Forecasting the Wind Generation Using a Two-Stage Network Based on Meteorological Information", *IEEE Transactions on Energy conversion,* Volume PP, Forthcoming, 2003 Page(s):1 – 9.

[2] Methaprayoon, K.; Yingvivatanapong, C.; Wei-Jen Lee; Liao, J.R.," An Integration of ANN Wind Power Estimation Into Unit Commitment Considering the Forecasting Uncertainty", *IEEE Transactions on Industry Applications,* Volume 43, Issue 6, Nov.-Dec. 2007 Page(s):1441 – 1448.

[3] Greiner, C.J.; Korpas, M.; Gjengedal, T.," Value of combining hydrogen production with wind power in short-term electricity markets", *IEEE 2nd International Power and Energy Conference, 2008* , 1-3 Dec. 2008 Page(s):1259 – 1264.

[4] Kiani, M.; Wei-Jen Lee," Effects of Voltage Unbalance and System Harmonics on the Performance of Doubly Fed Induction Wind Generators", *Industry Applications Society Annual Meeting, 2008. IAS '08. IEEE* 5-9 Oct. 2008 Page(s):1 – 7.

[5] E. Muljadi, et. al.,'' Understanding the unbalanced-voltage problem in wind turbine generation", *Proceedings of IEEE-IAS Annual meeting*, 1999, Vol. 2, pp. 1359-1365.

[6] Ted K. A. Brekken, Ned Mohan," Control of a doubly fed induction wind generator under unbalanced grid voltage conditions", *IEEE Transactions on Energy Conversion*, Vol. 22, No.1, March 2007, pp. 129-135.

[7] Santiago D. Rubira, M. D. McCulloch," Control method comparison of doubly fed wind generators connected to the grid by asymmetric transmission lines", IEEE *Transactions on Industry Applications*, Vol.36, No. 4, July/August 2000, pp. 986-991.

[8] Lie Xu, Yi Wang,'' Dynamic Modeling and Control of DFIG-Based Wind Turbines under Unbalanced Network Conditions'', *IEEE Transactions on Power Systems*, Vol. 22, No.1, February 2007.

[9] Lopez, J.; Sanchis, P.; Roboam, X.; Marroyo, L.," Dynamic Behavior of the Doubly Fed Induction Generator During Three-Phase Voltage Dips", *IEEE Transactions on Energy Conversion,* Volume 22, Issue 3, Sept. 2007 Page(s):709 – 717.

[10] Ekanayake, J.B.; Holdsworth, L.; XueGuang Wu; Jenkins, N.," Dynamic modeling of doubly fed induction generator wind turbines", *IEEE Transactions on Power Systems* ,Volume 18, Issue 2, May 2003 Page(s):803 – 809.

[11] Ledesma, P.; Usaola, J., "Effect of neglecting stator transients in doubly fed induction Generators models", *IEEE Transactions on Energy Conversion,* Volume 19, Issue 2, June 2004 Page(s):459 – 461.

[12] Wangsathitwong, S.; Sirisumrannukul, S.; Chatratana, S.; Deleroi, W.," Symmetrical Components-Based Control Technique of Doubly Fed Induction

Generators under Unbalanced Voltages for Reduction of Torque and Reactive Power Pulsations", *International Conference on Power Electronics and Drive Systems, 2007,* 27-30 Nov. 2007 Page(s):1325 – 1330.

[13] Tao Sun; Zhe Chen; Blaabjerg, F., "Flicker study on variable speed wind turbines with doubly fed induction generators", *IEEE Transactions on Energy Conversion,* Volume 20, Issue 4, Dec. 2005 Page(s):896 - 905.

[14] Xu, P.; Wei, J.; Lee, F.C.," The active-clamp couple-buck converter-a novel high efficiency voltage regulator modules", *IEEE Applied Power Electronics Conference and Exposition, 2001.* March 2001 Page(s):252 - 257 vol.1.

[15] Fernandez, L.M.; Garcia, C.A.; Jurado, F.; Saenz, J.R.," Control system of doubly fed induction generators based wind turbines with production limits", *IEEE International Conference on Electric Machines and Drives,* 12-15 May 2005 Page(s):1936-1941.

[16] Elkington, K.; Knazkins, V.; Ghandhari, M.," On the rotor angle stability of power systems with Doubly Fed Induction Generators", *IEEE Power Tech, 2007 Lausanne*
1-5 July 2007 Page(s):213 – 218.

[17] Elkington, K.; Knazkins, V.; Ghandhari, M.," Modal analysis of power systems with doubly fed induction generators", *2007 iREP Symposium on Bulk Power System Dynamics and Control - VII. Revitalizing Operational Reliability,* 19-24 Aug. 2007 Page(s):1 – 8.

[18] Auddy, S.; Varma, R.K.; Dang, M.," Field Validation of a Doubly Fed Induction Generator (DFIG) Model", *IEEE Electrical Power Conference, 2007. Canada* 25-26 Oct. 2007 Page(s):484 – 489.

[19] Xiyun Yang; Lingfeng Xu; Yibing Liu; Daping Xu," Multivariable Predictive Functional Control for Doubly Fed Induction Generator", *IEEE International Conference on Control and Automation, 2007,* May 30 2007-June 1 2007 Page(s):80 – 83.

[20] Mullane, A.; O'Malley, M.," The Inertial Response of Induction-Machine-Based Wind Turbines", *IEEE Transactions on Power Systems,* Volume 20, Issue 3, Aug. 2005 Page(s):1496 – 1503.

[21] Karimi-Davijani, H.; Sheikholeslami, A.; Livani, H.; Norouzi, N.," Fault ride-through capability improvement of wind farms using doubly fed induction generator", *43rd International Universities Power Engineering Conference,* 2008, 1-4 Sept. 2008 Page(s):1 – 5.

[22] Gomez, S.A.; Amenedo, J.L.R.," Grid synchronization of doubly fed induction generators using direct torque control", *28th Annual conference of Industrial Electronics Society, 2002,* Volume 4, 5-8 Nov. 2002 Page(s):3338 - 3343 vol.4.

[23] Wei Qiao; Venayagamoorthy, G.K.; Harley, R.G.," Real-Time Implementation of a STATCOM on a Wind Farm Equipped With Doubly Fed Induction Generators", *IEEE Transactions on Industry Application,* Volume 45, Issue 1, Jan.-Feb. 2009 Page(s):98 – 107.

[24] Gomis-Bellmunt, O.; Junyent-Ferre, A.; Sumper, A.; Bergas-Jan, J.," Ride-Through Control of a Doubly Fed Induction Generator Under Unbalanced Voltage

Sags", *IEEE Transactions on Energy Conversion*, Volume 23, Issue 4, Dec. 2008 Page(s):1036 – 1045.

[25] Santos-Martin, D.; Rodriguez-Amenedo, J.L.; Arnalte, S.," Direct Power Control Applied to Doubly Fed Induction Generator Under Unbalanced Grid Voltage Conditions", *IEEE Transactions on Power Electronics*, Volume 23, Issue 5, Sept. 2008 Page(s):2328 – 2336.

[26] Dawei Xiang; Li Ran; Tavner, P.J.; Yang, S.," Control of a doubly fed induction generator in a wind turbine during grid fault ride-through", *IEEE Transactions on Energy Conversion*, Volume 21, Issue 3, Sept. 2006 Page(s):652 – 662.

[27] Feng Wu; Xiao-Ping Zhang; Ping Ju; Sterling, M.J.H.," Decentralized Nonlinear Control of Wind Turbine With Doubly Fed Induction Generator", *IEEE Transactions on Power Systems*, Volume 23, Issue 2, May 2008 Page(s):613 – 621.

[28] Lopez, J.; Gubia, E.; Sanchis, P.; Roboam, X.; Marroyo, L.," Wind Turbines Based on Doubly Fed Induction Generator Under Asymmetrical Voltage Dips", *IEEE Transactions on Energy Conversion*, Volume 23, Issue 1, March 2008 Page(s):321 – 330.

[29] Dawei Xiang; Li Ran; Bumby, J.R.; Tavner, P.J.; Yang, S.," Coordinated control of an HVDC link and doubly fed induction generators in a large offshore wind farm", *IEEE Transactions on Power Delivery*, Volume 21, Issue 1, Jan. 2006 Page(s):463 – 471.

[30] Li, H.; Chen, Z.; Pederson, J.K.," Optimal Power Control Strategy of Maximizing Wind Energy Tracking and Conversion for VSCF Doubly Fed Induction Generator System", *International Power Electronics and Motion Control Conference, 2006. IPEMC 2006.* Volume 3, 14-16 Aug. 2006 Page(s):1 – 6.

[31] Guofeng Yuan; Jianyun Chai; Yongdong Li," Vector control and synchronization of doubly fed induction wind generator system", International Power Electronics and Motion Control Conference, 2004. IPEMC 2004, Volume 2, 14-16 Aug. 2004 Page(s):886 – 890.

[32] El-helw, H.M.; Tennakoon, S.B.," Vector Control of a Doubly Fed Induction Generator for Standalone Wind Energy Application", *Wind Power to the Grid - EPE Wind Energy Chapter 1st Seminar, 2008. EPE-WECS 2008*, 27-28 March 2008 Page(s):1 – 6.

[33] Li, H.; Chen, Z.; Pedersen, J.K.," Optimal Power Control Strategy of Maximizing Wind Energy Tracking and Conversion for VSCF Doubly Fed Induction Generator System", *International IEEE Power Electronics and Motion Control Conference, 2006*, Volume 3, 14-16 Aug. 2006 Page(s):1 – 6.

[34] Muller, S.; Deicke, M.; De Doncker, R.W.," Doubly fed induction generator systems for wind turbines", *Industry Applications Magazine, IEEE*, Volume 8, Issue 3, May-June 2002 Page(s):26 – 33.

[35] Yazhou Lei; Mullane, A.; Lightbody, G.; Yacamini, R.," Modeling of the wind turbine with a doubly fed induction generator for grid integration studies", *IEEE Transactions on Energy Conversion*, Volume 21, Issue 1, March 2006 Page(s):257 – 264.

[36] Pena, R.; Cardenas, R.; Escobar, E.; Clare, J.; Wheeler, P.," Control System for Unbalanced Operation of Stand-Alone Doubly Fed Induction Generators", *IEEE Transactions on Energy Conversion,* Volume 22, Issue 2, June 2007 Page(s):544 – 545.

[37] Shima, Z.; Ide, K.; Nishihama, K.; Fujigaki, T.; Mizutani, S.; Iizuka, M.," Finite element analysis for field currents and reactances of doubly fed induction generators for wind turbines", *IEEE International Conference on Electric Machines and Drives,* May 12-15 May 2005 Page(s):981 – 986.

[38] Lopez, J.; Sanchis, P.; Gubia, E.; Ursua, A.; Marroyo, L.; Roboam, X.," Control of Doubly Fed Induction Generator under symmetrical voltage dips", *IEEE International Symposium on Industrial Electronics, 2008.* June 30 2008-July 2 2008 Page(s):2456 – 2462.

[39] Won-Sang Kim; Kyo-Beum Lee; Byoung-Chang Jeong; Seung-Ho Song," A variable structure approach to control the active and reactive power for doubly fed induction generator", *International Conference on Power Electronics, 2007*, 22-26 Oct. 2007 Page(s):498 – 502.

[40] Jianyun Chai; Zhou Zhang," Calculation of equivalent circuit parameters of doubly fed induction generator based on magnetic field finite element analysis", *International Conference on Electrical Machines and Systems, 2008.* 17-20 Oct. 2008 Page(s):3767 - 3771.

[41] Pena, R.; Clare, J.C.; Asher, G.M.," Doubly fed induction generator using back-to-back PWM converters and its application to variable-speed wind-energy generation", *IEE Proceedings Electric Power Applications,* Volume 143, Issue 3, May 1996 Page(s):231 – 241.

[42] Tuohy, A.; Denny, E.; O'Malley, M.," Rolling Unit Commitment for Systems with Significant Installed Wind Capacity", IEEE Lausanne Power Tech, 2007, 1-5 July 2007 Page(s):1380 – 1385.

[43] W. Zhu, B. Fahimi, S. Pekarek, **"**A field reconstruction method for optimal excitation of permanent magnet synchronous machines"**,** *IEEE Trans. on Energy Conversion*, vol. 21, no.2, pp. 305 – 313, June 2006.

[44] W. Zhu, B. Fahimi, S. Pekarek, **"**Optimal excitation of permanent magnet synchronous machines via direct computation of electromagnetic force components", *IEEE Int. Conf. on Electrical machines and Drives*, pp. 918 - 925 , May 2005.

BIOGRAPHICAL INFORMATION

Morgan M. Kiani received her M.S. and PhD degrees from the department of Electrical Engineering at University of Texas at Arlington. She also holds a B.S. degree in Economics and a second B.S. in Electrical Engineering. She has conducted research in the general area of electric power system and in particular fault monitoring and treatment of distributed wind generation units. She is a member of HKN honor society and is a university scholar in the University of Texas at Arlington. She can be contacted by C/O Prof. Wei-Jen Lee at Electrical Engineering department, UTA.